USGS
science for a changing world

Prepared in cooperation with the U.S. Environmental Protection Agency, Great Lakes Restoration Initiative

Basin-Scale Simulation of Current and Potential Climate Changed Hydrologic Conditions in the Lake Michigan Basin, United States

Scientific Investigations Report 2014–5175

U.S. Department of the Interior
U.S. Geological Survey

Cover. Modified from satellite image of the Great Lakes Region, National Aeronautics and Space Administration, http://modis.gsfc.nasa.gov/gallery/individual.php?db_date=2010-09-06.

Basin-Scale Simulation of Current and Potential Climate Changed Hydrologic Conditions in the Lake Michigan Basin, United States

By Daniel E. Christiansen, John F. Walker, and Randall J. Hunt

Prepared in cooperation with the U.S. Environmental Protection Agency, Great Lakes Restoration Initiative

Scientific Investigations Report 2014–5175

U.S. Department of the Interior
U.S. Geological Survey

U.S. Department of the Interior
SALLY JEWELL, Secretary

U.S. Geological Survey
Suzette M. Kimball, Acting Director

U.S. Geological Survey, Reston, Virginia: 2014

Suggested citation:
Christiansen, D.E., Walker, J.F., and Hunt, R.J., 2014, Basin-scale simulation of current and potential climate changed hydrologic conditions in the Lake Michigan Basin, United States: U.S. Geological Survey Scientific Investigations Report 2014–5175, 74 p., *http://dx.doi.org/10.3133/sir20145175.*

ISSN 2328-0328 (online)

Contents

Figures

Tables

Conversion Factors

Inch/Pound to SI

Multiply	By	To obtain
	Length	
mile (mi)	1.609	kilometer (km)
	Area	
acre	4,047	square meter (m^2)
acre	0.004047	square kilometer (km^2)
square mile (mi^2)	2.590	square kilometer (km^2)
	Volume	
cubic foot (ft^3)	0.02832	cubic meter (m^3)
	Flow rate	
foot per second (ft/s)	0.3048	meter per second (m/s)
cubic foot per second (ft^3/s)	0.02832	cubic meter per second (m^3/s)
foot per day (ft/d)	0.3048	meter per day (m/d)

Temperature in degrees Fahrenheit (°F) may be converted to degrees Celsius (°C) as follows:

°C=(°F-32)/1.8

Vertical coordinate information is referenced North American Vertical Datum of 1988 (NAVD 88).

Horizontal coordinate information is referenced to World Geodetic System (WGS 84).

Altitude, as used in this report, refers to distance above the vertical datum.

Water year, as used in this report, refers to the 12-month period October 1 through September 30. It is designated by the calendar year in which it ends.

Basin-Scale Simulation of Current and Potential Climate Changed Hydrologic Conditions in the Lake Michigan Basin, United States

By Daniel E. Christiansen, John F. Walker, and Randall J. Hunt

Abstract

The Great Lakes Restoration Initiative (GLRI) is the largest public investment in the Great Lakes in two decades. A task force of 11 Federal agencies developed an action plan to implement the initiative. The U.S. Department of the Interior was one of the 11 agencies that entered into an interagency agreement with the U.S. Environmental Protection Agency as part of the GLRI to complete scientific projects throughout the Great Lakes basin. The U.S. Geological Survey, a bureau within the Department of the Interior, is involved in the GLRI to provide scientific support to management decisions as well as measure progress of the Great Lakes basin restoration efforts. This report presents basin-scale simulated current and forecast climatic and hydrologic conditions in the Lake Michigan Basin. The forecasts were obtained by constructing and calibrating a Precipitation-Runoff Modeling System (PRMS) model of the Lake Michigan Basin; the PRMS model was calibrated using the parameter estimation and uncertainty analysis (PEST) software suite. The calibrated model was used to evaluate potential responses to climate change by using four simulated carbon emission scenarios from eight general circulation models released by the World Climate Research Programme's Coupled Model Intercomparison Project phase 3. Statistically downscaled datasets of these scenarios were used to project hydrologic response for the Lake Michigan Basin.

In general, most of the observation sites in the Lake Michigan Basin indicated slight increases in annual streamflow in response to future climate change scenarios. Monthly streamflows indicated a general shift from the current (2014) winter-storage/snowmelt-pulse system to a system with a more equally distributed hydrograph throughout the year. Simulated soil moisture within the basin illustrates that conditions within the basin are also expected to change on a monthly timescale. One effect of increasing air temperature as a result of the changing climate was the appreciable increase in the length of the growing season in the Lake Michigan Basin. The increase in growing season will cause an increase in evapotranspiration across the Lake Michigan Basin, which will directly affect soil moisture and late growing season streamflows. Output from the Lake Michigan Basin PRMS model is available through an online dynamic web mapping service available at (*http://pubs.usgs.gov/sir/2014/5175/*). The map service includes layers for each of the 8 global climate models and 4 carbon emission scenarios combinations for 12 hydrologic model state variables. The layers are pre-rendered maps of annual hydrologic response from 1977 through 2099 that provide an easily accessible online method to examine climate change effects across the Lake Michigan Basin.

Introduction

The Great Lakes Restoration Initiative (GLRI) is the largest public investment in the Great Lakes in two decades. A task force of 11 federal agencies developed an action plan to implement the initiative. The U.S. Department of the Interior was one of the 11 agencies that entered into an interagency agreement with the U.S. Environmental Protection Agency (EPA) as part of the GLRI to complete scientific projects throughout the Great Lakes basin. The U.S. Geological Survey (USGS), a bureau within the Department of the Interior, is involved in the GLRI to provide scientific support to management decisions as well as measure progress of the Great Lakes restoration efforts. The USGS is involved in multiple projects in the GLRI intended to provide a scientific basis to support management decisions and measure progress of the Great Lakes restoration efforts; a list of projects can be accessed at *http://greatlakesrestoration.us/projects/usgs.html*.

As part of the scientific support, the USGS designed a hydrologic model of the Lake Michigan Basin, referred to as the Lake Michingan Basin Precipitation-Runoff Modeling System (PRMS) model in this report, to act as a Great Lakes decision support tool that can be used to answer potential questions about long-term restoration investments related to potential changes in land use and climate change. For example, coupling the hydrological output (streamflows) from the Lake Michigan Basin PRMS model with the Spatially Referenced Regression on Watershed (SPARROW) model framework can be used to estimate nutrient concentrations in

streams and loadings to Lake Michigan in response to changes in land use and climate. The Lake Michigan Basin PRMS model also can be applied to wildlife diseases; indices of hydrologic alteration can be related to historical spatial and temporal changes in wildlife diseases, and the relations can be used to forecast potential impacts of land use and climate on wildlife diseases. It is expected that a varietly of biological, ecological, and hydrological efforts the GLRI could benefit from forecasts of hydrologic outputs from the Lake Michigan Basin PRMS model.

Purpose and Scope

This report documents the development of a distributed-parameter, physically based, hydrologic model of the Lake Michigan Basin using the PRMS (Markstrom and others, 2008). A basin-scale hydrologic model was constructed and calibrated to current (2014) climatic conditions. Model calibration used the model-independent parameter estimation and uncertainty computer code (PEST; Doherty, 2010a, 2010b). Construction and calibration of the Lake Michigan Basin PRMS model focused on use for forecasts of monthly and annual streamflows; daily streamflows were not emphasized in the development and calibration because of the inappropriately large basin discretization needed to simulate the large areal extent of the Lake Michigan Basin PRMS model domain. Downscaled model output from four carbon emissions scenarios and eight general circulation models (GCMs) were used as input to the Lake Michigan Basin PRMS model to forecast potential future hydrologic changes within the Lake Michigan Basin caused by potential future climate change scenarios.

Previous Studies

The Lake Michigan Basin is a large geographic area, approximately 44,922 square miles of earth surface that has numerous hydrologic studies (for example; National Geophysical Data Center, 1998) as well as many modeling efforts present within, including but not limited to a compilation of basin models for tributaries to the Great Lakes (Coon and others, 2011); a compilation of regional groundwater divides for principal aquifers corresponding to the Great Lakes Basin, United States (Sheets and Simonson, 2006); a Basin-scale groundwater flow model constructed in support of the USGS Great Lakes Basin Water Availability and Use Study (Feinstein and others, 2010); and a study on nutrient inputs to the Lauretian Great Lakes by source and basin estimated using Spatially Referenced Regression on Watershed (SPARROW) models (Robertson and Saad, 2011). Furthermore, there have been several climate change models developed for the area such as a study on the response of Great Lakes water levels to future climate scenarios (Mackay and Seglenieks, 2013), and with emphasis on Lake Michigan-Huron (Angel and Kunkel, 2010); the hydrologic impacts of projected future climate change in the Lake Michigan region (Cherkauer and Sinha, 2010); assessing effects of climate change on Chicago and the regional climate change projections (Hayhoe and others, 2010; Wuebbles and others, 2010); and the methodological approaches to projecting the hydrologic impacts of climate change (Lofgren and Gronewold, 2013; Lofgren and others, 2013). Climate change effects simulated by PRMS models of 17 basins located throughout the United States are given by Markstrom and others (2011).

Description of Study Area

The Lake Michigan Basin is bounded by Michigan, Indiana, Illinois, and Wisconsin (fig. 1). Lake Michigan is the only Great Lake that is entirely located within the United States and is the second largest of the five Great Lakes. Lake Michigan has more than 1,600 miles of shoreline, and drains approximately 44,922 square miles (Government of Canada and U.S. Environmental Protection Agency, 1995; National Geophysical Data Center, 1998). Land cover in the Lake Michigan Basin consists of 32 percent agricultural, 29 percent forest, 7 percent urban, 20 percent wetland, 6 percent water, and 6 percent in a combination of grassland, scrub, and barren (National Oceanic and Atmospheric Administration, 2010). Many rivers and streams flow into Lake Michigan; a few of the major tributaries are Fox-Wolf, Grand, Kalamazoo, and St. Joseph Rivers (Rutherford, 2008).

The climate of the Lake Michigan Basin is controlled by movement of air masses from the Arctic and the Gulf of Mexico and also is moderated by the size and position of Lake Michigan within a large continental land mass (Sheets and Simonson, 2006). In winter, cold, arctic air moves across the basin and absorbs moisture from the comparatively warmer Great Lakes; condensation as the air masses reach land creates heavy snowfalls on the leeward sides of the Great Lakes. In summer, most of the Great Lakes Basin is dominated by warm, humid air from the Gulf of Mexico, and only the most northern part of the basin receives cooler and drier air from the Canadian northwest (Government of Canada and U.S. Environmental Protection Agency, 1995).

The physiography of the Great Lakes Basin is mostly the result of a series of continental glaciers that scoured the area, the latest of which is the Laurentide Ice Sheet of the Wisconsin-stage glaciation during the Pleistocene Epoch. Most of the Great Lakes Basin is covered by glacial landforms such as moraines and till plains (Fenneman and Johnson, 1946).

The southern part of Lake Michigan Basin contains the Milwaukee and Chicago metropolitan areas, whereas the northern part of Lake Michigan Basin is less developed. Lake Michigan has the second largest amount of water withdrawals and consumption of the Great Lakes, only second to Lake Erie, with 26,190 cubic feet per second of water withdrawals, and 1,310 cubic feet per second of water consumption; most of the water use is for power and manufacturing, with municipal use trailing (Government of Canada and U.S. Environmental Protection Agency, 1995).

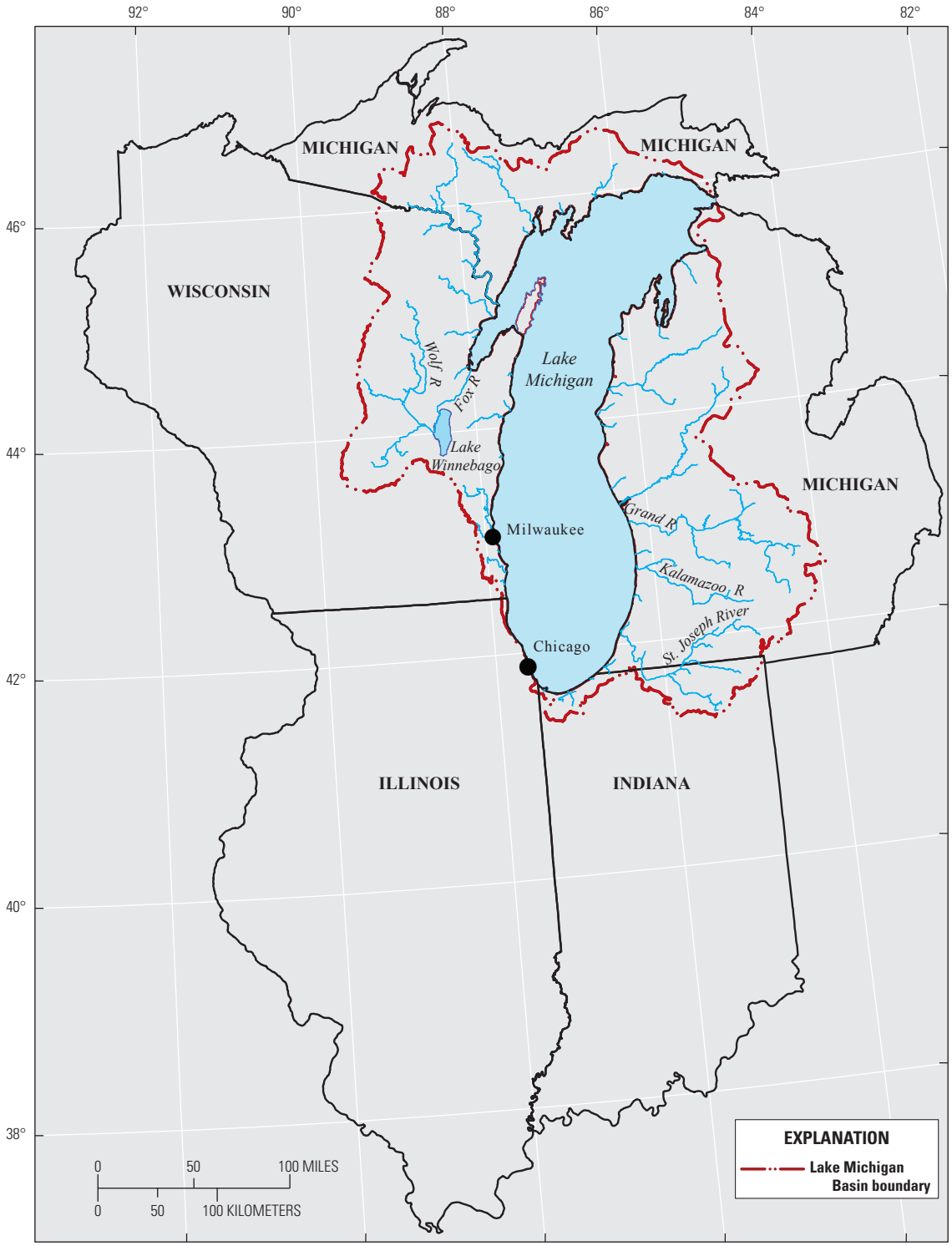

Base from U.S. Geolgocial Survey digital data, 2011, 1:2,000,000
Albers Equal-Area Conic projection
Standard parallels 29°30'N and 45°30'N,
Central meridian 96°W, Latitude of orgin 23°00'N

Horizontal coordinate information is referenced to the
World Geodetic System of 1984 (WGS 84)

Figure 1. Lake Michigan Basin location, extent, and hydrography.

Modeling Methods and Techniques

A Lake Michigan PRMS model was constructed over the entire Lake Michigan Basin area. The model was constructed and parameterized using available geographic information system (GIS) datasets, and calibrated using available observed (measured) streamflow, solar radiation, and potential evapotranspiration data. The observation data were processed using the Time-Series Processor TSPROC (Westenbroek and others, 2012) and automated calibration was completed using the parameter estimation code PEST (Doherty, 2010a, 2010b). Details of the PRMS model design and PEST calibration are discussed in the following sections.

Precipitation-Runoff Modeling System Model

The PRMS code used for the Lake Michigan Basin PRMS model is a modular, distributed-parameter, physically based process model developed to simulate basin conditions and surface-water runoff resulting from the effects of precipitation, climate, and land cover using physical laws and empirical relations (Markstrom and others, 2008). A schematic diagram of how basin and climate inputs are simulated within PRMS is shown in figure 2. The basin is divided into a series of piecewise-constant contiguous spatial units, called hydrologic response units (HRUs). The division of the basin into HRUs is based on hydrologic and physical characteristics such as land-surface altitude, slope, aspect, plant type and cover, land use, soil morphology, geology, drainage boundaries, distribution of precipitation, air temperature, solar radiation, and flow direction (Markstrom and others, 2008). The HRUs are deemed piecewise constant, internally homogenous (each parameter representing hydrologic and physical characteristics is defined using only one value), and are considered instantaneously and fully mixed. An energy balance and a water balance are computed for each HRU on a daily time step (Markstrom and others, 2008).

The Lake Michigan Basin PRMS model used minimum and maximum temperature, and precipitation as the primary climate drivers (fig. 2). The climate datasets were collected and formatted for model input using the USGS Downsizer program (Ward-Garrison and others, 2009), applied to climate stations with data that covered the time period from October 1, 1969 through September 30, 2008. Climate stations with large amounts of missing or erroneous data values were removed from the PRMS input data list, resulting in a total of 157 climate stations included in the PRMS model data file (table 1). The Downsizer program also was used to retrieve streamgage daily observations at 148 streamgage stations within the Lake Michigan Basin. The 148 streamgages were selected based on period of record and proximity to ecological points of interest developed by the SPAtially Referenced Regression On Watershed attributes model (Great Lakes SPARROW model; D. Robertson, written commun., 2009). The sites colocated with output nodes within the SPARROW model allow translation of potential effects of climate and land use changes to other societally relevant endpoints such as nutrient loads. The streamgages that were included in the model are listed in table 2, and figures 3 and 4 show the locations of the climate stations and streamgages, respectively, across the entire basin.

Parameter Development for the Lake Michigan Basin Precipitation-Runoff Modeling System Model

For this study, a geospatial database was created for use within a GIS, the GIS Weasel (Viger and Leavesley, 2007), to support model discretization, to characterize the physical features of the basin, and to estimate PRMS model parameters. The geospatial database consisted of: (1) the 2001 National Land Cover Database, (2) percent impervious, (3) U.S. forest types, (4) U.S. forest density, (5) State Soil Geographic Database (STATSGO) general soil maps, (6) National Hydrography Dataset (NHD) layers, and (7) a digital elevation model (DEM) derived from USGS National Elevation Dataset (NED) (U.S. Geological Survey, 2007; Homer and others, 2004; U.S. Department of Agriculture, 1994; Simley, 2008). A raster dataset representing Lake Winnebago was overlain onto the original HRUs and merged. Lake Winnebago and Lake Michigan are both represented as individual HRUs in the model. After processing, the Lake Michigan PRMS model consists of 766 HRUs and 467 stream segments (fig. 5). Depression storage, a parameter that facilitates accounting of within-HRU surface-water storage that can attenuate precipitation events, was also incorporated into the Lake Michigan Basin PRMS model.

The Lake Michigan Basin PRMS model requires the use of meteorological data as inputs to simulate streamflows. The meteorological data were distributed to each HRU using the climate_hru module (LaFontaine and others, 2013), which reads pre-processed values of minimum and maximum temperature, and precipitation for each HRU. The distribution by HRU enables the model to be adjusted for changes in temperature and precipitation relations over large distances compared to using the climate-station network, improving the representation of the climatic driver within the model. The Lake Michigan Basin PRMS model HRU development was based on rightbank/leftbank flow planes upgradient of the 148 streamgages (fig. 4). The Lake Michigan Basin PRMS model contains 766 HRUs and 245 subbasins that drain 44,904 square miles, and was developed as a coarse-resolution model intended to answer regional questions; however, potential improvements could be made by smaller discretization of the HRUs in the Lake Michigan Basin PRMS model in future modeling. Subbasins were developed by combining all HRUs that drain to each of the 148 streamgages (148 subbasins related to each streamgage) and the remaining subbasins that drain to Lake Michigan (fig. 6).

The depression storage feature of PRMS (Viger and others, 2010) helps account for within-HRU storage that can

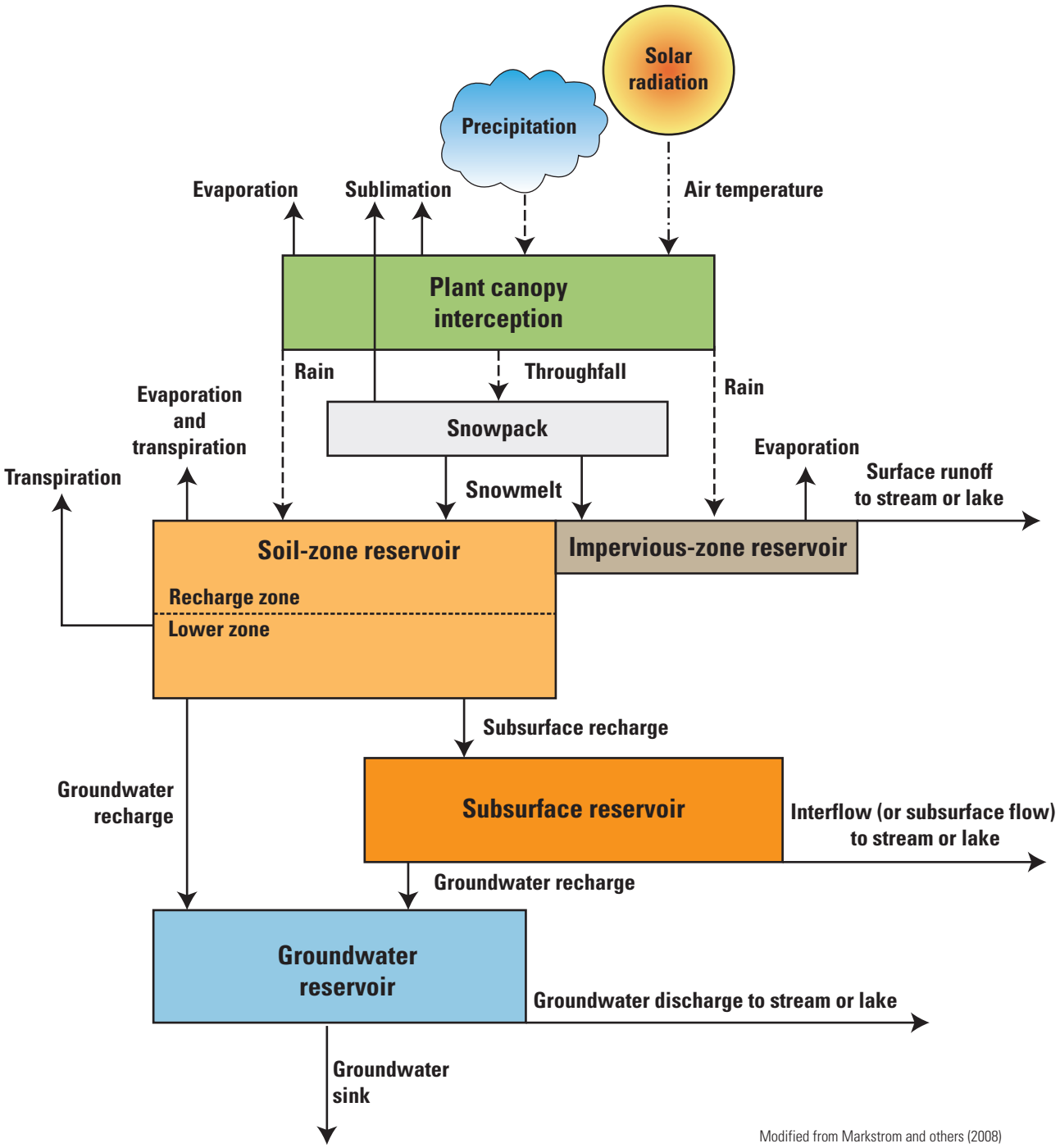

Figure 2. Schematic diagram of a basin and climate inputs simulated by the Precipitation-Runoff Modeling System model (modified from Markstrom and others, 2008).

Table 1. National Oceanic and Atmospheric Administration's National Weather Service Cooperative Observer Program meteorological stations used in the Lake Michigan Basin Precipitation Runoff-Modeling System model.

Map number (fig. 3)	Station number	State	Meteorological station name	Latitude (north)	Longitude (west)	Altitude (meters)
1	110338	Illinois	Aurora	41.781	88.309	201
2	110442	Illinois	Barrington 3 Southwest	42.115	88.164	267
3	111420	Illinois	Channahon Dresden Island	41.398	88.282	154
4	111497	Illinois	Chicago Botanical Garden	42.141	87.787	192
5	111549	Illinois	Chicago O'Hare International Airport	41.995	87.934	201
6	111572	Illinois	Chicago University	41.783	87.6	181
7	111577	Illinois	Chicago Midway Airport	41.737	87.777	189
8	112736	Illinois	Elgin	42.063	88.286	233
9	113369	Illinois	Gebhard Woods State Park	41.35	88.433	154
10	114530	Illinois	Joliet Brandon Road Dam	41.503	88.103	166
11	114603	Illinois	Kankakee Metro Wastewater Treatment Plant	41.138	87.886	195
12	119221	Illinois	Wheaton 3 Southeast	41.813	88.073	207
13	120200	Indiana	Angola	41.64	84.99	308
14	120676	Indiana	Berne Wastewater Treatment Plant	40.668	84.931	265
15	120830	Indiana	Bluffton 1 North	40.748	85.174	251
16	121739	Indiana	Columbia City	41.145	85.49	258
17	122096	Indiana	Decatur 1 North	40.848	84.929	250
18	123037	Indiana	Fort Wayne Weather Service Office Airport	41.006	85.206	252
19	123418	Indiana	Goshen 3 West	41.557	85.882	267
20	124181	Indiana	Huntington	40.856	85.498	221
21	125174	Indiana	Lowell	41.265	87.418	203
22	125337	Indiana	Marion 2 North	40.58	85.659	241
23	127298	Indiana	Rensselaer	40.936	87.156	198
24	127482	Indiana	Rochester	41.066	86.209	235
25	128187	Indiana	South Bend Weather Service Office Airport	41.707	86.333	236
26	129222	Indiana	Wanatah 2 West Northwest	41.444	86.93	224
27	129670	Indiana	Winamac 2 South Southeast	41.027	86.587	210
28	200146	Michigan	Alma	43.386	84.649	224
29	200230	Michigan	Ann Arbor Universtiy of Michigan	42.295	83.711	274
30	200710	Michigan	Benton Harbor Airport	42.129	86.422	191
31	200718	Michigan	Bergland Dam	46.587	89.548	396
32	200925	Michigan	Boyne Falls	45.167	84.914	222
33	201492	Michigan	Cheboygan	45.653	84.473	179
34	201896	Michigan	Cross Village 1 East	45.641	85.014	220
35	202015	Michigan	Dearborn	42.317	83.231	184
36	202094	Michigan	Detour Village	45.998	83.901	181
37	202103	Michigan	Detroit Metro Airport	42.231	83.331	192
38	202250	Michigan	Dowagiac 1 West	41.984	86.132	226
39	202298	Michigan	Dunbar Forest Experiment Station	46.317	84.233	183
40	202381	Michigan	East Jordan	45.152	85.132	178
41	202445	Michigan	Eau Claire 4 Northeast	42.014	86.242	265

Table 1. National Oceanic and Atmospheric Administration's National Weather Service Cooperative Observer Program meteorological stations used in the Lake Michigan Basin Precipitation Runoff-Modeling System model.—Continued

Map number (fig. 3)	Station number	State	Meteorological station name	Latitude (north)	Longitude (west)	Altitude (meters)
42	202846	Michigan	Flint Bishop International Airport	42.967	83.749	235
43	203096	Michigan	Gaylord	45.03	84.678	412
44	203170	Michigan	Gladwin	43.976	84.491	236
45	203306	Michigan	Grand Ledge 1 Northwest	42.763	84.762	244
46	203319	Michigan	Grand Marais 2 East	46.667	85.95	190
47	203333	Michigan	Grand Rapids International Airport	42.882	85.524	245
48	203391	Michigan	Grayling	44.654	84.699	346
49	203429	Michigan	Greenville 2 North Northeast	43.202	85.242	269
50	203661	Michigan	Hastings	42.642	85.287	250
51	203858	Michigan	Holland	42.787	86.123	186
52	203908	Michigan	Hancock Houghton County Airport	47.168	88.489	327
53	203936	Michigan	Houghton Lake Roscommon Airport	44.359	84.674	351
54	204078	Michigan	Ionia 2 South Southwest	42.953	85.078	245
55	204090	Michigan	Iron Mountain Kingsford Wastewater Treatment Plant	45.786	88.084	326
56	204150	Michigan	Jackson Airport	42.26	84.459	304
57	204502	Michigan	Lake City Experiment Farm	44.309	85.205	375
58	204641	Michigan	Lansing Capital City Airport	42.78	84.579	256
59	204655	Michigan	Lapeer Wastewater Treatment Plant	43.061	83.308	250
60	204944	Michigan	Lowell	42.929	85.34	195
61	204954	Michigan	Ludington 4 Southeast	43.907	86.394	210
62	205065	Michigan	Manistee 3 Southeast	44.211	86.294	204
63	205097	Michigan	Maple City 1 East	44.855	85.835	244
64	205178	Michigan	Sturgeon Bay Experiment Farm	46.546	87.379	203
65	205184	Michigan	Marquette Weather Service Office Airport	46.531	87.549	431
66	205434	Michigan	Midland	43.609	84.201	195
67	205558	Michigan	Monroe	41.914	83.394	180
68	205567	Michigan	Montague 4 Northwest	43.461	86.418	198
69	205712	Michigan	Muskegon County Airport	43.171	86.237	191
70	206184	Michigan	Onaway 4 North	45.411	84.223	227
71	206220	Michigan	Ontonagon 6 Southeast	46.834	89.207	241
72	206438	Michigan	Pellston Regional Airport	45.564	84.793	215
73	206507	Michigan	Petoskey	45.373	84.977	183
74	207094	Michigan	Rogers City	45.417	83.816	187
75	207222	Michigan	Saginaw Number 3	43.412	83.956	183
76	207227	Michigan	Saginaw Airport	43.533	84.08	201
77	207274	Michigan	St. Ignace Mackinac Bridge	45.849	84.723	181
78	207366	Michigan	Sault Ste. Marie Sanderson Field	46.479	84.357	220
79	207812	Michigan	Stambaugh 2 South Southeast	46.056	88.628	442
80	207820	Michigan	Standish 5 Southwest	43.947	84.038	197
81	207867	Michigan	Stephenson 8 West Northwest	45.45	87.75	216
82	208184	Michigan	Three Rivers	41.93	85.639	247

Table 1. National Oceanic and Atmospheric Administration's National Weather Service Cooperative Observer Program meteorological stations used in the Lake Michigan Basin Precipitation Runoff-Modeling System model.—Continued

Map number (fig. 3)	Station number	State	Meteorological station name	Latitude (north)	Longitude (west)	Altitude (meters)
83	208251	Michigan	Traverse City Federal Aviation Administration Airport	44.741	85.582	188
84	208800	Michigan	West Branch 3 Southeast	44.254	84.201	270
85	208920	Michigan	Whitefish Point	46.753	84.979	184
86	209218	Michigan	Ypsilanti East Michigan University	42.248	83.625	238
87	332098	Ohio	Defiance	41.278	84.385	213
88	333421	Ohio	Grover Hill	41.019	84.477	223
89	335438	Ohio	Montpelier	41.58	84.608	262
90	336465	Ohio	Paulding	41.124	84.592	221
91	338357	Ohio	Toledo Express Airport	41.589	83.801	204
92	338822	Ohio	Wauseon Water Treatment Plant	41.518	84.145	229
93	470265	Wisconsin	Appleton	44.279	88.439	236
94	470516	Wisconsin	Baraboo	43.458	89.727	251
95	470645	Wisconsin	Beaver Dam	43.445	88.848	256
96	470696	Wisconsin	Beloit	42.504	89.031	238
97	471205	Wisconsin	Burlington	42.651	88.254	229
98	471568	Wisconsin	Chilton	44.033	88.147	256
99	471667	Wisconsin	Clinton	42.549	88.875	293
100	471676	Wisconsin	Clintonville	44.623	88.747	244
101	471970	Wisconsin	Dalton	43.656	89.203	262
102	472314	Wisconsin	Eagle River	45.909	89.253	501
103	472447	Wisconsin	Eau Pleine Reservoir	44.725	89.757	347
104	472839	Wisconsin	Fond Du Lac	43.796	88.451	232
105	472869	Wisconsin	Fort Atkinson	42.905	88.859	244
106	473058	Wisconsin	Germantown	43.239	88.122	259
107	473182	Wisconsin	Goodrich 1 East	45.149	90.067	424
108	473269	Wisconsin	Green Bay Austin Straubel International Airport	44.479	88.138	209
109	473405	Wisconsin	Hancock Experiment Farm	44.119	89.534	328
110	473654	Wisconsin	Hillsboro	43.654	90.334	287
111	474174	Wisconsin	Kenosha	42.561	87.816	183
112	474195	Wisconsin	Kewaunee	44.463	87.505	179
113	474383	Wisconsin	Lac Vieux Desert	46.121	89.119	515
114	474457	Wisconsin	Lake Geneva	42.594	88.435	258
115	474523	Wisconsin	Lakewood 3 Northeast	45.333	88.498	365
116	474582	Wisconsin	Laona 6 Southwest	45.513	88.759	465
117	474829	Wisconsin	Long Lake Dam	45.888	89.139	497
118	474961	Wisconsin	Madison Dane Regional Airport	43.141	89.345	264
119	475017	Wisconsin	Manitowoc	44.069	87.739	221
120	475091	Wisconsin	Marinette	45.091	87.629	180
121	475120	Wisconsin	Marshfield Experiment Farm	44.632	90.131	381
122	475164	Wisconsin	Mather 3 Northwest	44.175	90.348	298
123	475178	Wisconsin	Mauston 1 Southeast	43.79	90.06	264

Table 1. National Oceanic and Atmospheric Administration's National Weather Service Cooperative Observer Program meteorological stations used in the Lake Michigan Basin Precipitation Runoff-Modeling System model.—Continued

Map number (fig. 3)	Station number	State	Meteorological station name	Latitude (north)	Longitude (west)	Altitude (meters)
124	475364	Wisconsin	Merrill	45.179	89.662	381
125	475474	Wisconsin	Milwaukee Mount Mary College	43.072	88.029	221
126	475479	Wisconsin	Milwaukee Mitchell Airport	42.955	87.904	204
127	475516	Wisconsin	Minocqua	45.886	89.732	489
128	475581	Wisconsin	Montello	43.781	89.317	240
129	475786	Wisconsin	Necedah 2 Southeast	43.997	90.035	276
130	476200	Wisconsin	Oconomowoc	43.1	88.504	261
131	476208	Wisconsin	Oconto 4 West	44.884	87.954	201
132	476330	Wisconsin	Oshkosh	44.012	88.556	229
133	476678	Wisconsin	Plymouth	43.73	87.971	254
134	476718	Wisconsin	Portage	43.528	89.434	236
135	476764	Wisconsin	Port Washington	43.394	87.864	181
136	476922	Wisconsin	Racine	42.702	87.786	181
137	476939	Wisconsin	Rainbow Reservoir Tomahawk	45.834	89.549	488
138	477113	Wisconsin	Rhinelander	45.629	89.423	467
139	477121	Wisconsin	Rib Falls	44.967	89.896	393
140	477140	Wisconsin	Rice Reservoir Tomahawk	45.541	89.748	447
141	477158	Wisconsin	Richland Center	43.331	90.389	222
142	477708	Wisconsin	Shawano 2 South Southwest	44.764	88.618	247
143	477725	Wisconsin	Sheboygan	43.75	87.717	198
144	478018	Wisconsin	Spirit Falls	45.449	89.967	448
145	478171	Wisconsin	Stevens Point	44.51	89.586	329
146	478241	Wisconsin	Stratford 1 Northwest	44.809	90.089	399
147	478267	Wisconsin	Sturgeon Bay Experiment Farm	44.872	87.335	200
148	478288	Wisconsin	Sugar Camp	45.865	89.382	489
149	478672	Wisconsin	Two Rivers	44.143	87.569	179
150	478905	Wisconsin	Washington Island	45.386	86.911	218
151	478919	Wisconsin	Watertown	43.174	88.736	251
152	478951	Wisconsin	Waupaca	44.355	89.059	265
153	478968	Wisconsin	Wausau	44.929	89.627	365
154	479050	Wisconsin	West Bend	43.368	88.086	287
155	479190	Wisconsin	Whitewater	42.851	88.725	267
156	479236	Wisconsin	Willow Reservoir	45.708	89.849	467
157	479335	Wisconsin	Wisconsin Rapids	44.388	89.806	315

Table 2. U.S. Geological Survey streamgages used in the Lake Michigan Basin Precipitation Runoff-Modeling System model.

[USGS, U.S. Geological Survey; latitude and longitude in decimal degrees; mi², square miles; MI, Michigan; WI, Wisconsin; IN, Indiana]

Map number (fig. 4)	USGS station number	USGS station name	Latitude (north)	Longitude (west)	Drainage area measured at gage (mi²)	Period of record used
1	04105700	Augusta Creek near Augusta, MI	42.353	85.354	38.9	9/30/1964–09/29/1995
2	04046000	Black River near Garnet, MI	46.118	85.365	28	9/30/1964–9/29/1995
3	[1]04049500	Manistique River at Germfask, MI	46.233	85.928	341	9/30/1964–9/29/1966
4	[1]04055000	Manistique River at Cookson Bridge near Blaney, MI	46.086	86.06	704	9/30/1964–9/29/1966
5	04056500	Manistique River near Manistique, MI	46.031	86.161	1,100	9/30/1964–9/29/1995
6	[1]04057000	Indian River near Manistique, MI	45.991	86.288	302	9/30/1964–9/29/1989
7	04057510	Sturgeon River near Nahma Junction, MI	45.943	86.706	183	9/30/1964–9/29/1995
8	04057800	Middle Branch Escanaba River at Humboldt, MI	46.499	87.887	46	9/30/1964–9/29/1995
9	[1]04058000	Middle Branch Escanaba River near Ishpeming, MI	46.397	87.759	128	9/30/1964–9/29/1971
10	04058100	Middle Branch Escanaba River near Princeton, MI	46.317	87.502	210	9/30/1964–9/29/1995
11	04058200	Schweitzer Creek near Palmer, MI	46.411	87.624	23.6	9/30/1964–9/29/1995
12	04058500	East Branch Escanaba River at Gwinn, MI	46.282	87.435	124	9/30/1964–9/29/1976
13	04059000	Escanaba River at Cornell, MI	45.909	87.214	870	9/30/1964–9/29/1995
14	04059500	Ford River near Hyde, MI	45.755	87.202	450	9/30/1964–9/29/1995
15	04060500	Iron River at Caspian, MI	46.059	88.627	92.1	9/30/1964–9/29/1976
16	04060993	Brule River at U.S. Highway 2 near Florence, WI	45.961	88.316	366	9/30/1964–9/29/1995
17	04061000	Brule River near Florence, WI	45.959	88.266	389	9/30/1964–9/6/1990
18	04061500	Paint River at Crystal Falls, MI	46.106	88.335	597	9/30/1964–9/29/1992
19	[1]04062000	Paint River near Alpha, MI	46.011	88.258	631	9/30/1964–9/29/1995
20	04062200	Peshekee River near Champion, MI	46.557	88.003	133	9/30/1964–9/29/1974
21	[1]04062500	Michigamme River near Crystal Falls, MI	46.114	88.216	656	9/30/1964–9/29/1995
22	04063000	Menominee River near Florence, WI	45.951	88.189	1,760	9/30/1964–9/29/1995
23	04063500	Menominee River at Twin Falls near Iron Mountain, MI	45.871	88.07	1,800	9/30/1964–9/29/1995

Table 2. U.S. Geological Survey streamgages used in the Lake Michigan Basin Precipitation Runoff-Modeling System model.—Continued

[USGS, U.S. Geological Survey; latitude and longitude in decimal degrees; mi², square miles; MI, Michigan; WI, Wisconsin; IN, Indiana]

Map number (fig. 4)	USGS station number	USGS station name	Latitude (north)	Longitude (west)	Drainage area measured at gage (mi²)	Period of record used
24	04063700	Popple River near Fence, WI	45.764	88.464	139	9/30/1964–9/29/1995
25	04064500	Pine River Below Pine River Powerplant near Florence, WI	45.837	88.225	533	9/30/1964–9/29/1995
26	[1]04065106	Menominee River at Niagara, WI	45.768	87.981	2,470	9/30/1988–9/29/1995
27	04065300	West Branch Sturgeon River near Randville, MI	46.012	87.979	56.1	9/30/1964–9/29/1977
28	04065500	Sturgeon River near Foster City, MI	45.91	87.757	237	9/30/1964–9/29/1976
29	04066003	Menominee River Below Pemene Creek near Pembine, WI	45.579	87.787	3,140	9/30/1964–9/29/1995
30	[1]04066030	Menominee River at White Rapids Dam near Banat, MI	45.482	87.802	3,190	9/30/1994–9/29/1995
31	[1]04066500	Pike River at Amberg, WI	45.5	88	255	9/30/1964–11/10/1966
32	04066800	Menominee River at Koss, MI	45.387	87.702	3,700	9/30/1964–9/29/1995
33	04067000	Menominee River near Koss, MI	45.354	87.649	3,720	9/30/1964–9/29/1977
34	04067500	Menominee River near McAllister, WI	45.326	87.663	3,930	9/30/1975–9/29/1995
35	[1]04067958	Peshtigo River near Wabeno, WI	45.388	88.305	447	5/31/1994–9/29/1995
36	04069500	Peshtigo River at Peshtigo, WI	45.047	87.745	1,080	9/30/1964–9/29/1995
37	04071000	Oconto River near Gillett, WI	44.865	88.3	705	9/30/1964–9/29/1995
38	[1]04071765	Oconto River near Oconto, WI	44.861	87.984	966	9/30/1984–9/29/1995
39	04071858	Pensaukee River near Pensaukee, WI	44.819	87.954	134	9/30/1968–9/29/1992
40	04072150	Duck Creek near Howard, WI	44.536	88.13	108	4/30/1984–9/29/1995
41	[1]04073468	Green Lake Inlet at County Highway A near Green Lake, WI	43.824	88.927	53.5	1/31/1983–9/29/1995
42	[1]04073473	Puchyan River downstream North Lawson Drive near Green Lake, WI	43.857	88.947	105	10/31/1992–9/29/1995
43	04073500	Fox River at Berlin, WI	43.954	88.953	1,340	9/30/1964–9/29/1995
44	04074950	Wolf River at Langlade, WI	45.19	88.733	463	9/30/1964–9/29/1995
45	04077400	Wolf River near Shawano, WI	44.836	88.625	816	9/30/1981–9/29/1995
46	[1]04077630	Red River at Morgan Road near Morgan, WI	44.898	88.844	114	9/30/1988–9/29/1995

Table 2. U.S. Geological Survey streamgages used in the Lake Michigan Basin Precipitation Runoff-Modeling System model.—Continued

[USGS, U.S. Geological Survey; latitude and longitude in decimal degrees; mi², square miles; MI, Michigan; WI, Wisconsin; IN, Indiana]

Map number (fig. 4)	USGS station number	USGS station name	Latitude (north)	Longitude (west)	Drainage area measured at gage (mi²)	Period of record used
47	04078500	Embarrass River near Embarrass, WI	44.725	88.736	384	9/30/1964–9/29/1995
48	04079000	Wolf River at New London, WI	44.392	88.74	2,260	9/30/1964–9/29/1995
49	[1]04080000	Little Wolf River at Royalton, WI	44.412	88.865	507	9/30/1964–9/29/1981
50	[1]04081000	Waupaca River near Waupaca, WI	44.329	88.996	265	9/30/1978–9/29/1981
51	04082400	Fox River at Oshkosh, WI	44.014	88.541	5,310	9/30/1987–9/29/1995
52	04084445	Fox River at Appleton, WI	44.248	88.423	5,950	6/30/1982–9/29/1995
53	04084500	Fox River at Rapide Croche Dam near Wrightstown, WI	44.317	88.197	6,010	9/30/1964–9/29/1995
54	04085200	Kewaunee River near Kewaunee, WI	44.458	87.556	127	9/30/1964–9/29/1995
55	04085281	East Twin River at MIshicot, WI	44.238	87.636	110	7/24/1968–9/29/1992
56	04085427	Manitowoc River at Manitowoc, WI	44.107	87.715	526	7/25/1968–9/29/1995
57	04086000	Sheboygan River at Sheboygan, WI	43.742	87.754	418	9/30/1964–9/29/1995
58	04086500	Cedar Creek near Cedarburg, WI	43.323	87.979	120	9/30/1964–9/29/1995
59	04086600	Milwaukee River near Cedarburg, WI	43.28	87.943	607	10/31/1977–9/29/1995
60	04087000	Milwaukee River at Milwaukee, WI	43.1	87.909	696	9/30/1964–9/29/1995
61	04087030	Menomonee River at Menomonee Falls, WI	43.173	88.104	34.7	10/31/1970–9/29/1995
62	04087088	Underwood Creek at Wauwatosa, WI	43.055	88.046	18.2	10/31/1970–9/29/1995
63	04087120	Menomonee River at Wauwatosa, WI	43.046	88	123	9/30/1964–9/29/1995
64	04087159	Kinnickinnic River at South 11th Street at Milwaukee, WI	42.998	87.926	18.8	9/30/1978–9/29/1995
65	[1]04087170	Milwaukee River at Mouth at Milwaukee, WI	43.024	87.898	872	3/31/1990–10/30/1991
66	04087204	Oak Creek at South Milwaukee, WI	42.925	87.87	25	9/30/1964–9/29/1995
67	04087220	Root River near Franklin, WI	42.874	87.996	49.2	9/30/1964–9/29/1995
68	04087233	Root River Canal near Franklin, WI	42.816	87.995	57	9/30/1964–9/29/1995
69	04087240	Root River at Racine, WI	42.751	87.824	190	9/30/1964–9/29/1995

Table 2. U.S. Geological Survey streamgages used in the Lake Michigan Basin Precipitation Runoff-Modeling System model.—Continued

[USGS, U.S. Geological Survey; latitude and longitude in decimal degrees; mi², square miles; MI, Michigan; WI, Wisconsin; IN, Indiana]

Map number (fig. 4)	USGS station number	USGS station name	Latitude (north)	Longitude (west)	Drainage area measured at gage (mi²)	Period of record used
70	04087257	Pike River near Racine, WI	42.647	87.861	38.5	9/30/1967–9/29/1995
71	[1]04092750	Indiana Harbor Canal at East Chicago, IN	41.649	87.469	0	10/4/1987–9/29/1995
72	04093000	Deep River at Lake George Outlet at Hobart, IN	41.536	87.257	124	9/30/1964–9/29/1995
73	04094000	Little Calumet River at Porter, IN	41.622	87.087	66.2	9/30/1964–9/29/1995
74	04094500	Salt Creek near McCool, IN	41.597	87.144	74.6	9/30/1964–9/29/1987
75	[1]04095090	Burns Ditch at Portage, IN	41.622	87.176	331	9/30/1990–9/29/1995
76	04095300	Trail Creek at Michigan City, IN	41.717	86.86	54.1	5/31/1965–9/29/1990
77	04096100	Galena River near Laporte, IN	41.748	86.675	17.2	9/30/1965–9/29/1995
78	04096400	St. Joseph River near Burlington, MI	42.103	85.04	201	9/30/1964–9/29/1987
79	04096405	St. Joseph River at Burlington, MI	42.103	85.08	206	9/30/1964–9/29/1995
80	04096515	South Branch Hog Creek near Allen, MI	41.949	84.828	48.7	9/30/1965–9/29/1995
81	04096600	Coldwater River near Hodunk, MI	42.029	85.106	293	9/30/1964–9/29/1985
82	04096900	Nottawa Creek near Athens, MI	42.056	85.308	162	9/30/1964–9/29/1993
83	04097500	St. Joseph River at Three Rivers, MI	41.94	85.633	1,350	9/30/1964–9/29/1995
84	04097540	Prairie River near Nottawa, MI	41.888	85.409	106	9/30/1964–9/29/1995
85	04099000	St. Joseph River at Mottville, MI	41.801	85.756	1,866	9/30/1964–9/29/1995
86	04099510	Pigeon Creek near Angola, IN	41.634	85.11	106	9/30/1964–9/29/1995
87	04099750	Pigeon River near Scott, IN	41.749	85.576	361	9/30/1964–9/29/1995
88	04099808	Little Elkhart River at MIddlebury, IN	41.675	85.7	97.6	9/19/1975–9/29/1995
89	04099850	Pine Creek near Elkhart, IN	41.681	85.882	31	9/30/1975–9/29/1995
90	04100222	North Branch Elkhart River at Cosperville, IN	41.482	85.476	142	9/30/1967–9/29/1995
91	04100252	Forker Creek near Burr Oak, IN	41.333	85.424	19.2	5/31/1965–9/29/1995
92	04100295	Rimmell Branch near Albion, IN	41.385	85.371	10.7	11/27/1975–9/29/1995

Table 2. U.S. Geological Survey streamgages used in the Lake Michigan Basin Precipitation Runoff-Modeling System model.—Continued

[USGS, U.S. Geological Survey; latitude and longitude in decimal degrees; mi², square miles; MI, Michigan; WI, Wisconsin; IN, Indiana]

Map number (fig. 4)	USGS station number	USGS station name	Latitude (north)	Longitude (west)	Drainage area measured at gage (mi²)	Period of record used
93	04100500	Elkhart River at Goshen, IN	41.593	85.849	594	9/30/1964–9/29/1995
94	04101000	St. Joseph River at Elkhart, IN	41.692	85.975	3,370	9/30/1964–9/29/1995
95	04101500	St. Joseph River at Niles, MI	41.829	86.26	3,666	9/30/1964–9/29/1995
96	04101800	Dowagiac River at Sumnerville, MI	41.913	86.213	255	9/30/1964–9/29/1995
97	04102500	Paw Paw River at Riverside, MI	42.186	86.369	390	9/30/1964–9/29/1995
98	04102700	South Branch Black River near Bangor, MI	42.354	86.188	83.6	9/30/1964–9/29/1995
99	04103010	Kalamazoo River near Marengo, MI	42.262	84.856	267	9/30/1982–9/29/1995
100	04103500	Kalamazoo River at Marshall, MI	42.265	84.964	449	9/30/1964–3/30/1978
101	04105000	Battle Creek at Battle Creek, MI	42.331	85.154	241	09/30/1964–9/29/1995
102	04105500	Kalamazoo River near Battle Creek, MI	42.324	85.197	824	9/30/1964–9/29/1995
103	04106000	Kalamazoo River at Comstock, MI	42.286	85.514	1,010	9/30/1964–9/29/1995
104	04106500	Portage Creek at Kalamazoo, MI	42.274	85.576	46.8	5/31/1971–9/29/1982
105	04108600	Rabbit River near Hopkins, MI	42.642	85.722	71.4	9/30/1964–9/29/1995
106	04108800	Macatawa River at State Road near Zeeland, MI	42.779	86.018	65.8	9/30/1964–9/29/1995
107	04108801	Macatawa River near Zeeland, MI	42.784	86.036	68.5	9/30/1964–9/29/1995
108	04109000	Grand River at Jackson, MI	42.284	84.409	174	9/30/1964–9/29/1995
109	04111000	Grand River near Eaton Rapids, MI	42.535	84.623	661	9/30/1964–9/29/1995
110	04111379	Red Cedar River near WIlliamston, MI	42.683	84.219	163	7/9/1971–9/29/1985
111	04111500	Deer Creek near Dansville, MI	42.609	84.319	16.3	9/30/1964–9/29/1995
112	04112000	Sloan Creek near WIlliamston, MI	42.676	84.364	9.34	9/30/1964–9/29/1995
113	04112500	Red Cedar River at East Lansing, MI	42.727	84.478	355	9/30/1964–9/29/1995
114	04113000	Grand River at Lansing, MI	42.751	84.555	1,230	9/30/1964–9/29/1995
115	04114000	Grand River at Portland, MI	42.856	84.912	1,385	9/30/1964–9/29/1995

Table 2. U.S. Geological Survey streamgages used in the Lake Michigan Basin Precipitation Runoff-Modeling System model.—Continued

[USGS, U.S. Geological Survey; latitude and longitude in decimal degrees; mi², square miles; MI, Michigan; WI, Wisconsin; IN, Indiana]

Map number (fig. 4)	USGS station number	USGS station name	Latitude (north)	Longitude (west)	Drainage area measured at gage (mi²)	Period of record used
116	04114498	Looking Glass River near Eagle, MI	42.828	84.759	280	9/30/1964–9/29/1992
117	04114500	Looking Glass River at Hinman Road near Eagle, MI	42.829	84.779	281	9/30/1964–9/29/1992
118	04115000	Maple River at Maple Rapids, MI	43.11	84.693	434	9/30/1964–9/29/1995
119	04115265	Fish Creek near Crystal, MI	43.25	84.981	39.7	9/30/1983–9/29/1995
120	04116000	Grand River at Ionia, MI	42.972	85.069	2,840	9/30/1964–9/29/1995
121	04116500	Flat River at Smyrna, MI	43.053	85.265	528	9/30/1964–9/29/1982
122	04117000	Quaker Brook near Nashville, MI	42.566	85.094	7.6	9/30/1964–9/29/1995
123	04117500	Thornapple River near Hastings, MI	42.616	85.236	385	9/30/1964–9/29/1995
124	04118000	Thornapple River near Caledonia, MI	42.811	85.483	773	9/30/1964–9/29/1990
125	04118500	Rogue River near Rockford, MI	43.082	85.591	234	9/30/1964–9/29/1995
126	04119000	Grand River at Grand Rapids, MI	42.964	85.676	4,900	9/30/1964–9/29/1995
127	[1]04121000	Muskegon River near Merritt, MI	44.336	84.89	355	9/30/1964–12/30/1969
128	04121300	Clam River at Vogel Center, MI	44.201	85.053	243	9/30/1964–9/29/1995
129	04121500	Muskegon River at Evart, MI	43.899	85.255	1,433	9/30/1964–9/29/1995
130	04121900	Little Muskegon River near Morley, MI	43.503	85.343	121	9/30/1964–9/29/1992
131	[1]04121944	Little Muskegon River near Oak Grove, MI	43.431	85.596	345	9/30/1991–9/29/1995
132	[1]04121970	Muskegon River near Croton, MI	43.435	85.665	2,313	9/30/1991–9/29/1995
133	04122000	Muskegon River at Newaygo, MI	43.422	85.801	2,350	9/30/1964–9/29/1989
134	04122100	Bear Creek near Muskegon, MI	43.289	86.223	16.7	9/30/1964–09/30/1964
135	04122200	White River near Whitehall, MI	43.464	86.233	406	9/30/1964–9/29/1995
136	04122500	Pere Marquette River at Scottville, MI	43.945	86.279	681	9/30/1964–9/29/1995
137	[1]04123000	Big Sable River near Freesoil, MI	44.12	86.28	127	9/30/1964–12/30/1969
138	[1]04123500	Manistee River near Grayling, MI	44.693	84.847	123	9/30/1964–12/30/1969

Table 2. U.S. Geological Survey streamgages used in the Lake Michigan Basin Precipitation Runoff-Modeling System model.—Continued

[USGS, U.S. Geological Survey; latitude and longitude in decimal degrees; mi², square miles; MI, Michigan; WI, Wisconsin; IN, Indiana]

Map number (fig. 4)	USGS station number	USGS station name	Latitude (north)	Longitude (west)	Drainage area measured at gage (mi²)	Period of record used
139	04124000	Manistee River near Sherman, MI	44.436	85.699	857	9/30/1964–9/29/1995
140	[1]04124200	Manistee River near Mesick, MI	44.363	85.821	1,018	11/30/1992–9/29/1995
141	04124500	East Branch Pine River near Tustin, MI	44.103	85.517	60	9/30/1987–9/29/1995
142	04125460	Pine River at High School Bridge near Hoxeyville, MI	44.193	85.77	245	9/30/1964–9/29/1995
143	04125500	Pine River near Hoxeyville, MI	44.203	85.8	251	9/30/1964–9/29/1978
144	04126000	Manistee River near Manistee, MI	44.271	86.199	1,677	9/30/1964–9/29/1989
145	04126740	Platte River at Honor, MI	44.668	86.035	125	3/26/1986–9/29/1995
146	04127000	Boardman River near Mayfield, MI	44.638	85.52	182	9/30/1964–9/29/1985
147	04127800	Jordan River near East Jordan, MI	45.103	85.098	67.9	9/30/1964–9/29/1995
148	040851385	Fox River at Oil Tank Depot at Green Bay, WI	44.529	88.01	6,330	9/30/1984–9/29/1995

[1]Sites not included in calibration because of control structures or short period of record.

attenuate precipitation events. Depression storage parameters for the Lake Michigan Basin PRMS model were developed using the ArcGIS Desktop GIS software program (Environmental Systems Research Institute, Inc., 2004) according to the methods and techniques described by Viger and others (2010). The NHD data layers of water bodies and flow lines were used in the development of the depression storage parameters using GIS analyses (Horizon Systems Corporation, 2006). ArcGIS was used to determine the percent of the HRU pervious land surface that flows into the depression storage features. Surface depressions that are entirely beyond 984 feet from the stream network were determined to be the most hydrologically realistic for the Lake Michigan Basin PRMS model. The results of the GIS analyses were then used to populate the depression storage parameters in the Lake Michigan PRMS model. The parameters in table 3 were derived from GIS analyses.

Surface-Water Model Calibration

The model was calibrated using the universal parameter estimation and uncertainty analysis computer code PEST (Doherty, 2010a, 2010b). PEST uses automated adjustment of PRMS input parameters (for example, maximum contributing area, slow interflow coefficient) and evaluation of model outputs (for example, streamflow) to obtain a quantitative best fit between simulated model outputs and observed data. Simulated outputs of streamflow, solar radiation, and potential evapotranspiration were compared to current measurements during the calibration process. Parameter estimation continued until a best fit between simulated and observed targets was attained and the optimal model input parameters were deemed reasonable. The calibration approach used here differs from traditional nonlinear regression parameter estimation in two primary areas, specifically by the use of (1) soft-knowledge constraints on parameters (Tikhonov regularization; Tikhonov, 1963a, 1963b; Doherty, 2003), and (2) reducing the parameter space to an unconditionally stable subspace using singular value decomposition (Tonkin and Doherty, 2005; Hunt and others, 2007; Doherty and Hunt, 2010). Additional information regarding the overview of the advantages of using these more sophisticated tools for parameter estimation is discussed by Hunt and others (2007). The tools were applied using the guidelines given by Doherty and Hunt (2010). The specific parameter estimation tools used to calibrate the PRMS model are briefly summarized in the following sections.

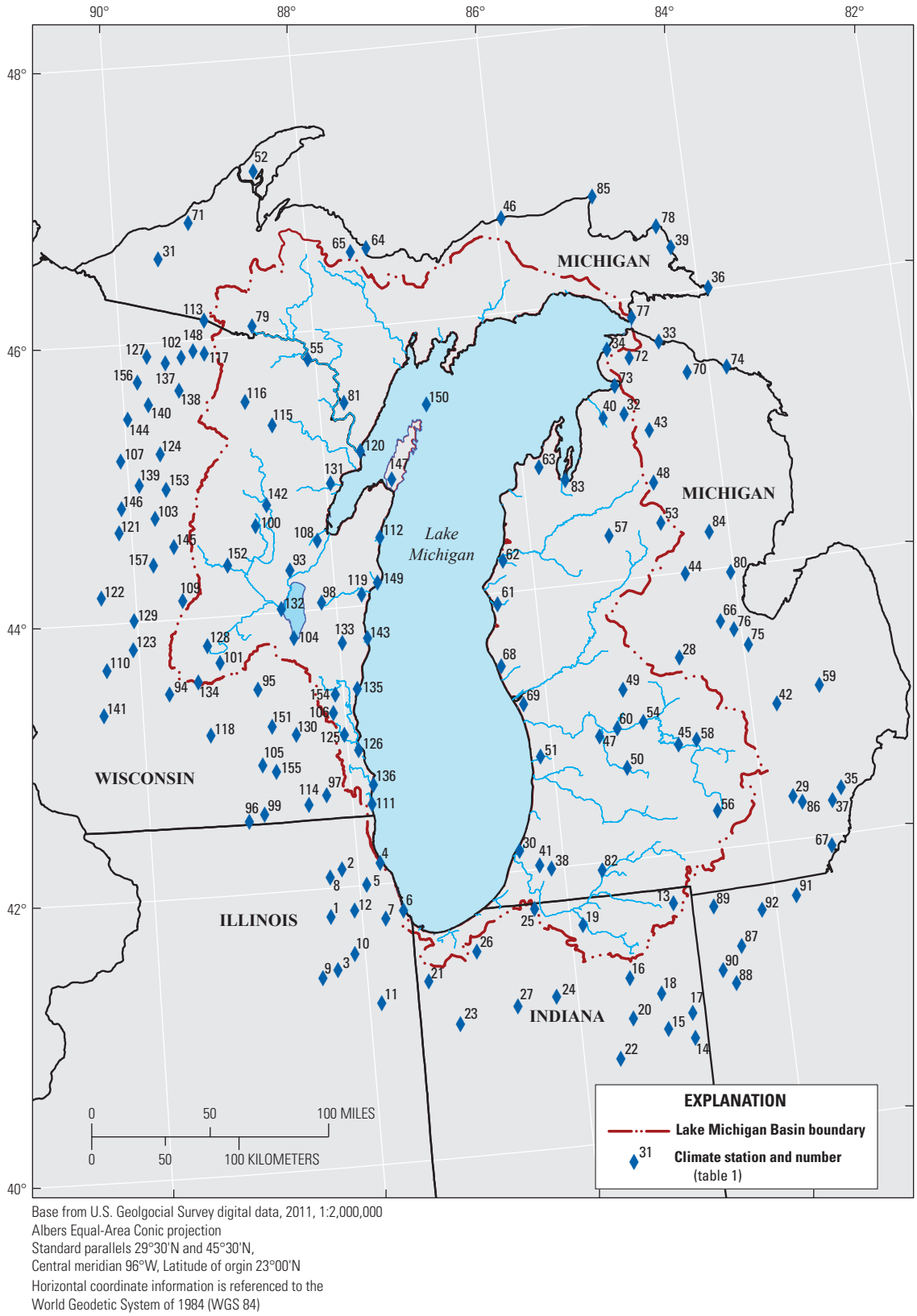

Base from U.S. Geolgocial Survey digital data, 2011, 1:2,000,000
Albers Equal-Area Conic projection
Standard parallels 29°30'N and 45°30'N,
Central meridian 96°W, Latitude of orgin 23°00'N
Horizontal coordinate information is referenced to the
World Geodetic System of 1984 (WGS 84)

Figure 3. National Oceanic and Atmospheric Administration's National Weather Service Cooperative Observer Program meteorological stations used in the Lake Michigan Basin Precipitation Runoff-Modeling System model. Station numbers are cross-referenced in table 1.

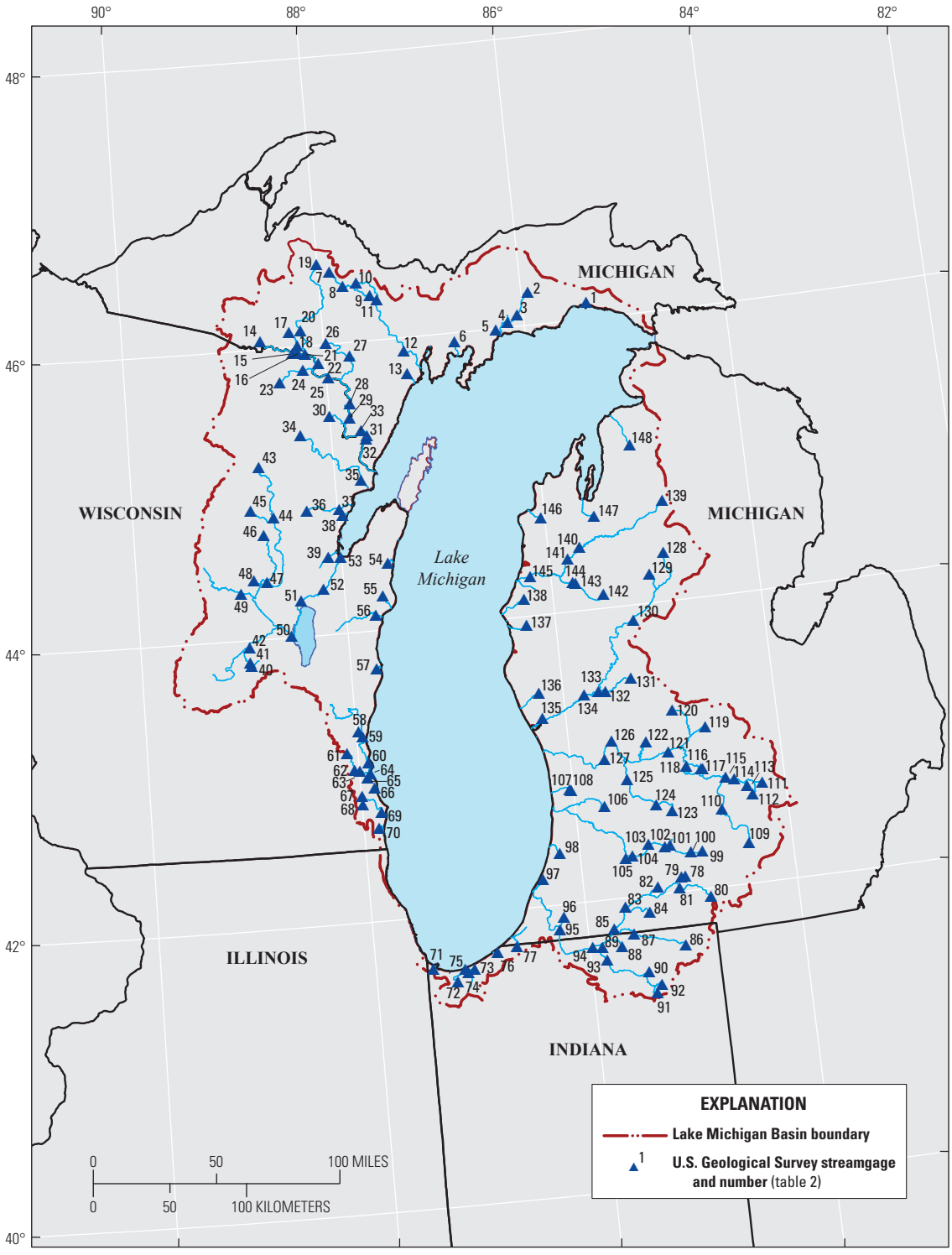

Base from U.S. Geolgocial Survey digital data, 2011, 1:2,000,000
Albers Equal-Area Conic projection
Standard parallels 29°30'N and 45°30'N,
Central meridian 96°W, Latitude of orgin 23°00'N
Horizontal coordinate information is referenced to the
World Geodetic System of 1984 (WGS 84)

Figure 4. U.S. Geological Survey streamgages used in the Lake Michigan Basin Precipitation Runoff-Modeling System model. Streamgage numbers are cross-referenced in table 2.

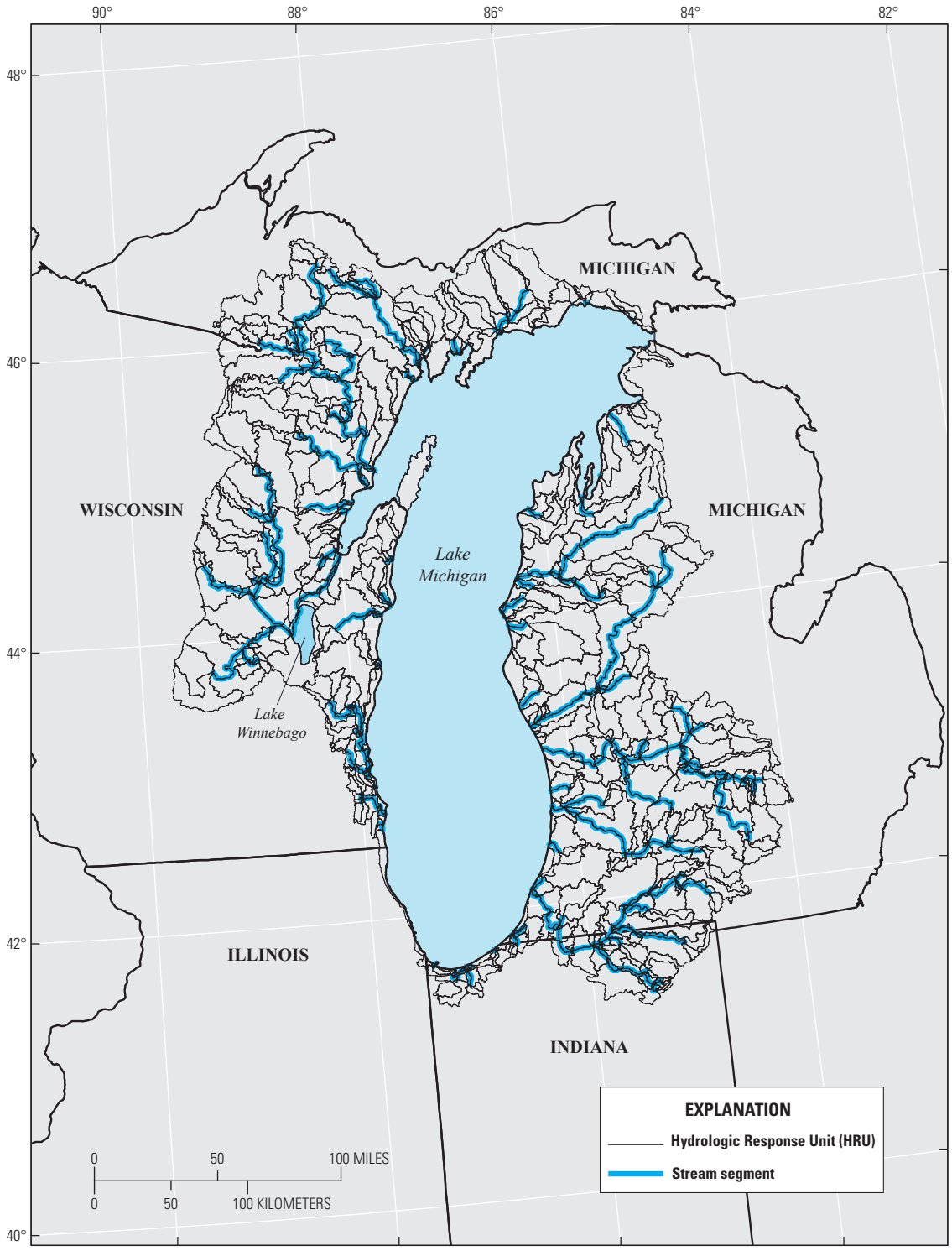

Base from U.S. Geolgocial Survey digital data, 2011, 1:2,000,000
Albers Equal-Area Conic projection
Standard parallels 29°30'N and 45°30'N,
Central meridian 96°W, Latitude of orgin 23°00'N
Horizontal coordinate information is referenced to the
World Geodetic System of 1984 (WGS 84)

Figure 5. Hydrologic response units and stream segments for the Lake Michigan Basin Precipitation-Runoff Modeling System model.

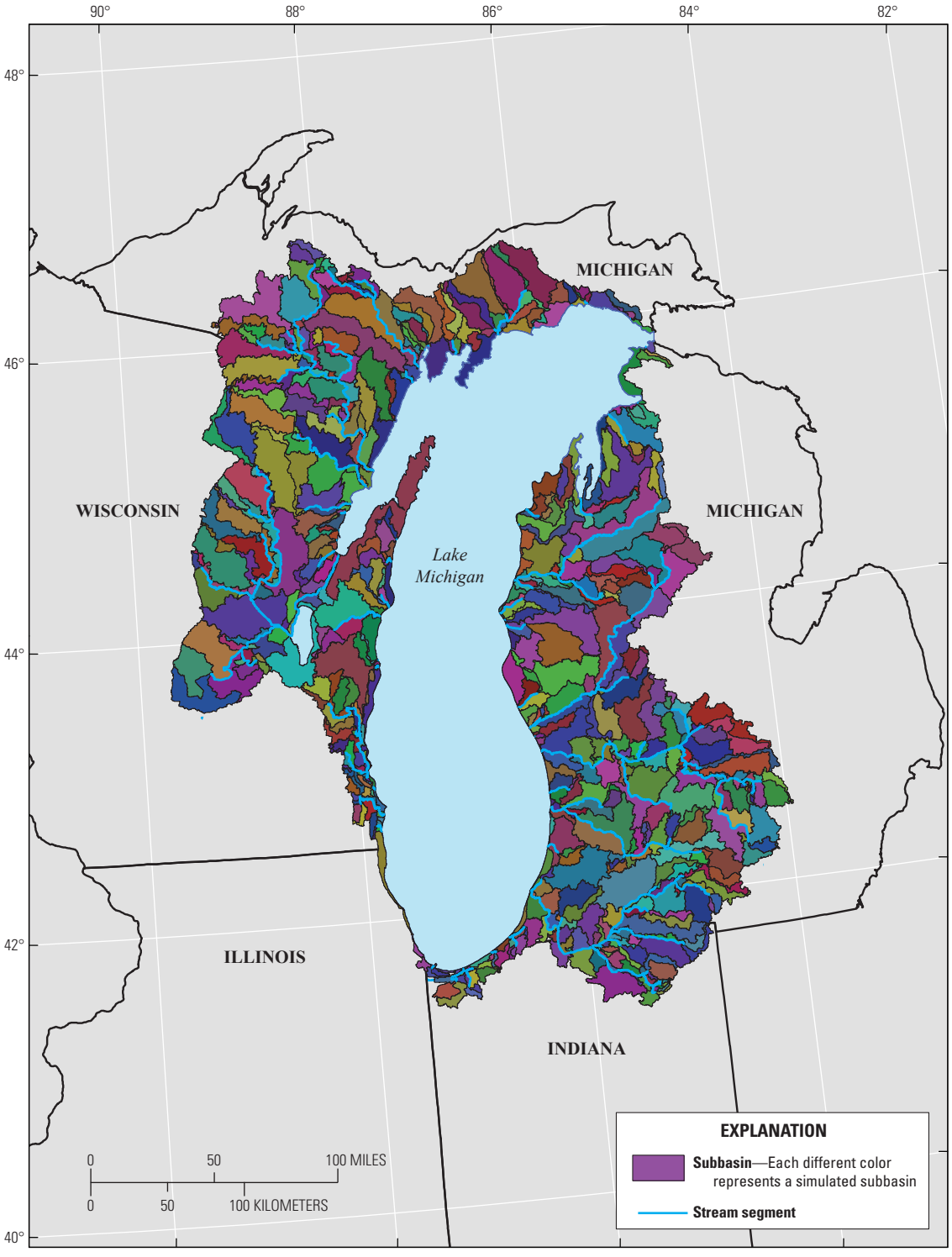

Base from U.S. Geolgocial Survey digital data, 2011, 1:2,000,000
Albers Equal-Area Conic projection
Standard parallels 29°30'N and 45°30'N,
Central meridian 96°W, Latitude of orgin 23°00'N
Horizontal coordinate information is referenced to the
World Geodetic System of 1984 (WGS 84)

Figure 6. Two hundred forty-five subbasins delineated for the Lake Michigan Basin Precipitation-Runoff Modeling System model.

Table 3. Depression storage parameters derived from geographic information systems analyses.

[nhru, number of hydrologic response units; HRU, hydrologic response unit]

Parameter	Dimension	Description	Units	Default value (range)
dprst_area	nhru	Aggregate sum of surface depression areas of each HRU	Acres	0 (0–1,000,000,000)
dprst_frac_open	nhru	Fraction of open surface depression storage area within an HRU that can generate surface runoff as a function of storage volume	Decimal percent	0 (0–1)
sro_to_dprst	nhru	Fraction of pervious and impervious surface runoff that flows into surface depression storage	Decimal percent	0.2 (0–1)

Soft-Knowledge Constraints Through Tikhonov Regularization

The reasonableness of optimal parameters is as important a consideration as the model's fit of simulated to observed values, where reasonableness is based on expert knowledge of basin characteristics and behavior. Tikhonov regularization provides a vehicle for incorporation of this soft knowledge into the calibration process, which allows the adherence to the soft knowledge to be formally balanced against the simulated to observed best fit (Tikhonov, 1963a, 1963b). Moreover, the addition of soft knowledge can provide a means for achievement of a unique solution to the inverse problem of model calibration, an issue well recognized in surface-water modeling (Beven, 1993). Understanding of a site can enter into the calibration process through definition of a preferred system condition (for example, preferred value such as the hydraulic conductivity should have a value around 3.2808 ft/d, or preferred difference such as the hydraulic conductivity should be uniform in this area). Parameter estimation stability is achieved by supplementing the calibration observed dataset with a suite of "pseudo observations" each of these pertaining to one or more parameters used by the model. Collectively, these provide a default position for parameters, or for relations between parameters, in the event that little or no information resides in the observations of the calibration dataset. When the information content of a calibration dataset is insufficient for unique estimation of certain parameters, or combinations of parameters, the fallback position prevails.

Apart from providing a fallback or default condition for parameters, and for relations between them, Tikhonov regularization also provides constraints on the manner in which heterogeneity that is supported by the calibration dataset emerges in the estimated parameter field. If properly formulated, Tikhonov constraints can promulgate the introduction of realistic departures from background parameter fields, in contrast to ad-hoc departures from those fields which may provide a good fit with the calibration dataset, but erode the credibility of the estimated parameter field. In fact, part of the "art" of formulating appropriate Tikhonov constraints for a particular parameter estimation problem is to achieve this end.

Reducing the Parameter Space Using Singular Value Decomposition

In contrast to Tikhonov regularization, which adds information that expresses professional expertise to the calibration process to promote unique estimability of parameters, subspace methods subtract from the calibration process the need to estimate either individual parameters, or combinations of correlated parameters, that are inestimable on the basis of the current calibration dataset. These combinations are determined through initiating singular value decomposition (SVD) of the weighted Jacobian matrix (Moore and Doherty, 2005; Tonkin and Doherty, 2005; Doherty and Hunt, 2010). The Jacobian matrix encapsulates the sensitivities of model outputs corresponding to field measurements to all adjustable model parameters; each column of the Jacobian matrix contains the sensitivity of all model outputs for which there are corresponding field measurements to a single adjustable parameter. Individual parameters, or combinations of parameters, that are deemed to be estimable (comprising the so-called "calibration solution space") are then estimated on the basis of the calibration dataset. Those parameters, and parameter combinations, that are deemed to be inestimable (comprising the so-called "calibration null space") are not adjusted during calibration but rather retain their initial values.

Time-Series Processing Approach

In addition to issues of parameter insensitivity and correlation inherent to highly parameterized models, surface-water models like PRMS can be affected by issues with measurement noise and redundant information in the time-series observations used to calibrate the model. Surface-water datasets, such as those used to calibrate the Lake Michigan Basin PRMS model, commonly include many observations with high temporal density across a spatially distributed monitoring network. Each data point does not convey equal insight into the hydrologic system; however, data collected at the same location on different days can carry redundant insight into the system. Without time series processing, each observation contributes to measurement noise that affects the extraction of information from the observed data to the calibration,

regardless of insight provided. To enhance the signal-to-noise ratio within the observation data, a time-series processing approach was used in addition to simply comparing every raw observed value to the simulated equivalent. That is, the raw observations were processed and distilled into characteristic aspects of the system important for calibration such as base flow, peak flow, and so forth (Walker and others, 2009). The simulated PRMS output was then processed in the same way as the raw observations and directly compared during the parameter estimation process. The processing was completed using TSPROC (Westenbroek and others, 2012). The following calibration targets were computed:

1. Mean monthly solar radiation—Daily solar radiation averaged for each month across all years in the simulation period was used to capture the seasonal variation of solar radiation.

2. Mean monthly potential evapotranspiration—Daily potential evapotranspiration averaged for each month across all years in the simulation period was used to capture the seasonal variation of potential evapotranspiration.

3. Mean monthly streamflow—mean streamflow for each month averaged across all years in the simulation period and represents the seasonal variation of streamflow.

4. Annual mean streamflow—average streamflow for each year during the simulation period and represents the streamflow part of the annual hydrologic budget.

5. Monthly mean streamflow—average streamflow for each month during the simulation and represents the total volume of streamflow for each month.

6. Monthly maximum streamflow—maximum streamflow for each month during the simulation and represents the largest daily streamflow for each month.

7. Monthly base flow—average base flow for each month during the simulation and represents the groundwater contribution to streamflow.

8. Hydrograph peaks—Selected hydrographs corresponding to peaks above a minimum value were used to represent daily streamflow dynamics. The minimum value for each gage was selected to give a reasonable (3–12) number of peaks per year based on graphical inspection of the hydrograph.

Approach, Parameters, and Observations Used in Parameter Estimation

Issues with surface-water calibration are well documented (for example, Beven, 1993). One fundamental issue is that only a handful of the many parameters that may be used by a hydrologic model are actually estimable on the basis of most calibration datasets (for example, Beven and Binley, 1992; Jakeman and Hornberger, 1993; Beven and Freer, 2001; Doherty and Hunt, 2010). Although many processes can be included in a model code, the ability to constrain the parameters needed to use the additional functionality is not commensurate. For this application, a "stepwise" calibration approach was used for the period October 1, 1969 to September 30, 1999. The PEST software was used to perform multiple optimization steps, with a different set of parameters and objective function for each step in the process (table 4.). Such an approach is outlined by Hay and others (2006). As pointed out by Hunt and Doherty (2006), basin models can be improved by calibrating to a variety of data types. Thus, parameters estimated and observations used for calibration depended on the calibration step, and those parameters not estimated in a particular calibration step were fixed. Parameters estimated for the four calibration steps are described below and listed in table 5.

Table 4. Hydrologic processes associated with the individual steps of the stepwise calibration procedure.

Step	Hydrologic processes	Number of parameters	Number of observation groups
1	Solar radiation, potential evapotranspiration	183	2
2	Annual water balance	144	1
3	Runoff, infiltration, depression storage, groundwater flow	4,696	4
4	Streamflow routing	934	1

In general, an estimate of uncertainty in the observations was used for the weights for each observation group. The weight was assigned to be the reciprocal of the uncertainty for each group (σ_g), thus

$$w_g = \frac{1}{\sigma_g} \quad (1)$$

where:

w_g is the weight for a particular observation group, and

σ_g is the standard deviation of the uncertainty for the observations.

The uncertainties were estimated using the coefficient of variation (standard deviation divided by the mean) and an average value for each observation group, thus the weight is estimated as

$$w_g = \frac{1}{\mu_g CV_g} \quad (2)$$

Table 5. Calibrated parameters and calibration steps modified from Hay and others (2006).

[Dimensions: nmonth, number of months equals 12; °F, degrees Fahrenheit; HRU, hydrologic response unit; nhru, number of hydrologic response units equals 766; x; times; nsub, number of subbasins equals 245; °C, degrees Celsius; nsegment, number of stream segments equals 466]

Name	Description	Calibration step	Dimension	Units	Default value (range)
	ccsolrad_hru_prms module				
ccov_intcp	Intercept in temperature cloud cover relationship	1	nmonth	unitless	1.83 (0–5)
ccov_slope	Slope in temperature cloud cover relationship	1	nmonth	unitless	-0.13 (-0.5–-0.01)
crad_coef	Coefficient in cloud cover/solar radiation relationship	1	one	unitless	0.4 (0.1–0.7)
crad_exp	Exponent in cloud cover/solar radiation relationship	1	one	unitless	0.61 (0.2–0.8)
	potet_jh_prms module				
jh_coef	Monthly air temperature coefficient–Jensen-Haise	1	nmonth	°F	0.014 (0.005–0.06)
jh_coef_hru	HRU air temperature coefficient–Jensen-Haise	1	nhru	°F	13 (5–20)
	climate_hru_prms module				
rain_sub_adj	Rain adjustment factor for each subbasin and each month	2	nmonths x nsub	decimal fraction	1 (0–3)
snow_sub_adj	Snow adjustment factor for each subbasin and each month	2	nmonths x nsub	decimal fraction	1 (0–3)
	gwflow_casc_prms module				
gwflow_coef	Groundwater routing coefficient	3	nhru	1/day	0.015 (0–1)
gwsink_coef	Groundwater sink coefficient	3	nhru	1/day	0 (0–1)
gwstor_min	Minimum storage in each groundwater reservoir	3	nhru	inches	0 (0–5)
	climate_hru_prms module				
adjmix_rain	Adjustment factor for rain in a rain/snow mix	3	nmonth	decimal fraction	1 (0–3)
tmax_allrain	Precip all rain if HRU maximum temperature above this value	3	nmonth	temperature units	40 (0–90)
tmax_allsnow	Precip all snow if HRU maximum temperature below this value	3	one	temperature units	32 (-10–-40)
	intcp_prms module				
potet_sublim	Proportion of potential evapotranspiration that is sublimated from snow surface	3	one	decimal fraction	0.5 (0.1–0.75)
	snowcomp_prms module				
cecn_coef	Convection condensation energy coefficient	3	nmonth	calories per °C above 0	5 (0–20)
emis_noppt	Emissivity of air on days without precipitation	3	one	decimal fraction	0.757 (0.757–1)
freeh2o_cap	Free-water holding capacity of snowpack	3	one	decimal fraction	0.05 (0.01–0.2)

Table 5. Calibrated parameters and calibration steps modified from Hay and others (2006).–Continued

[Dimensions: nmonth, number of months equals 12; °F, degrees Fahrenheit; HRU, hydrologic response unit; nhru, number of hydrologic response units equals 766; x; times; nsub, number of subbasins equals 245; °C, degrees Celsius; nsegment, number of stream segments equals 466]

Name	Description	Calibration step	Dimension	Units	Default value (range)
	soilzone_prms module				
fastcoef_lin	Linear preferential-flow routing coefficient	3	nhru	1/day	0.1 (0–1)
fastcoef_sq	Nonlinear preferential-flow routing coefficient	3	nhru	unitless	0.8 (0–1)
pref_flow_den	Preferential-flow pore density	3	nhru	decimal fraction	0 (0 -1)
slowcoef_lin	Linear gravity-flow reservoir routing coefficient	3	nhru	1/day	0.015 (0–1)
slowcoef_sq	Nonlinear gravity-flow reservoir routing coefficient	3	nhru	unitless	0.1 (0–1)
soil_rechr_max	Maximum value for soil recharge zone	3	nhru	inches	2 (0.001–10)
soil2gw_max	Maximum value for soil water excess to groundwater	3	nhru	inches	0 (0–5)
ssr2gw_rate	Coefficient to route water from subsurface to groundwater	3	nhru	1/day	0.1 (0–1)
soil_moist_max	Maximum value of water for soil zone	3	nhru	inches	6 (0.001–20)
	srunoff_smidx_prms module				
carea_max	Maximum contributing area	3	nhru	decimal fraction	0.6 (0–1)
smidx_coef	Coefficient in contributing area computations	3	nhru	decimal fraction	0.01 (0.0001–1)
smidx_exp	Exponent in contributing area computations	3	nhru	1/inch	0.3 (0.2–0.8)
	musroute_prms module				
K_coef	Storage coefficient	4	nsegment	hours	0 (0–240)
x_coef	Routing weighting factor	4	nsegment	hours	0.2 (0–0.5)

where:

CV_g is the coefficient of variation for the observation group, and

μ_g is the average value for the observation group.

For a log-transformed normally distributed variable, the standard deviation in log space was determined by rearranging the equations relating log-space (y) moments to real-space (x) (Miller and Freund, 1977):

$$\sigma_y = \sqrt{\log(1 + CV_x^{\,2})} \quad (3)$$

where:

σ_y is the standard deviation of the log-space observations, and

CV_x is the coefficient of variation of the real-space observations.

Because the groups contained observations at different time scales, there was a considerable difference in the number of observations within each group and from station to station. To compensate for the number of observations, the weights were adjusted to represent an equivalent number of annual observations for step 1 (solar radiation and potential evapotranspiration) and monthly observations for step 3 (runoff, infiltration, depression storage, groundwater flow). This reasoning follows from the basic identity that the standard

deviation of the mean from a random sample of size n is given by

$$\sigma_m = \frac{\sigma_g}{\sqrt{n}} \quad (4)$$

where:

σ_m is the standard deviation of the mean of the observations,

σ_g is the standard deviation for the observation group, and

n is the sample size.

Because the weights are equal to the inverse of the standard deviation, the weight for a mean statistic becomes

$$W_m = \frac{1}{\sigma_m} = \frac{\sqrt{n}}{\sigma_g} = W_g\sqrt{n} \quad (5)$$

where:

W_m is the resulting weight for the mean of the observation group, and

W_g is the base weight for the observation group (from equation 2).

The coefficients of variation for each observation group along with the observation size multiplier (n in eq. 5) for steps 1 and 3 are given in table 6.

Step 1—Solar Radiation and Potential Evapotranspiration

The first step involved the estimation of several parameters controlling incoming solar radiation and potential evapotranspiration. Solar radiation is a main driver for hydrologic processes simulated in the PRMS model (for example, snowmelt, evapotranspiration). If the model is able to simulate the incoming solar radiation correctly, parameters specific to other processes will be more constrained and are more apt to have representative values after calibration. Simulation of solar radiation, as done here, allows the amount of solar radiation to differ from current or historical conditions using physics of the system, whereas specification of solar radiation precludes simulation of future climate solar radiation. The measurements used for this observation group consisted of mean monthly solar radiation and potential evapotranspiration computed across all years for each month.

Mean monthly solar radiation observations were obtained from a dataset developed for the United States by Hay and others (2006). The dataset consists of mean monthly values estimated at a network of climate-station sites using multiple regression analysis (National Oceanic and Atmospheric Administration Cooperative Observer Program, 2014). The mean monthly values of solar radiation for the site closest to the centroid of Lake Michigan Basin were used as the solar radiation calibration target. Similar to solar radiation, representative simulations of potential evapotranspiration, an important sink of water, constrains associated simulation of infiltration, runoff, and groundwater flow processes. Observations of potential evapotranspiration (PET) estimates were obtained from mean monthly PET maps derived from the free-water evaporation atlas of Farnsworth and others (1982). The mean monthly values were averaged over Lake Michigan to develop the PET calibration target. Because the model is relatively insensitive to the spatial component of the Jenson-Haise relation (jh_coef_hru; Markstrom and others, 2008), an average PET target was used.

Parameters allowed to vary in this step included four parameters from the cloud cover module (ccsolrad_hru_prms; Markstrom and others, 2008) and two parameters from the potential evapotranspiration module (potet_jh_hru_prms module; Markstrom and others, 2008). Three of the parameters (ccov_intcp, ccov_slope, and jh_coef; Markstrom and others, 2008) were allowed to vary by month, one parameter (jh_coef_hru) was allowed to vary by HRU, and two of the parameters (crad_coef, crad_exp; Markstrom and others, 2008) were estimated as mean values. The most sensitive and identifiable parameters were the cloud-cover slope, intercept terms, and the monthly Jenson-Haise coefficients. Most of the remaining terms remained close to their pre-calibration starting values.

Table 6. Uncertainties (coefficient of variation) and weights (observation size multiplier) assigned to the observation groups for steps 1 and 3.

Observation group	Coefficient of variation	Observation size multiplier
Mean monthly solar radiation	0.05	12
Mean monthly potential evapotranspiration	0.1	12
Annual flow	0.1	12
Monthly mean flow	0.1	1
Monthly maximum flow	0.1	1
Monthly mean base flow	0.1	1

Step 2—Annual Water Budget

The second step (table 4 and 5) in the parameter estimation process involved calibration of two sets of parameters that control incoming precipitation. Calibrating to the annual water budget ensures that the distribution of monthly water budgets sum to a representative annual value. The objective function for this calibration step consisted of metrics associated with annual mean streamflow at each of the streamgages used for calibration.

Step two (as well as subsequent steps 3 and 4; table 4 and 5) relies on the processing of daily streamflow data for the parameter estimation objective function. The USGS streamflow data for the 1970–2010 water years (October 1, 1969–September 30, 2010) were processed for a selected set of stations across the United States with records that have been minimally affected by human activities as defined by Wolock (2003). The remaining USGS streamgages in the study area were examined, and additional sites were selected

for inclusion as calibration datasets, with a priority given to those stations having ancillary USGS data such as water-quality data. This process resulted in a set of 148 streamgages used for calibration. For this step of the calibration, temperature and precipitation were distributed to the individual HRUs using a new module (climate_hru_prms; LaFontaine and others, 2013). This module reads values from additional data files for three variables (maximum temperature, minimum temperature, and precipitation) for each HRU. The climate input to the module was generated by running the inverse-distance-elevation module in PRMS (ide_dist; Hunt and others, 2013) for 157 climate stations in the basin, and writing an output data file with daily values computed for each HRU. A Fortran program was used to convert the output data file to the three input files needed by the climate_hru_prms module. Parameters allowed to vary in step 2 of the calibration included two sets of parameters that adjust the rain and snow falling on each HRU using a coefficient that varies by HRU and month. Because an initial spatial distribution of these parameters was not well characterized using available data, the spatial variability was represented by the six regions used for the groundwater model of the Lake Michigan Basin developed by Feinstein and others (2010; fig. 7.). Dividing the Lake Michigan Basin into six regions facilitated in the calibration of the model and the discussion of results.

Step 3—Runoff, Infiltration and Groundwater Flow

The third step (table 4 and 5) in the parameter estimation process involved changes to a group of parameters that control runoff, infiltration into the soil zone, and the rate and volume of flow from the groundwater system to surface water. Observations used to calibrate these processes consisted of annual mean streamflow, monthly mean streamflow, monthly maximum streamflow, and monthly mean base flow. For the parameters that varied by HRU, the initial spatial distribution of parameters was modified by estimating a mean value for each of the 245 subbasins as shown in figure 6, and then distributing the post-calibration mean back to the HRUs, which resulted in 4,696 parameters being estimated in this step.

Step 4—Streamflow Routing

The fourth step (table 4 and 5) of the parameter estimation process involved parameters that control streamflow routing throughout the stream network. Observations used to constrain the associated parameters consisted of hydrographs corresponding to peaks above a specified minimum discharge. Parameters allowed to vary in this step included the Muskingum K- and x-coefficients (musroute_prms; *http://wwwbrr.cr.usgs.gov/projects/SW_MoWS/PRMS.html*). Initial results determined that the rain and snow adjusted HRU parameters imparted undesirable artifacts to results spatially distributed across HRUs; therefore, the calibration fourth step was completed again after the rain and snow adjusted parameters were reset to 1.0 (= no change to climate-derived data).

Calibration Results

Overall, the Lake Michigan Basin PRMS model constructed for this investigation is a reasonable predictor of streamflow throughout the Lake Michigan Basin study area (table 7, appendix 1). The Lake Michigan Basin PRMS model results were evaluated using four metrics: annual mean streamflow, monthly mean streamflow, mean monthly streamflows (for example, mean of January streamflows for all years), and monthly mean base flow. The utility of these metrics for calibration are shown by using two example subbasin areas within the Lake Michigan Basin (figs. 8 and 9, appendix 1). The graphs show that simulated streamflow values follow the observed streamflow values relatively well. Similar plots of simulated and observed values for 127 of 148 USGS streamgages that were used in model calibration are shown in appendix 1. Of these 148 streamgages, 21 sites (noted in table 2) were dropped from the model calibration because there were control structures affecting observed streamflow observations, or the period of record was appreciably shorter than the calibration time period.

The Nash-Sutcliffe efficiency (NSE) statistic (Moriasi and others, 2007; Nash and Sutcliffe, 1970; eq. 1) was used to determine model performance for selected outputs. The NSE is a normalized statistic that provides a measure of how well simulated values match observed datasets. The NSE is defined as

$$\mathrm{NSE} = \left[1 - \frac{\sum_{i=1}^{n} \left(Q_{obs,i} - Q_{sim,i} \right)^2}{\sum_{i=1}^{n} \left(Q_{obs,i} - \bar{Q}_{obs} \right)^2} \right], \qquad (6)$$

where:

$Q_{obs,i}$ is the ith observed streamflow value,

$Q_{sim,i}$ is the ith simulated streamflow value,

$\bar{Q}_{obs}$ is the mean of the observed streamflow values, and

n is the total number of measured observations.

The NSE values range from -∞ to 1. Values of zero or less indicate that the mean observed streamflow is a better predictor than the simulated streamflow. A value of zero indicates the simulated streamflow is as good as using the average value of all the observed data, and a value of 1 indicates a perfect fit between observed and simulated values. Moriasi and others (2007) suggest that an NSE of greater than 0.50 is satisfactory in basin models such as PRMS.

The NSE values for the Lake Michigan Basin PRMS model were computed for monthly mean streamflows and monthly mean base flow and are shown in table 7. The NSE values are above 0.50 for 85 percent of the calibration locations for monthly mean observations and 60 percent of the calibration locations for the monthly mean base flow observations. The higher NSE value for monthly mean streamflows across the Lake Michigan Basin reflects the greater importance these observations were given during the calibration

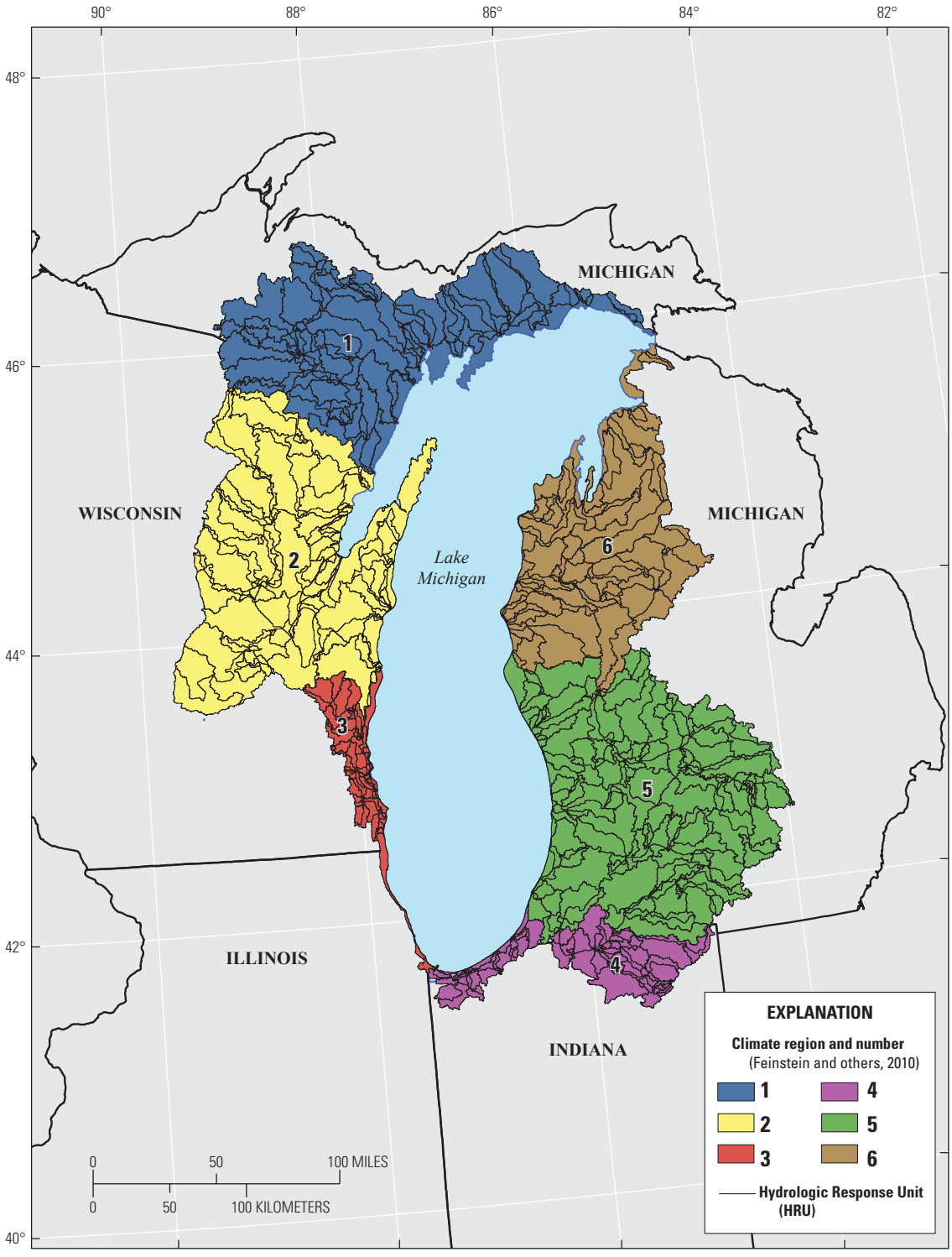

Figure 7. Lake Michigan Basin climate regions used for rain and snow characterization during model calibration. Climate regions are based on classification in Feinstein and others (2010).

Table 7. Nash-Sutcliffe efficiency (NSE) values for calibration streamgages in the Lake Michigan Basin Precipitation-Runoff Modeling System model.

[USGS, U.S. Geological Survey; MI, Michigan; WI, Wisconsin; IN, Indiana]

USGS station number	USGS station name	Monthly mean	Monthly mean base flow
04046000	Black River near Garnet, MI	0.62	0.64
04056500	Manistique River near Manistique, MI	0.83	0.53
04057510	Sturgeon River near Nahma Junction, MI	0.69	0.47
04057800	Middle Branch Escanaba River at Humboldt, MI	0.79	0.68
04058100	Middle Branch Escanaba River near Princeton, MI	0.86	0.70
04058200	Schweitzer Creek near Palmer, MI	0.68	0.54
04058500	East Branch Escanaba River at Gwinn, MI	0.90	0.39
04059000	Escanaba River at Cornell, MI	0.89	0.61
04059500	Ford River near Hyde, MI	0.85	0.26
04060500	Iron River at Caspian, MI	0.62	0.56
04060993	Brule River at US Highway 2 near Florence, WI	0.88	0.64
04061000	Brule River near Florence, WI	0.34	0.22
04061500	Paint River at Crystal Falls, MI	0.25	-0.34
04062200	Peshekee River near Champion, MI	0.83	0.73
04063000	Menominee River near Florence, WI	0.57	0.02
04063500	Menominee River at Twin Falls near Iron Mountain, MI	0.58	0.01
04063700	Popple River near Fence, WI	0.73	0.47
04064500	Pine River Below Pine River Powerplant near Florence, WI	0.91	0.75
04065300	West Branch Sturgeon River near Randville, MI	0.78	0.78
04065500	Sturgeon River near Foster City, MI	0.88	0.60
04066003	Menominee River below Pemene Creek near Pembine, WI	0.83	0.54
04066800	Menominee River at Koss, MI	0.88	0.64
04067000	Menominee River near Koss, MI	0.90	0.66
04067500	Menominee River near McAllister, WI	0.81	0.49
04069500	Peshtigo River at Peshtigo, WI	0.83	0.68
04071000	Oconto River near Gillett, WI	0.68	0.61
04071858	Pensaukee River near Pensaukee, WI	0.76	0.46
04072150	Duck Creek near Howard, WI	0.71	0.66
04073468	Green Lake Inlet at County Highway A near Green Lake, WI	0.70	0.40
04073500	Fox River at Berlin, WI	0.69	0.47
04074950	Wolf River at Langlade, WI	0.71	0.41
04077400	Wolf River near Shawano, WI	0.71	0.35
04078500	Embarrass River near Embarrass, WI	0.64	0.38
04079000	Wolf River at New London, WI	0.72	0.51
04082400	Fox River at Oshkosh, WI	0.80	-0.12
04084445	Fox River at Appleton, WI	0.70	0.41
04084500	Fox River at Rapide Croche Dam near Wrightstown, WI	0.65	0.47
04085200	Kewaunee River near Kewaunee, WI	0.51	0.50
04085281	East Twin River at Mishicot, WI	0.73	0.68
04085427	Manitowoc River at Manitowoc, WI	0.85	0.79
04086000	Sheboygan River at Sheboygan, WI	0.64	0.58
04086500	Cedar Creek near Cedarburg, WI	0.74	0.67

Table 7. Nash-Sutcliffe efficiency (NSE) values for calibration streamgages in the Lake Michigan Basin Precipitation-Runoff Modeling System model.—Continued

[USGS, U.S. Geological Survey; MI, Michigan; WI, Wisconsin; IN, Indiana]

USGS station mumber	USGS station name	Monthly mean	Monthly mean base flow
04086600	Milwaukee River near Cedarburg, WI	0.83	0.74
04087000	Milwaukee River at Milwaukee, WI	0.83	0.75
04087030	Menomonee River at Menomonee Falls, WI	0.72	0.59
04087088	Underwood Creek at Wauwatosa, WI	0.59	0.53
04087120	Menomonee River at Wauwatosa, WI	0.77	0.74
04087159	Kinnickinnic River at South 11th Street at Milwaukee, WI	0.62	-0.10
04087204	Oak Creek at South Milwaukee, WI	0.47	0.13
04087220	Root River near Franklin, WI	0.70	0.62
04087233	Root River Canal near Franklin, WI	0.74	0.65
04087240	Root River at Racine, WI	0.77	0.66
04087257	Pike River near Racine, WI	0.68	0.37
04093000	Deep River at Lake George Outlet at Hobart, IN	0.66	0.65
04094000	Little Calumet River at Porter, IN	0.35	0.12
04094500	Salt Creek near McCool, IN	0.66	0.55
04095300	Trail Creek at Michigan City, IN	0.59	0.41
04096100	Galena River near Laporte, IN	0.53	0.38
04096400	St. Joseph River near Burlington, MI	0.58	0.58
04096405	St. Joseph River at Burlington, MI	0.56	0.49
04096515	South Branch Hog Creek near Allen, MI	0.44	0.42
04096600	Coldwater River near Hodunk, MI	0.54	0.47
04096900	Nottawa Creek near Athens, MI	0.57	0.51
04097500	St. Joseph River at Three Rivers, MI	0.72	0.67
04097540	Prairie River near Nottawa, MI	0.63	0.61
04099000	St. Joseph River at Mottville, MI	0.72	0.62
04099510	Pigeon Creek near Angola, IN	0.52	0.37
04099750	Pigeon River near Scott, IN	0.51	0.46
04099808	Little Elkhart River at Middlebury, IN	0.68	0.68
04099850	Pine Creek near Elkhart, IN	0.70	0.62
04100222	North Branch Elkhart River at Cosperville, IN	0.63	0.59
04100252	Forker Creek near Burr Oak, IN	0.54	0.51
04100295	Rimmell Branch near Albion, IN	0.49	0.51
04100500	Elkhart River at Goshen, IN	0.69	0.66
04101000	St. Joseph River at Elkhart, IN	0.73	0.58
04101500	St. Joseph River at Niles, MI	0.75	0.66
04101800	Dowagiac River at Sumnerville, MI	0.66	0.56
04102500	Paw Paw River at Riverside, MI	-0.31	-1.02
04102700	South Branch Black River near Bangor, MI	0.54	0.52
04103010	Kalamazoo River near Marengo, MI	-0.18	-0.98
04103500	Kalamazoo River at Marshall, MI	0.30	-0.09
04105000	Battle Creek at Battle Creek, MI	0.74	0.59
04105500	Kalamazoo River near Battle Creek, MI	0.65	0.54

Table 7. Nash-Sutcliffe efficiency (NSE) values for calibration streamgages in the Lake MIchigan Basin Precipitation-Runoff Modeling System model.—Continued

[USGS, U.S. Geological Survey; MI, Michigan; WI, Wisconsin; IN, Indiana]

USGS station mumber	USGS station name	Monthly mean	Monthly mean base flow
04105700	Augusta Creek near Augusta, MI	0.24	0.05
04106000	Kalamazoo River at Comstock, MI	0.71	0.63
04106500	Portage Creek at Kalamazoo, MI	0.19	0.05
04108600	Rabbit River near Hopkins, MI	0.62	0.61
04108800	Macatawa River at State Road near Zeeland, MI	0.34	0.30
04108801	Macatawa River near Zeeland, MI	0.34	0.31
04109000	Grand River at Jackson, MI	0.46	0.35
04111000	Grand River near Eaton Rapids, MI	0.69	0.56
04111379	Red Cedar River near Williamston, MI	0.70	0.31
04111500	Deer Creek near Dansville, MI	0.52	0.49
04112000	Sloan Creek near Williamston, MI	0.70	0.58
04112500	Red Cedar River at East Lansing, MI	0.74	0.64
04113000	Grand River at Lansing, MI	0.74	0.67
04114000	Grand River at Portland, MI	0.75	0.65
04114498	Looking Glass River near Eagle, MI	0.54	0.39
04114500	Looking Glass River at Hinman Road near Eagle, MI	0.54	0.39
04115000	Maple River at Maple Rapids, MI	0.71	0.48
04115265	Fish Creek near Crystal, MI	0.46	0.34
04116000	Grand River at Ionia, MI	0.82	0.69
04116500	Flat River at Smyrna, MI	0.73	0.67
04117000	Quaker Brook near Nashville, MI	0.23	0.38
04117500	Thornapple River near Hastings, MI	0.78	0.60
04118000	Thornapple River near Caledonia, MI	0.76	0.62
04118500	Rogue River near Rockford, MI	0.66	0.52
04119000	Grand River at Grand Rapids, MI	0.83	0.67
04121300	Clam River at Vogel Center, MI	0.68	0.57
04121500	Muskegon River at Evart, MI	0.81	0.66
04121900	Little Muskegon River near Morley, MI	0.64	0.60
04122000	Muskegon River at Newaygo, MI	0.74	0.47
04122100	Bear Creek near Muskegon, MI	0.68	0.68
04122200	White River near Whitehall, MI	0.53	0.49
04122500	Pere Marquette River at Scottville, MI	0.54	0.46
04124000	Manistee River near Sherman, MI	0.64	0.39
04124500	East Branch Pine River near Tustin, MI	0.34	0.32
04125460	Pine River at High School Bridge near Hoxeyville, MI	0.64	0.44
04125500	Pine River near Hoxeyville, MI	0.70	0.59
04126000	Manistee River near Manistee, MI	0.66	0.41
04126740	Platte River at Honor, MI	-3.35	-2.79
04127000	Boardman River near Mayfield, MI	0.66	0.54
04127800	Jordan River near East Jordan, MI	-0.29	-1.68
040851385	Fox River at Oil Tank Depot at Green Bay, WI	0.74	0.47

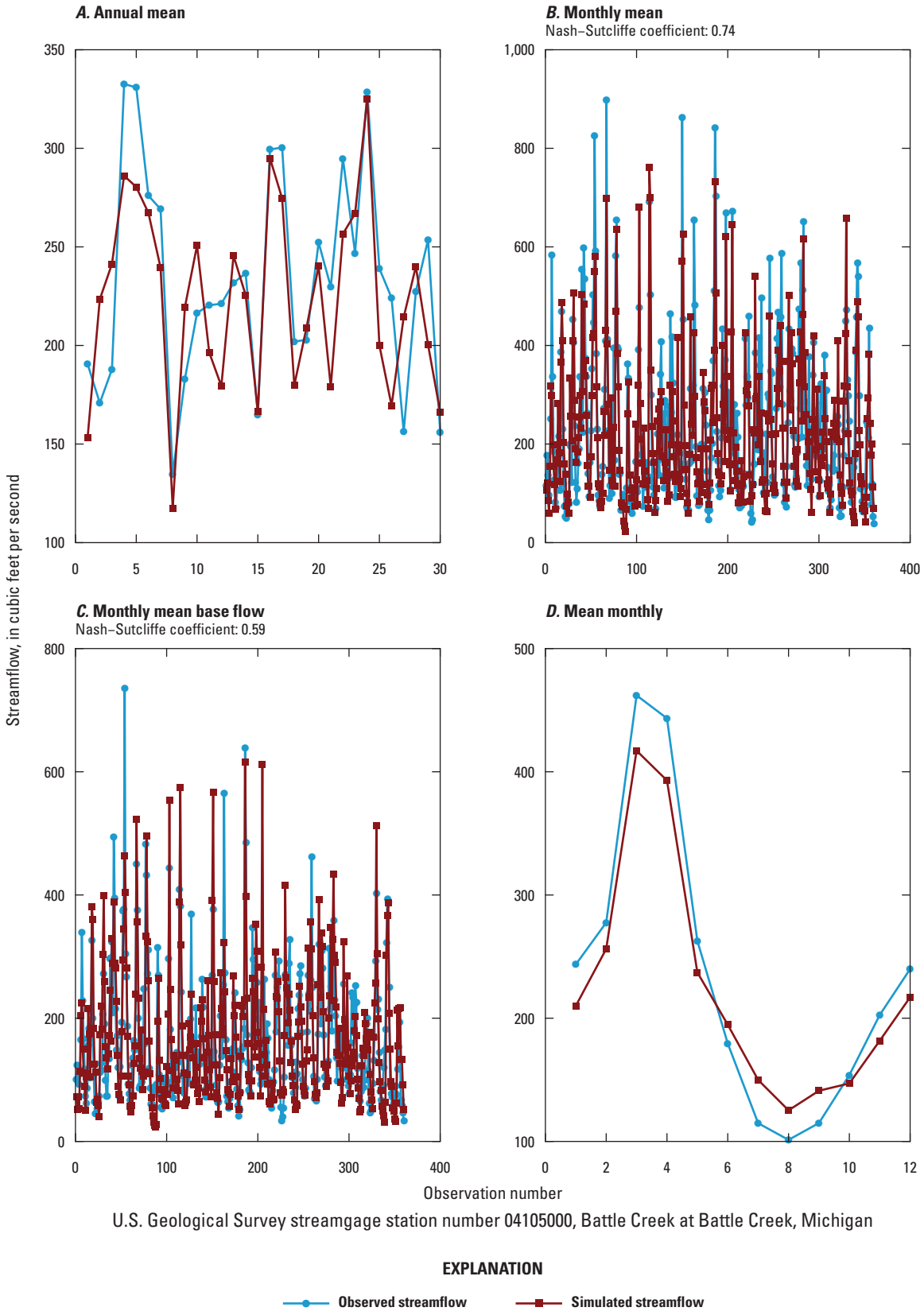

Figure 8. Streamflow statistics for *A*, annual mean; *B*, monthly mean; *C*, monthly mean base flow; and *D*, mean monthly for Battle Creek at Battle Creek, Michigan, U.S. Geological Survey streamgage number 04105000.

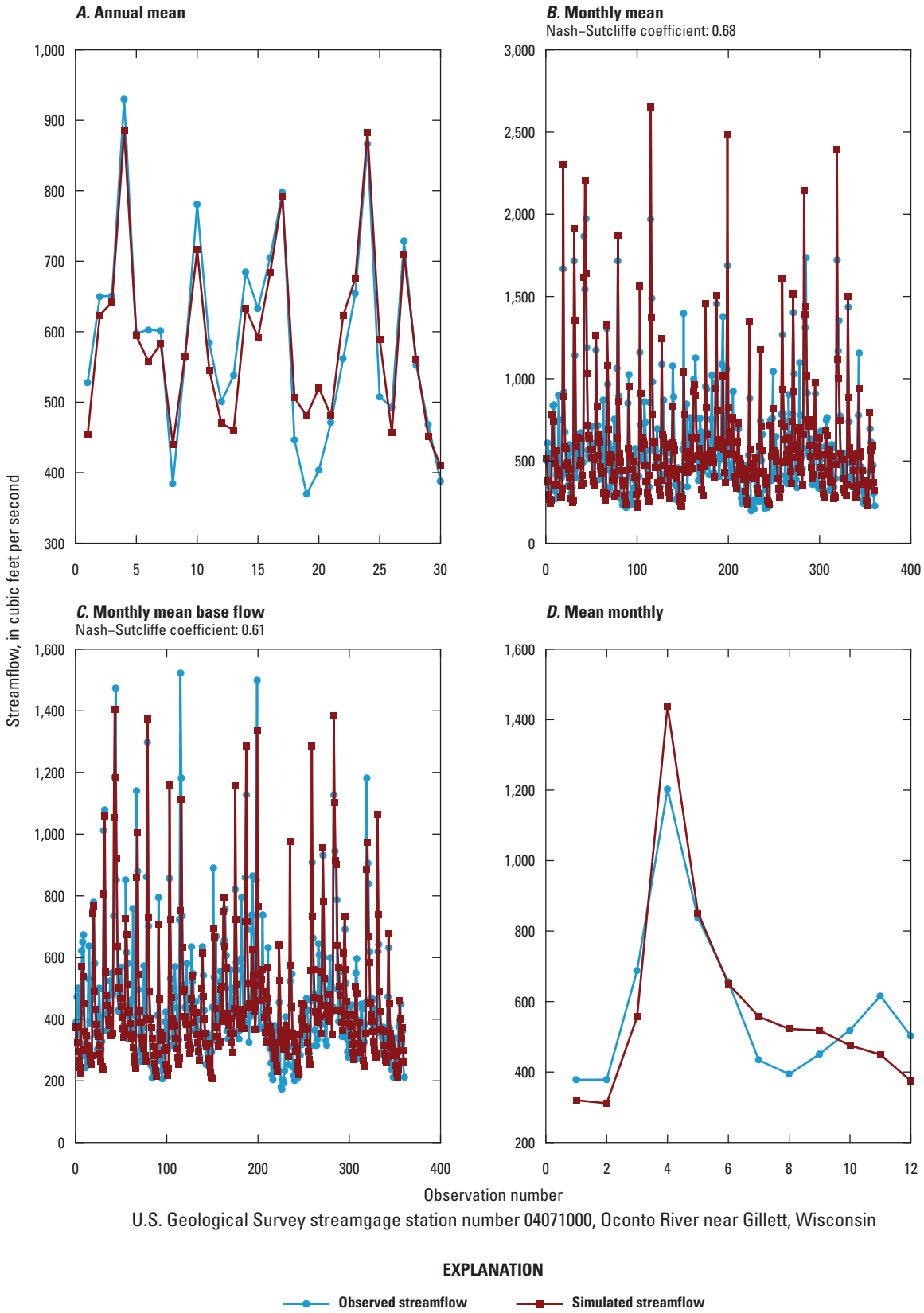

Figure 9. Streamflow statistics for *A*, annual mean; *B*, monthly mean; *C*, monthly mean base flow; and *D*, mean monthly for Oconto River near Gillett, Wisconsin, U.S. Geological Survey streamgage number 04071000.

process; these observations were given more weight than other calibration targets. Regional models are best suited to simulate regional systems well; therefore, the Lake Michigan Basin PRMS model is a coarse-scale model and represents the larger basin response well (for example, annual and monthly tributary flow). Further refinement by a more spatially detailed model will likely be required to improve the simulations of smaller basin areas, shorter time periods of interest (for example, daily streamflows), and to improve accuracy in the areas not currently well simulated (see "Limitations and Assumptions" section).

Climate Change Methods and Results

Once calibrated, the Lake Michigan Basin PRMS model was used to simulate basin-scale change in hydrologic flows resulting from using eight GCMs and four carbon emissions scenarios as climate input, thus providing a range of scenarios of potential future changes within the Lake Michigan Basin because of changes in climate. Carbon emission scenarios (Intergovernmental Panel on Climate Change, 2007) were simulated by several different GCMs (table 8). The results of the GCM simulations of the carbon emissions scenarios are referred to as the GCM projections. The GCM projections contain a wide range of future climatic conditions, each of which is used in PRMS to simulate hydrologic responses across the Lake Michigan Basin to the climate scenarios. Four carbon emission scenarios developed by the Intergovernmental Panel on Climate Change (IPCC) were used in this study (table 9).The first scenario (20C3M) corresponds to the 20th century and was used to determine the baseline current conditions (1989–1999). The three remaining scenarios represent different levels of carbon emissions leading to the different greenhouse gas emissions and concentrations during the 21st century, from relatively low (B1), to medium (A1B), to high (A2) concentrations (Intergovernmental Panel on Climate Change, 2007). GCMs were statistically downscaled so that the GCM output could be used as input into the Lake Michigan Basin PRMS model. The details of the downscaling procedure are described in detail by Notaro and others (2011).

Results of the climate change scenarios are presented here, but also can be evaluated through a dynamic web mapping service developed by the USGS available from *http://wim.usgs.gov/LakeModelDev/LakeModelMapper.html*. The map service includes layers for the 8 global climate models, 4 climate scenarios, and 12 PRMS state variables (table 10). The layers are pre-rendered maps of annual HRU state from 1977 through 2100. This web service is implemented as an Open Geospatial Consortium Standard Web Map Service (WMS) (Open Geospatial Consortium, 2006). To make the Lake Michigan Basin PRMS model results available through this service type, a custom data store (mapping from a format on disk to standard web services) was implemented in an open source geospatial server, and is briefly described below. This web mapping service will be used in future PRMS modeling efforts across the Great Lakes Basin.

The general approach was to join the shapefile of Lake Michigan Basin HRUs to a PRMS output data file, which stores the time series of HRU state for each model HRU. This approach is readily transferable to any PRMS modeling domain and can be used with any time step model result or summary of model results stored in the PRMS animation file format. Generally, an ASCII data store format would not be optimal for performance reasons because of its large file size, but the approach in this report generates cached map images for map zoom levels that would otherwise require reading large amounts of geospatial and time series data. The resulting map service is available for any client software with a network connection to display the spatial distribution of basin state parameters represented by the service.

Table 8. General circulation model (GCM) outputs used in this study from the World Climate Research Programme's Coupled Model Intercomparison Project phase 3 (CMIP3) multimodel dataset archive.

GCM[1]	Description
CGCM3.2	Canadian Centre for Climate Modeling and Analysis, Canada.
CNRM-CM3	Météo-France/Centre National de Recherches Météorologiques, France.
CSIRO-MK3.5	Commonwealth Scientific and Industrial Research Organisation (CSIRO) Atmospheric Research, Australia.
ECHAM5/MPI-OM	Max Planck Institute for Meteorology, Germany.
ECHO-G	Meteorological Institute of the University of Bonn, Meteorological Research Institute of the Korea Meteorological Administration (KMA), and Model and Data Group, Germany/Korea.
GFDL-CM2.0	U.S. Department of Commerce/ National Oceanic and Atmospheric Administration (NOAA)/ Geophysical Fluid Dynamics Laboratory.
GISS-ER	National Aeronautics and Space Administration (NASA)/ Goddard Institute for Space Studies (GISS), United States.
MRI-CGCM2.3.2	Meteorological Research Institute, Japan.

[1]CMIP3 GCM documentation, references, and links can be found at *http://www-pcmdi.llnl.gov/ipcc/model_documentation/ipcc_model_documentation.php*.

Table 9. General circulation model baseline and future emission scenarios chosen for this study (from Intergovernmental Panel on Climate Change, 2007).

Emission scenario	Description/assumptions
20C3M	20th century climate used to determine baseline (1989–1999) conditions.
A1B	Very rapid economic growth, a global population that peaks in mid-21st century and rapid introduction of new and more efficient technologies with a balanced emphasis on all energy sources.
B1	Convergent world, with the same global population as emission scenario A1B, but with more rapid changes in economic structures toward a service and information economy that is more ecologically friendly.
A2	Very heterogeneous world with high population growth, slow economic development, and slow technological change.

Table 10. Precipitation-Runoff Modeling System state variables presented in the Lake Michigan Mapper.

[in, inch; HRU, hydrologic response unit; GWR, groundwater reservoir; gw, groundwater; ssr, subsurface reservoir; ft, feet; ft^3/s, cubic feet per second]

State variable name	Statistic	Units	Description
soil_moist	average	in	Current moisture content of soil profile to the depth of the rooting zone of the major vegetation type on the HRU.
recharge	sum	in	Recharge to the associated GWR as sum of soil_to_gw and ssr_to_gw for each HRU.
hru_ppt	sum	in	Adjusted precipitation on each HRU.
hru_rain	sum	in	Computed rain on each HRU.
hru_snow	sum	in	Computed snow on each HRU.
tminf	average	ft	HRU adjusted daily minimum temperature.
tmaxf	average	ft	HRU adjusted daily maximum temperature.
potet	sum	in	Potential evapotranspiration on an HRU.
hru_actet	sum	in	Actual evapotranspiration on HRU, pervious plus impervious.
pkwater_equiv	maximum	in	Snowpack water equivalent on an HRU.
snowmelt	sum	in	Snowmelt from snowpack on an HRU.
hru_streamflow_out	average	ft^3/s	Total flow to stream network from each HRU.

Climate Change Scenarios and Precipitation-Runoff Modeling System Simulation

The GCMs predicted outputs of daily maximum temperature, minimum temperature, and precipitation, which were entered as new input to the calibrated Lake Michigan Basin PRMS model. Daily climate scenarios were generated using the USGS GeoData Portal (GDP; Blodgett, 2013) and the gridded downscaled dataset. The GDP computes zonal average values of daily maximum temperature, minimum temperature, and precipitation for each of the model HRUs. The resulting climate scenario data are read directly by the PRMS model code. Growing season onset dates and lengths are expected to change with increased temperature (for example, Christiansen and others, 2011); therefore, growing season dates used by PRMS were adjusted by pre-processing daily minimum temperature times-series (discussed previously in Time-series Processing Approach). Although maximum and minimum daily temperatures are forecasted to increase, minimum daily temperatures are expected to increase more (fig. 10). The results for precipitation are not as clear, with a general increase in the central tendency for the two periods; however, the variability across the GCMs and scenarios is relatively large (length of the box and "whiskers" in fig. 10). Moreover, figure 10 encompasses the entire Lake Michigan Basin; averaging such a large area results in some combinations exhibiting temperature and precipitation that are lower than current conditions and some combinations higher than current conditions.

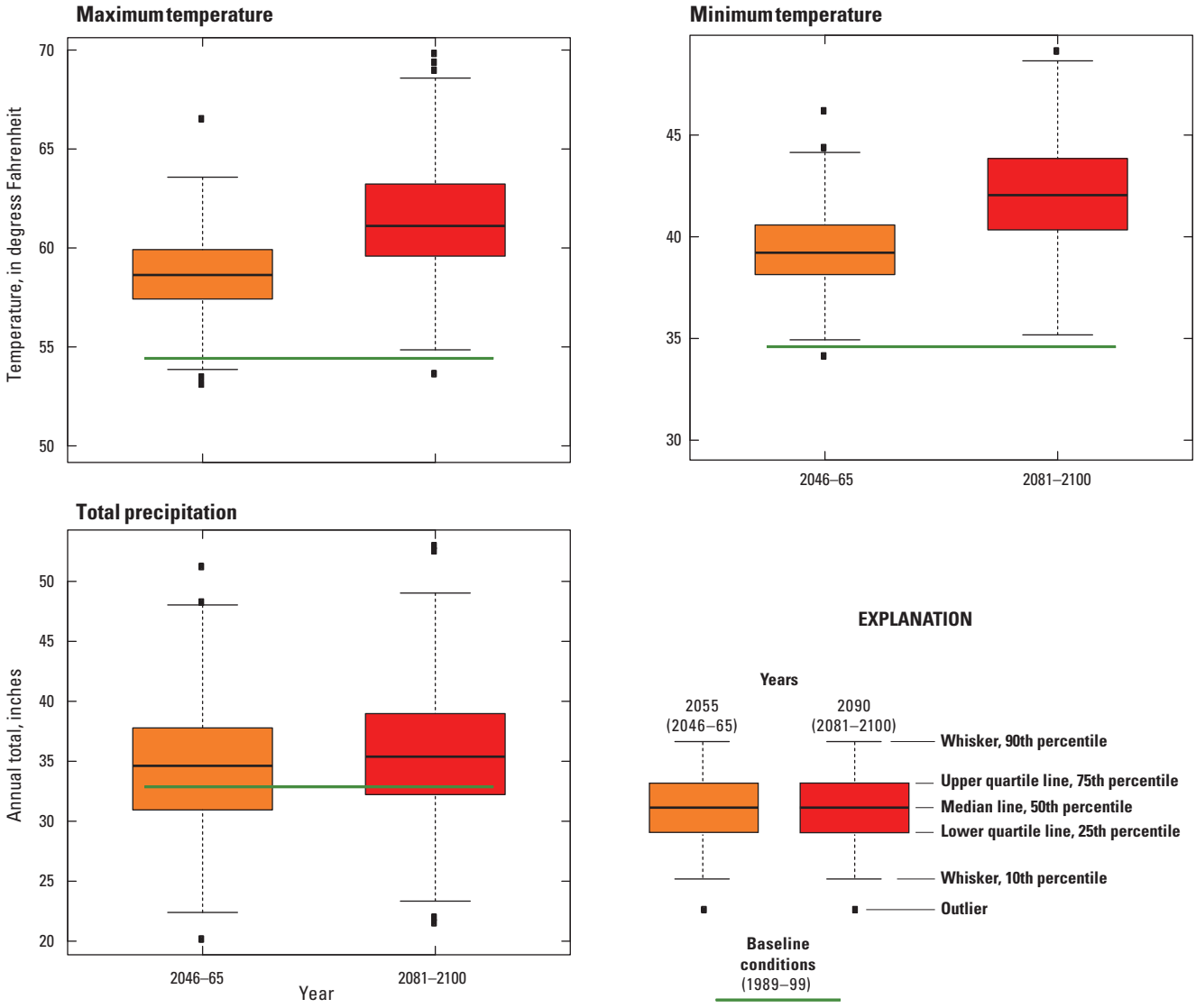

Figure 10. Lake Michigan Basin current and forecast minimum and maximum temperatures, and precipitation based on eight downscaled general circulation models and three carbon emissions scenarios.

Climate Change Outputs Considered for Discussion

Forecasts of climate change are dependent on the prediction specified and the tool constructed. In a Lake Michigan-scale representation, the regional scale of the hydrologic model does not allow accurate simulations of small basins or short (for example, daily) time periods; however, if the discussion only focused on time-integrated, large-scale outputs (for example, total annual tributary flow to Lake Michigan), the insight would be too coarse for assessing site-scale effects on ecosystems or restoration within the Lake Michigan Basin. Moreover, the amount of output generated from the Lake Michigan Basin PRMS model for all subbasins, all GCMs, and all emission scenarios precludes detailed discussion of all model outputs for all potential future climates. Therefore, to illustrate representative climate change scenario outputs, the discussion here is restricted to a subset of the model output, including the following:

1. Annual streamflow to Lake Michigan through time itself integrates shorter-term tributary flow, which gives utility to metrics involving annual timescales. Tributary-related base flow is the largest source of groundwater to the Great Lakes, and the second largest source of water after precipitation (Grannemann and others, 2000); therefore, forecasts of Lake Michigan stage can be inferred by estimates of median and ranges of expected annual streamflows for potential climate change scenarios.

2. Subbasin streamflow response to climate change, where the comparison divides the Lake Michigan Basin into the six areas (fig. 7) of Feinstein and others (2010) for discussion purposes. Two gages from each subbasin were selected for the comparison, from the gages that were well simulated during the calibration to current conditions (Nash-Sutcliffe greater than [>] 0.5). Observed and simulated streamflows are shown in figure 11 to illustrate the calibrated Lake Michigan Basin PRMS model's ability to simulate current conditions at all 12 streamgage locations used for climate comparisons. In addition to annual streamflows, comparison also focuses on ecologically relevant metrics of changes in annual Q_{10} (high-flow conditions) and Q_{90} (low-flow conditions). In addition, the mean monthly streamflows for the 20-year periods 2046–2065 and 2081–2100 also are discussed. Such a subbasin depiction allows regional analysis of variability and gradients of effects, which are important considerations when simulating a large basin. The use of subbasin grouping is especially relevant in this work given the large areal extent of the Lake Michigan Basin and the exhibited regional trends in climatic drivers that are observed during current conditions.

3. Comparisons of subbasin model output of mean soil moisture for the periods 2046–2065 and 2081–2100 also are discussed because soil moisture is an important driver for basin nutrient loading and aquatic habitat (for example, wetland) restoration.

Although only a subset of model outputs are discussed here, similar graphical representation for all gages calibrated in the Lake Michigan Basin are included in appendixes 1–5. Observation numbers on the graphs begin with observation 1 as the first year or month in the period of record used (table 2); however, for the mean monthly graphs, observations 1–12 represent months, beginning with January and ending with December.

Hydrologic Response to Climate Change Scenarios

The Lake Michigan Basin PRMS model documented here is designed to use climate inputs from any GCM results, downscaling methodology, or both; as such, the discussion here does not focus on specific GCM/carbon emission scenarios and the differences among the subset simulated in this work. Rather, the forecasts are considered an ensemble of potential scenarios given the statistical downscaling approach used by Notaro and others (2011).

When tributary stream dynamics are averaged into a single annual mean value, GCMs and emission scenarios do not exhibit strong trends when current conditions are compared to the future at the selected subbasins (fig. 12) or when summed within Lake Michigan itself (fig. 13). The box plots show a range of projected results, and higher and lower streamflows through the median values are not dissimilar to that shown for current conditions; however, annual streamflow over such a large spatial area is not an important driver for many Great Lakes restoration questions. Annual basin flows to Lake Michigan are calculated by summing stream tributary flow into Lake Michigan, direct surface runoff, and groundwater reservoir flow from directly adjacent subbasins to Lake Michigan. An annual mean flow into Lake Michigan can mask variability across the basin, as evidenced by the various magnitudes of individual tributary streamflows (fig. 12). Even minor flow duration post-processing of the simulated streamflows illustrates the potential for future changes to streamflow dynamics in the Lake Michigan Basin hidden by an annual average; for example, the forecasts indicate decreased high streamflows (Q_{10}) and increased low streamflows (Q_{90}) into Lake Michigan, compared to current conditions (fig. 13), which are changes that are not seen by analyzing forecasts of annual flow into Lake Michigan. Although the simulations forecast little change in time-integrated/annual inflows to Lake Michigan (fig. 13), this result alone cannot be used to determine forecasts of Lake Michigan stage (water level) because tributary inflows are only one component of the lake water budget that determines future lake stages.

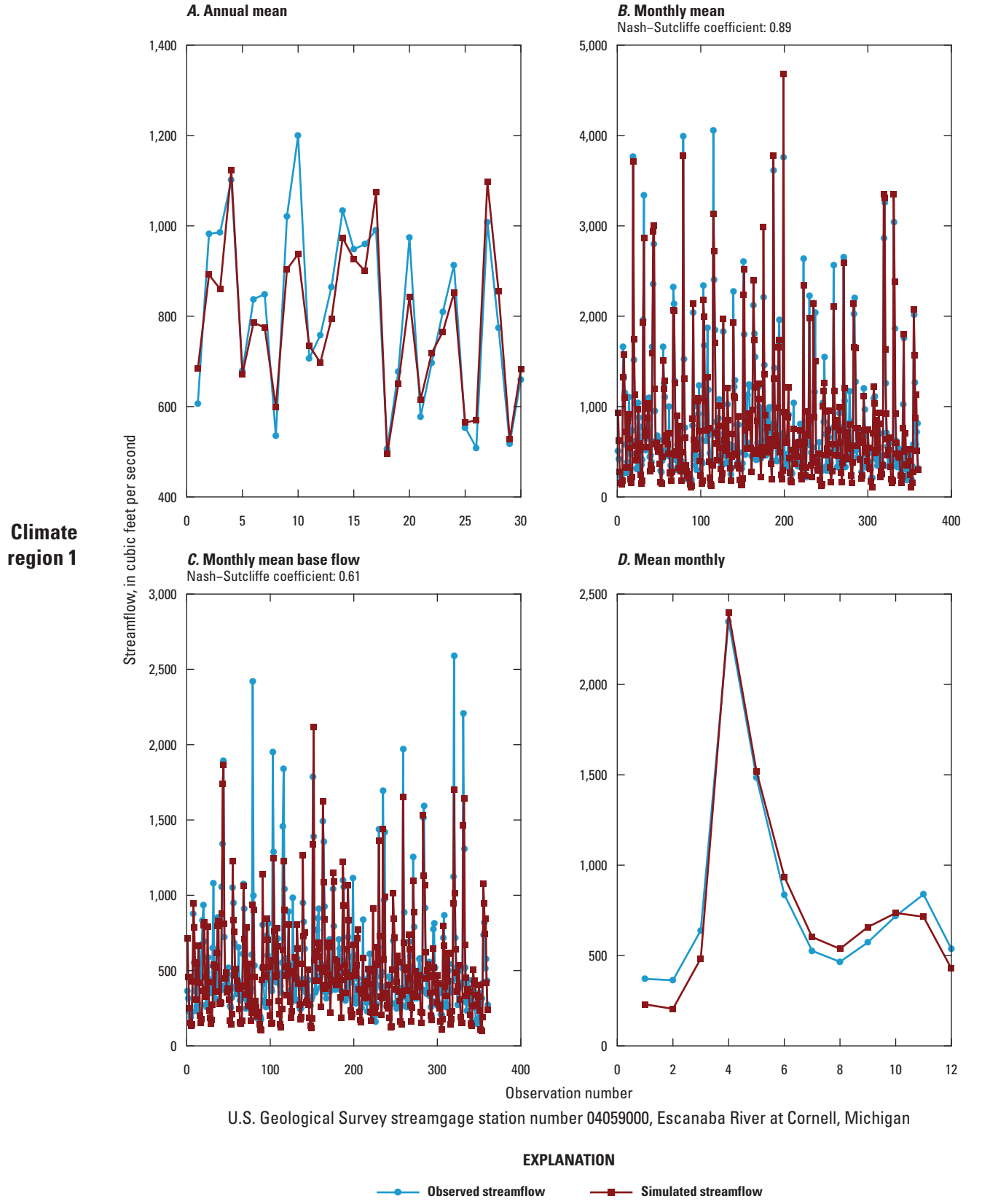

Figure 11. Streamflow statistics for *A*, annual mean; *B*, monthly mean; *C*, monthly mean base flow; and *D*, mean monthly for selected streamgages from the six climatic regions defined in Feinstein and others (2010). These locations are used for presenting simulations of climate change in figures 12–18.

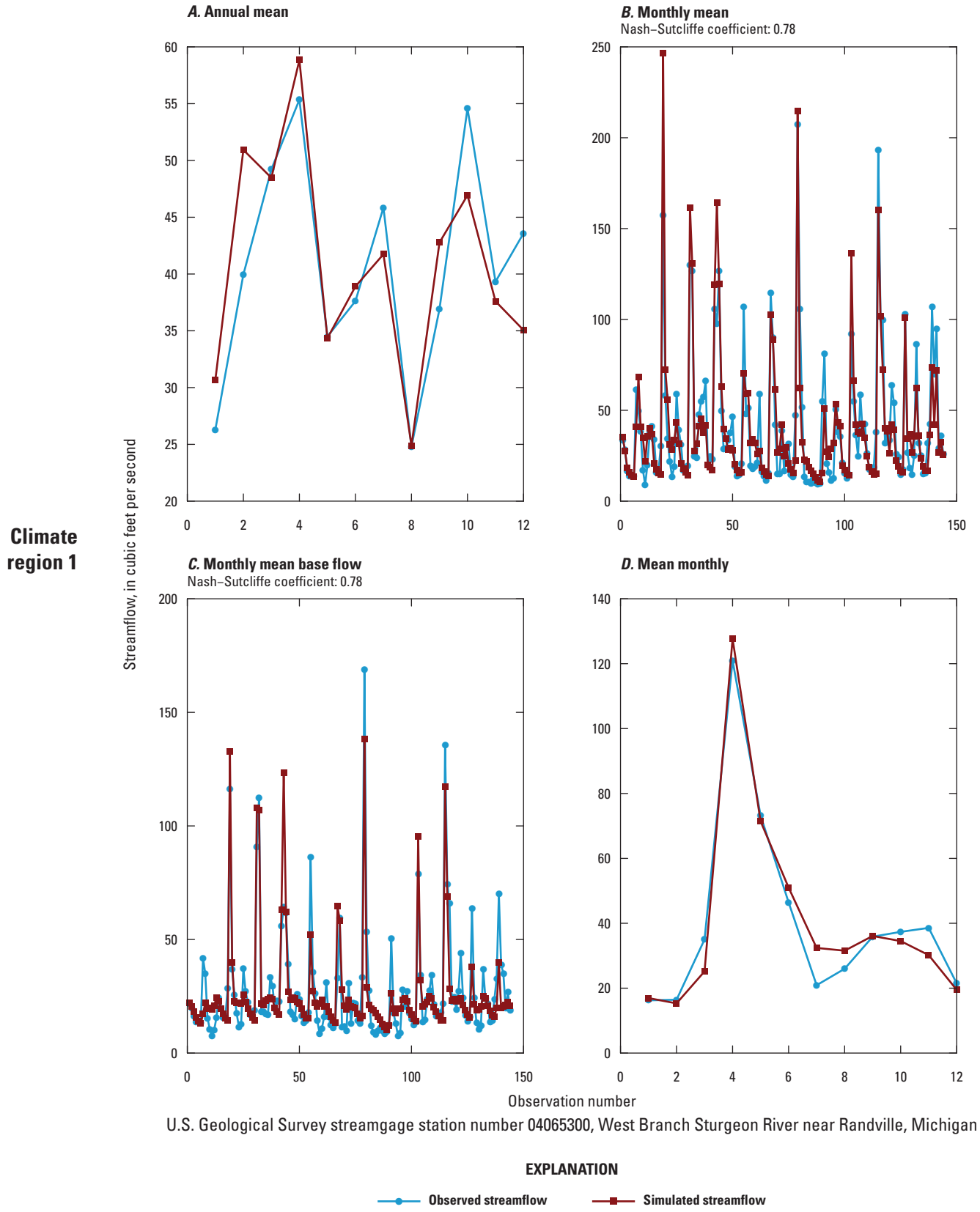

Figure 11. Streamflow statistics for *A*, annual mean; *B*, monthly mean; *C*, monthly mean base flow,; and *D*, mean monthly for selected streamgages from the six climatic regions defined in Feinstein and others (2010). These locations are used for presenting simulations of climate change in figures 12–18.—Continued

Climate region 2

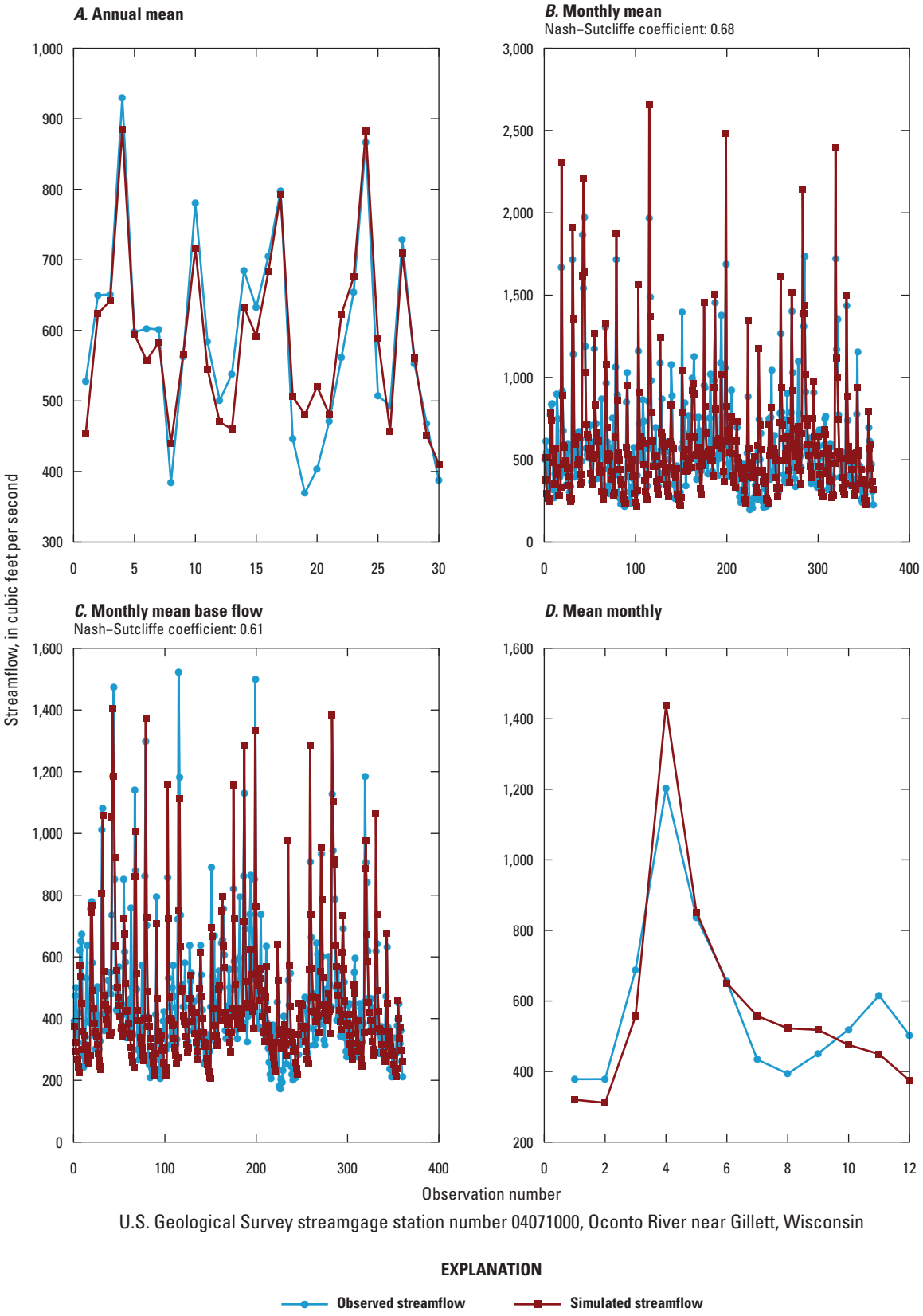

Figure 11. Streamflow statistics for *A*, annual mean; *B*, monthly mean; *C*, monthly mean base flow,; and *D*, mean monthly for selected streamgages from the six climatic regions defined in Feinstein and others (2010). These locations are used for presenting simulations of climate change in figures 12–18.—Continued

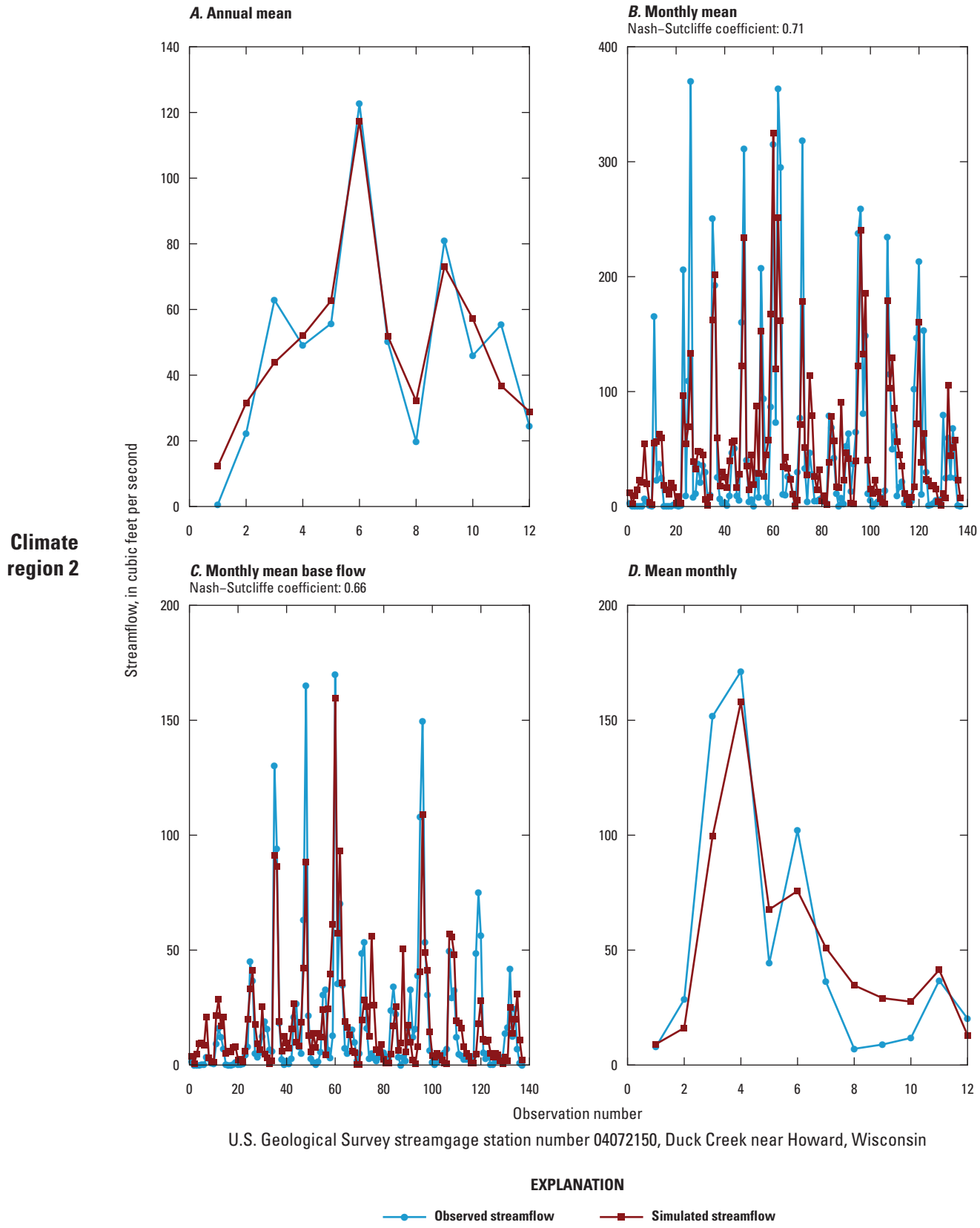

Figure 11. Streamflow statistics for *A*, annual mean; *B*, monthly mean; *C*, monthly mean base flow,; and *D*, mean monthly for selected streamgages from the six climatic regions defined in Feinstein and others (2010). These locations are used for presenting simulations of climate change in figures 12–18.—Continued

Climate region 3

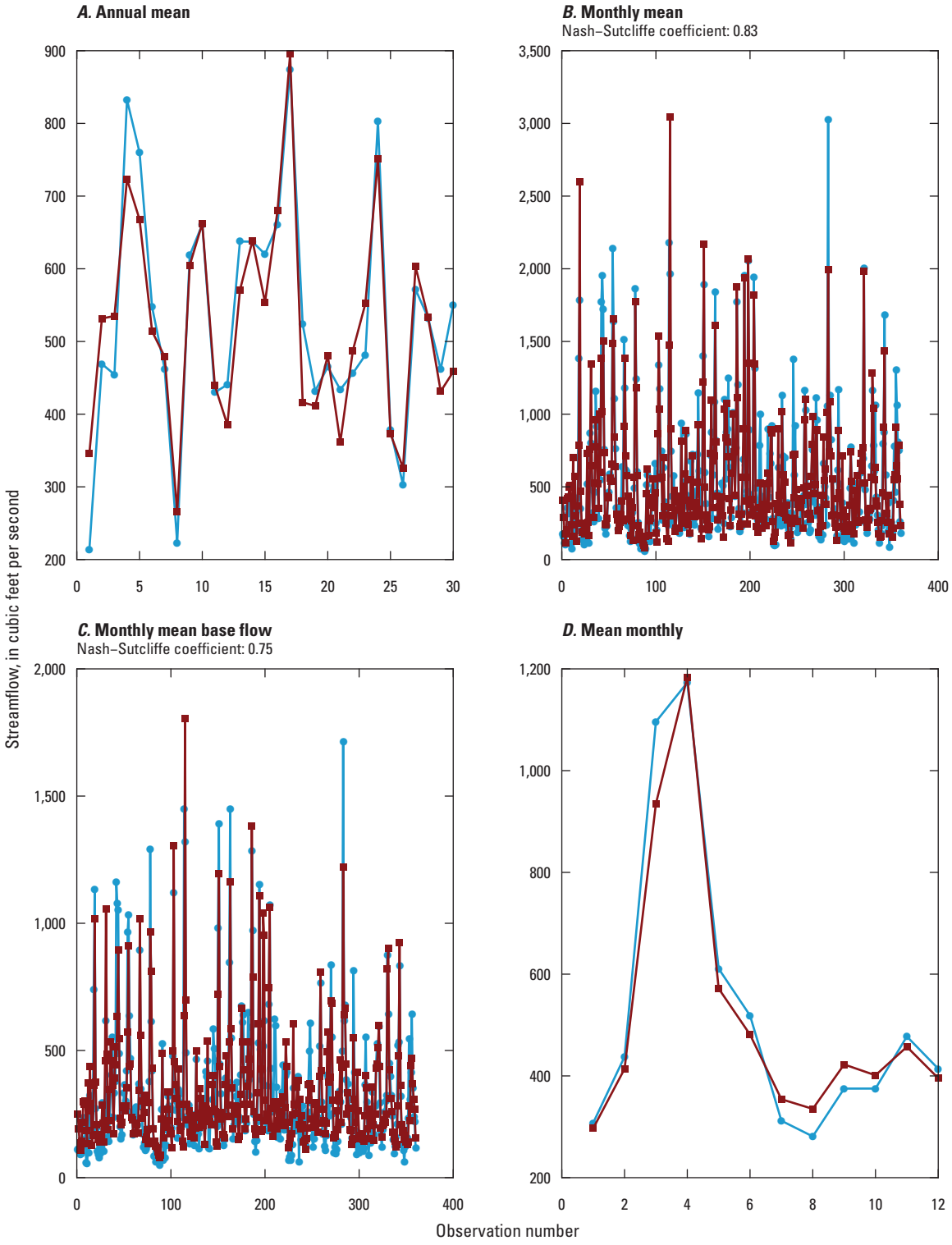

Figure 11. Streamflow statistics for *A*, annual mean; *B*, monthly mean; *C*, monthly mean base flow,; and *D*, mean monthly for selected streamgages from the six climatic regions defined in Feinstein and others (2010). These locations are used for presenting simulations of climate change in figures 12–18.—Continued

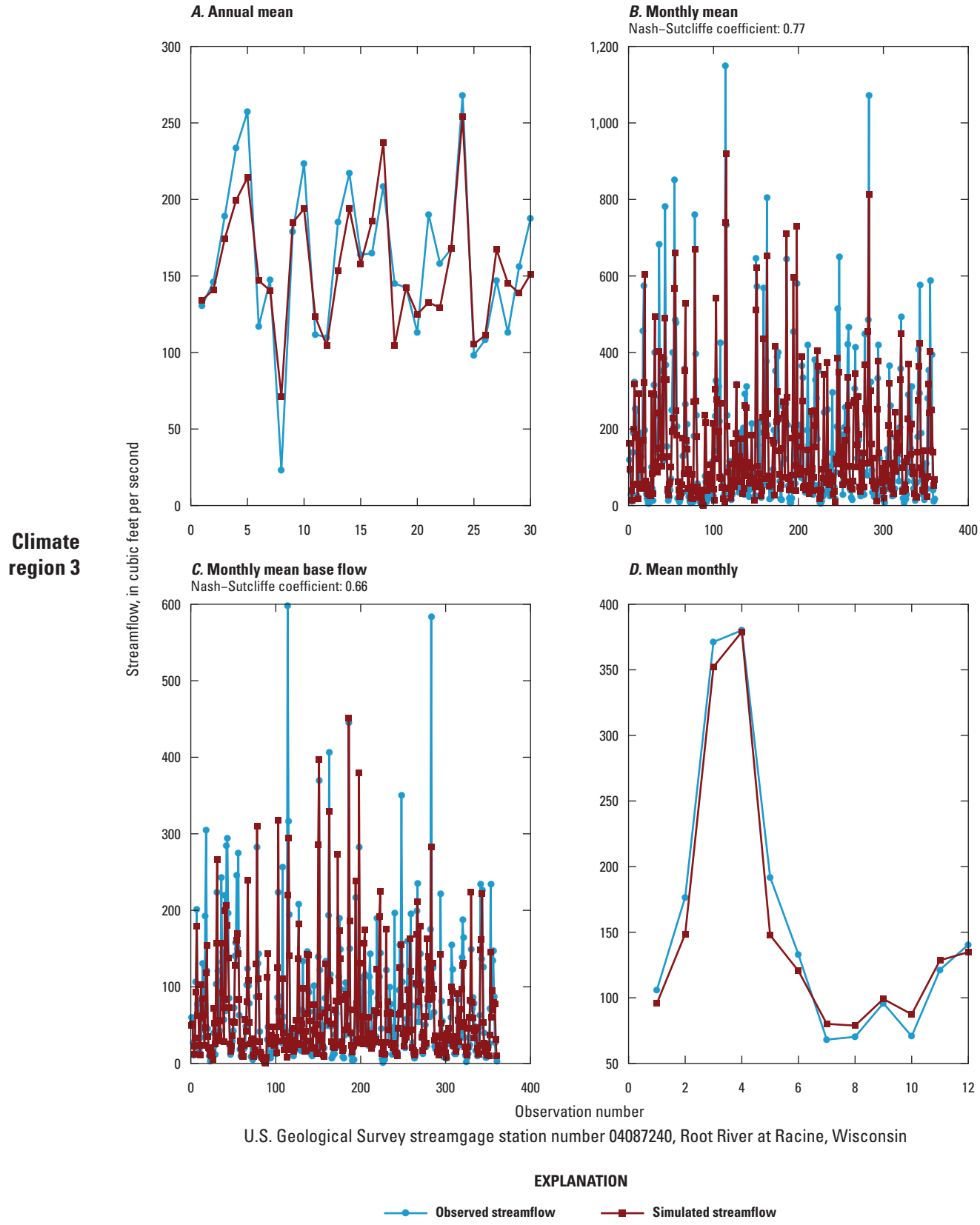

Figure 11. Streamflow statistics for *A*, annual mean; *B*, monthly mean; *C*, monthly mean base flow,; and *D*, mean monthly for selected streamgages from the six climatic regions defined in Feinstein and others (2010). These locations are used for presenting simulations of climate change in figures 12–18.—Continued

Climate region 4

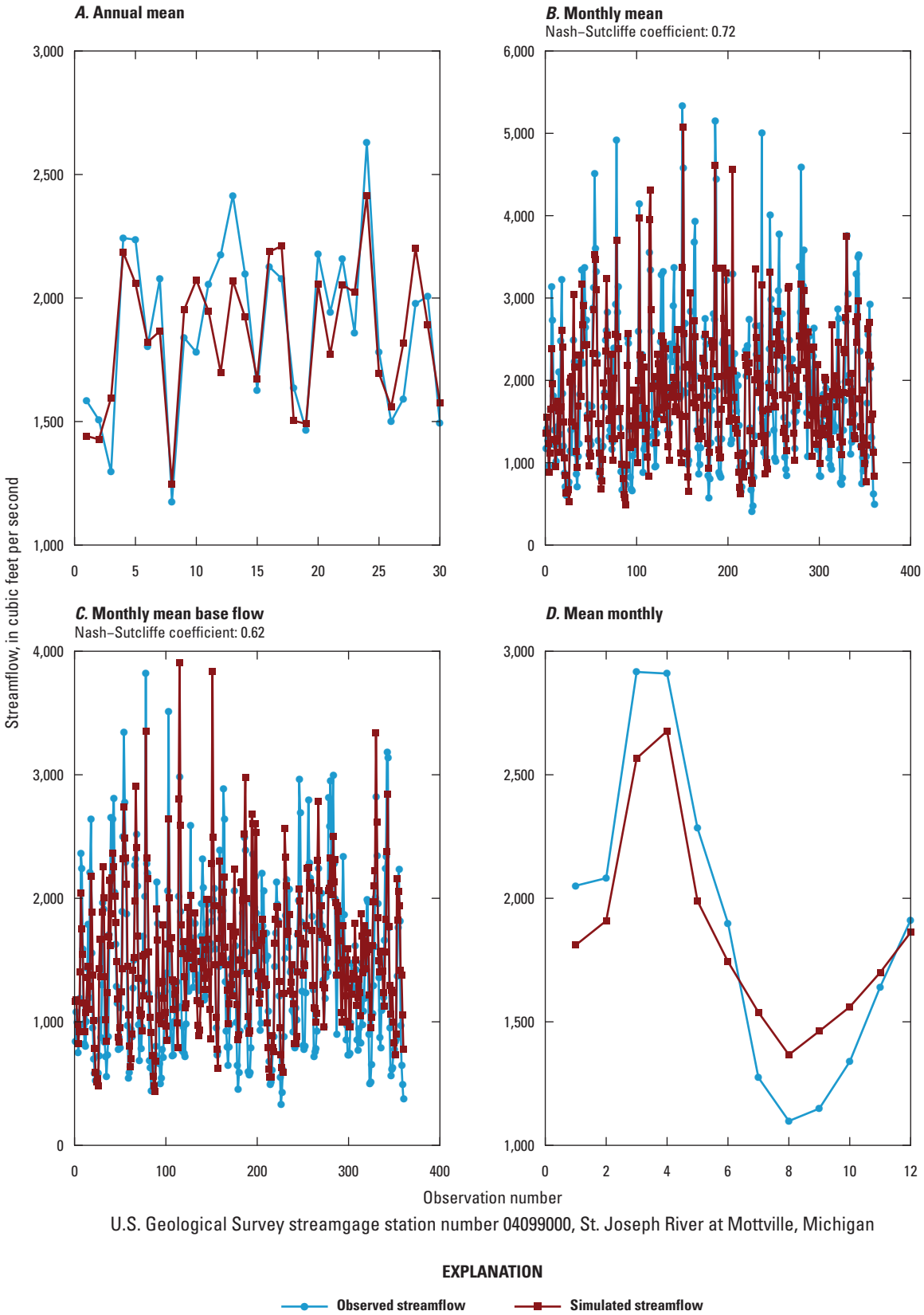

Figure 11. Streamflow statistics for *A*, annual mean; *B*, monthly mean; *C*, monthly mean base flow,; and *D*, mean monthly for selected streamgages from the six climatic regions defined in Feinstein and others (2010). These locations are used for presenting simulations of climate change in figures 12–18.—Continued

Climate region 4

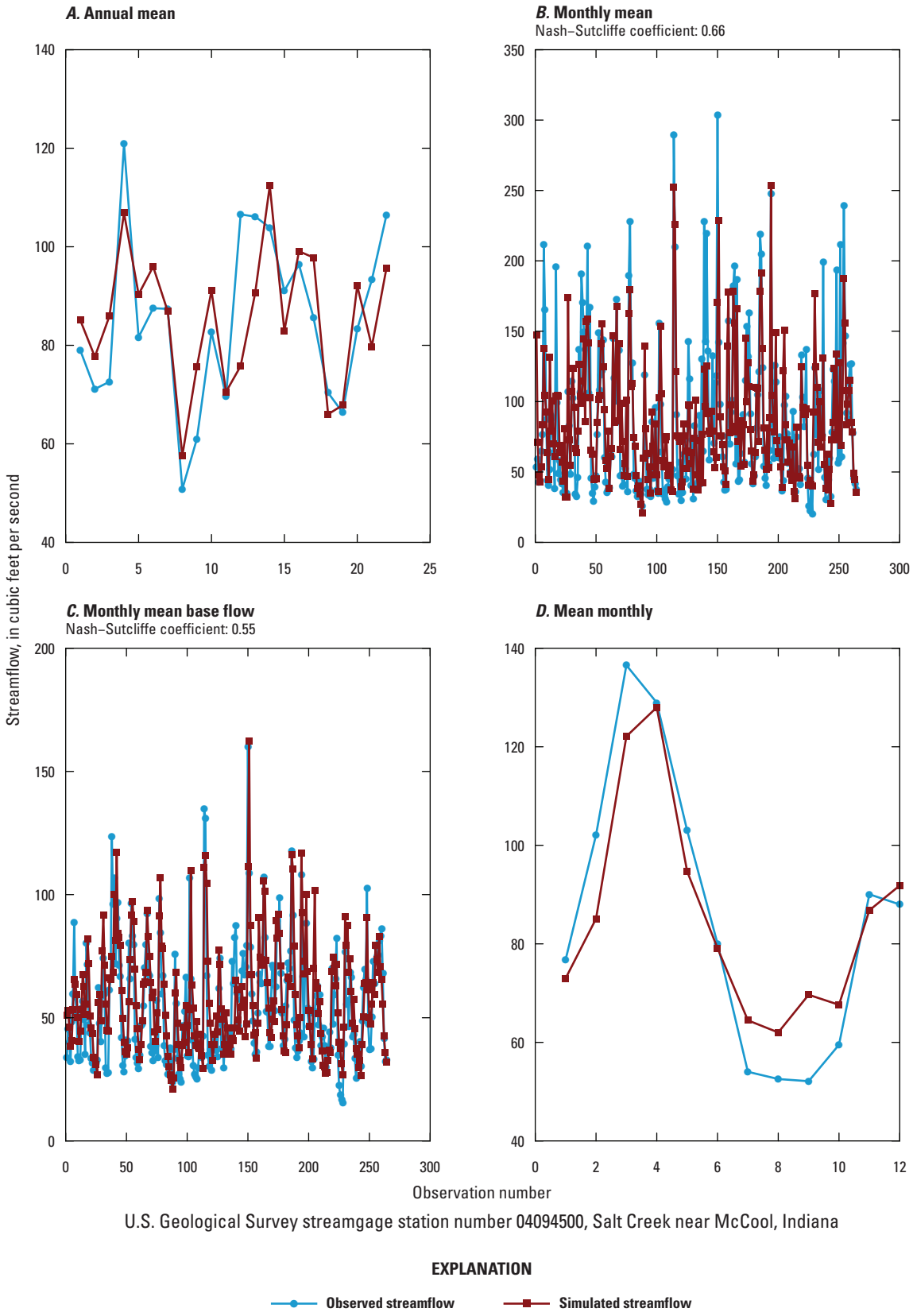

Figure 11. Streamflow statistics for *A*, annual mean; *B*, monthly mean; *C*, monthly mean base flow,; and *D*, mean monthly for selected streamgages from the six climatic regions defined in Feinstein and others (2010). These locations are used for presenting simulations of climate change in figures 12–18.—Continued

Climate region 5

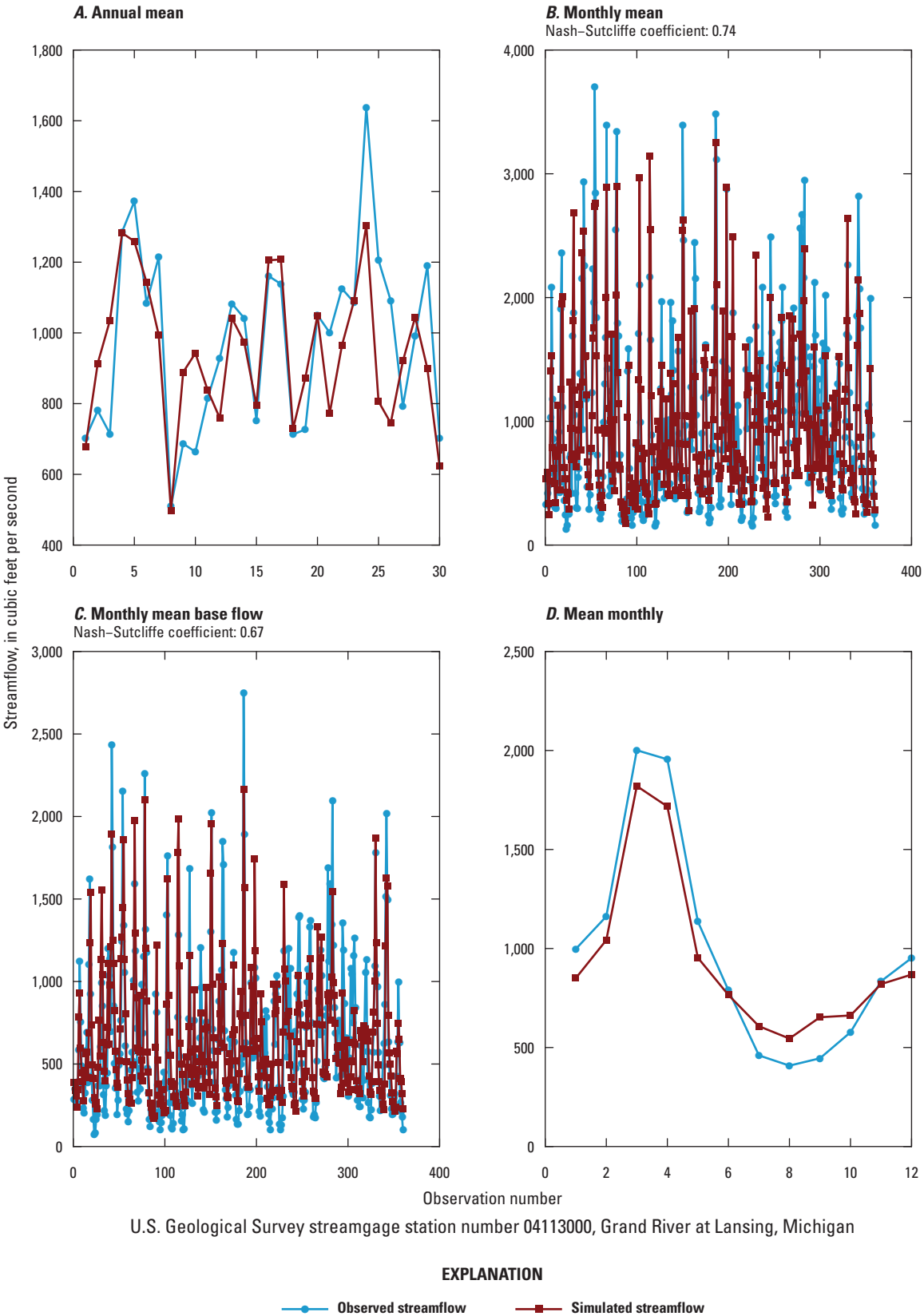

Figure 11. Streamflow statistics for *A*, annual mean; *B*, monthly mean; *C*, monthly mean base flow,; and *D*, mean monthly for selected streamgages from the six climatic regions defined in Feinstein and others (2010). These locations are used for presenting simulations of climate change in figures 12–18.—Continued

Climate region 5

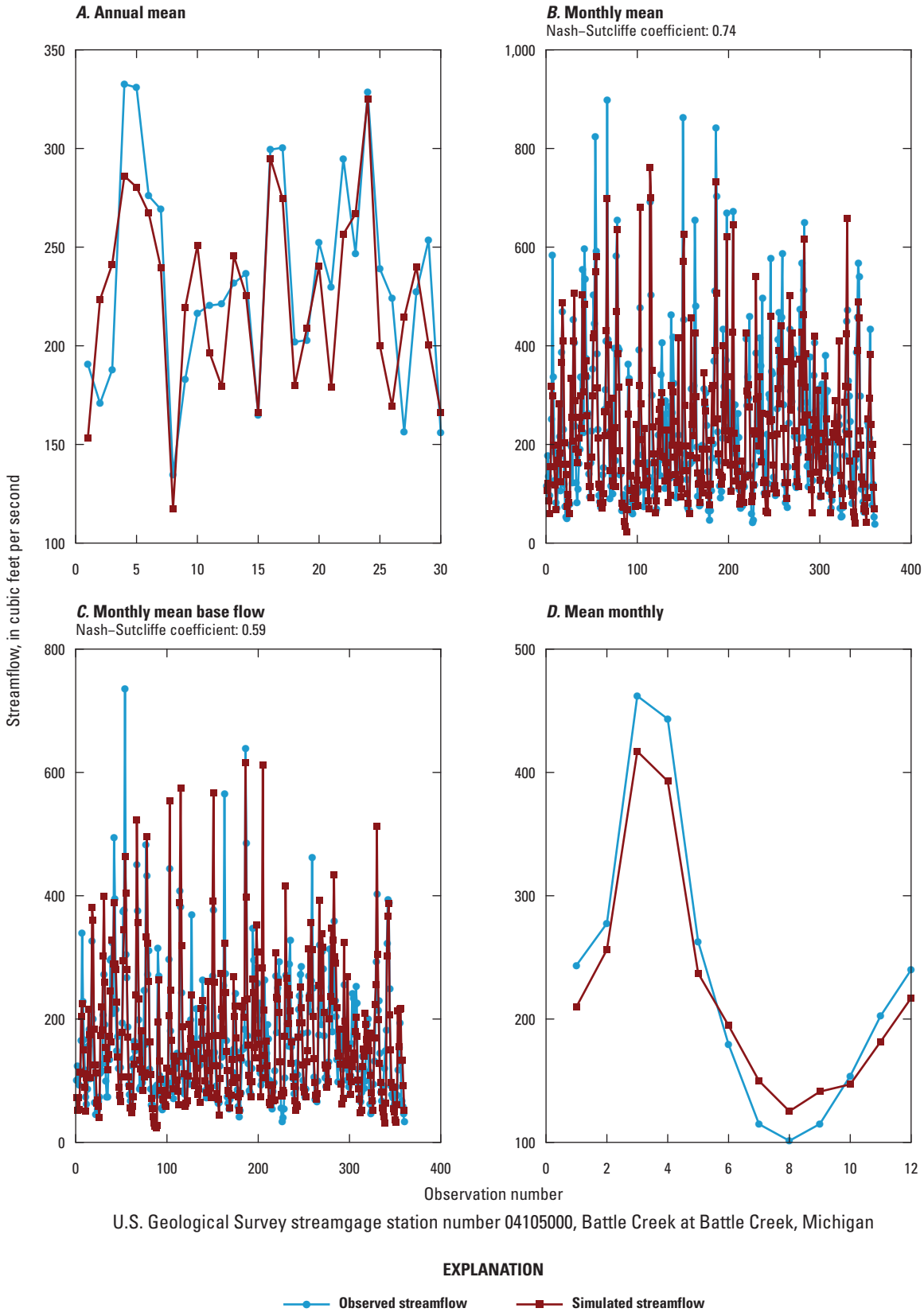

Figure 11. Streamflow statistics for *A*, annual mean; *B*, monthly mean; *C*, monthly mean base flow,; and *D*, mean monthly for selected streamgages from the six climatic regions defined in Feinstein and others (2010). These locations are used for presenting simulations of climate change in figures 12–18.—Continued

Climate region 6

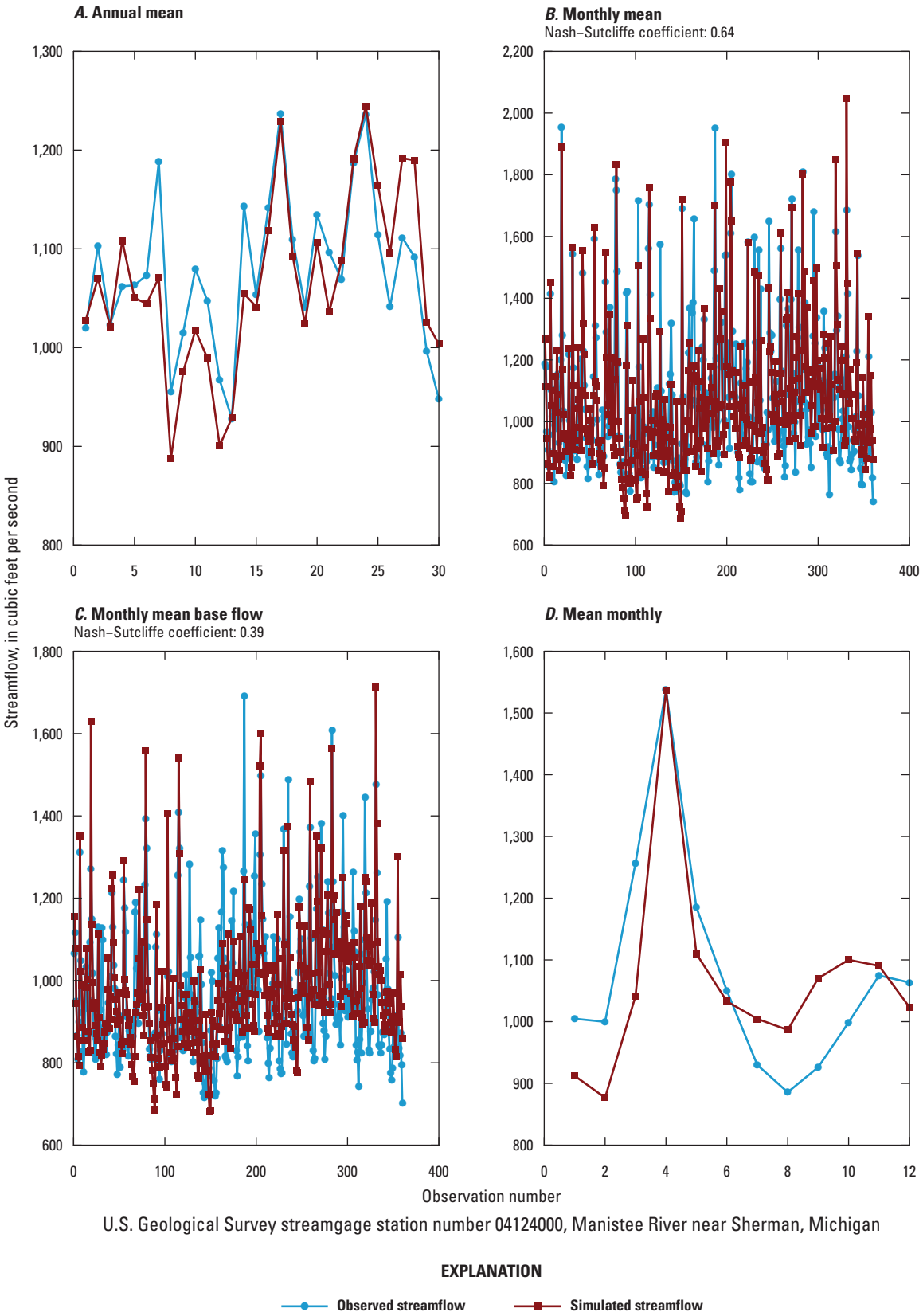

Figure 11. Streamflow statistics for *A*, annual mean; *B*, monthly mean; *C*, monthly mean base flow,; and *D*, mean monthly for selected streamgages from the six climatic regions defined in Feinstein and others (2010). These locations are used for presenting simulations of climate change in figures 12–18.—Continued

Climate region 6

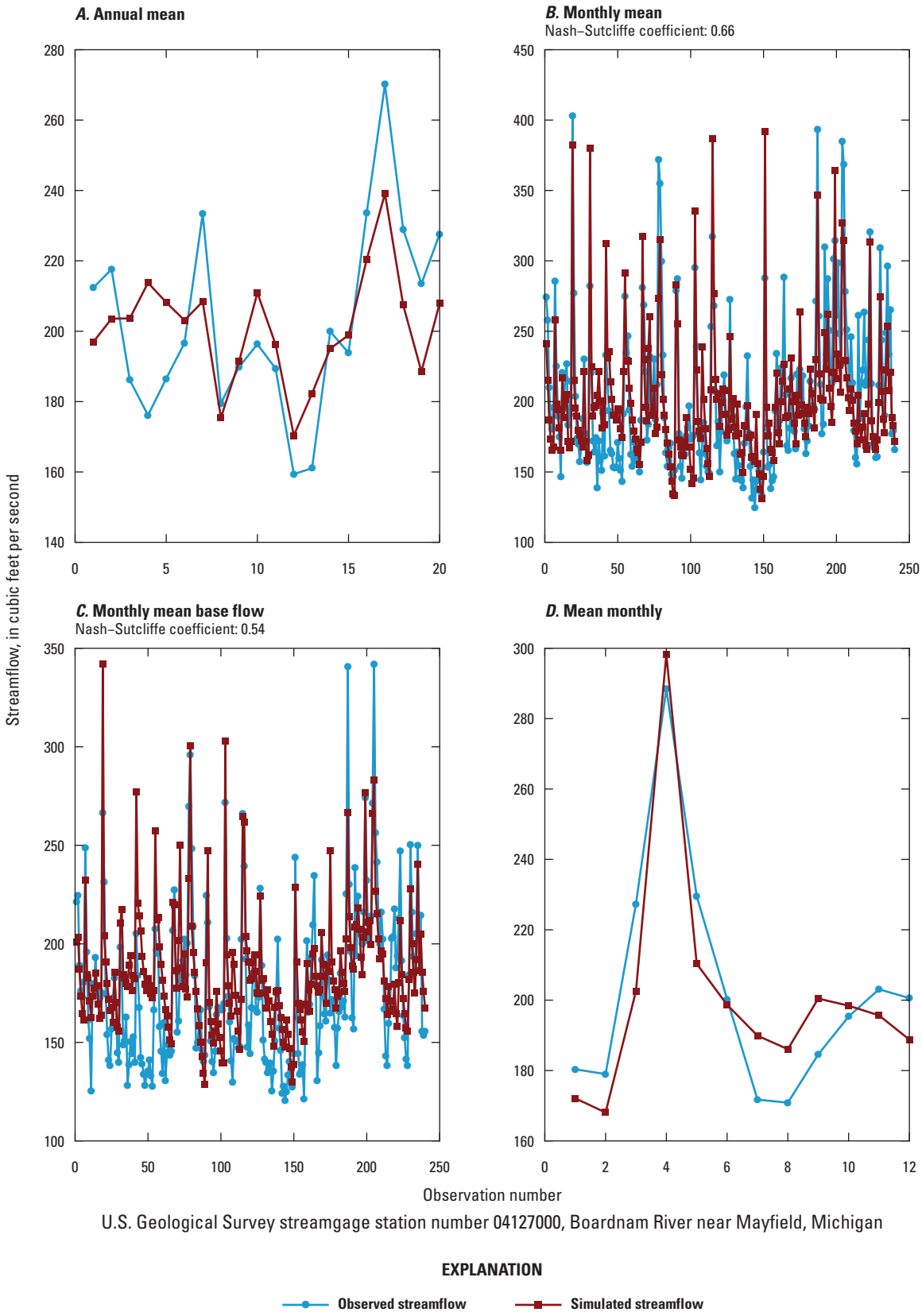

Figure 11. Streamflow statistics for *A*, annual mean; *B*, monthly mean; *C*, monthly mean base flow,; and *D*, mean monthly for selected streamgages from the six climatic regions defined in Feinstein and others (2010). These locations are used for presenting simulations of climate change in figures 12–18.—Continued

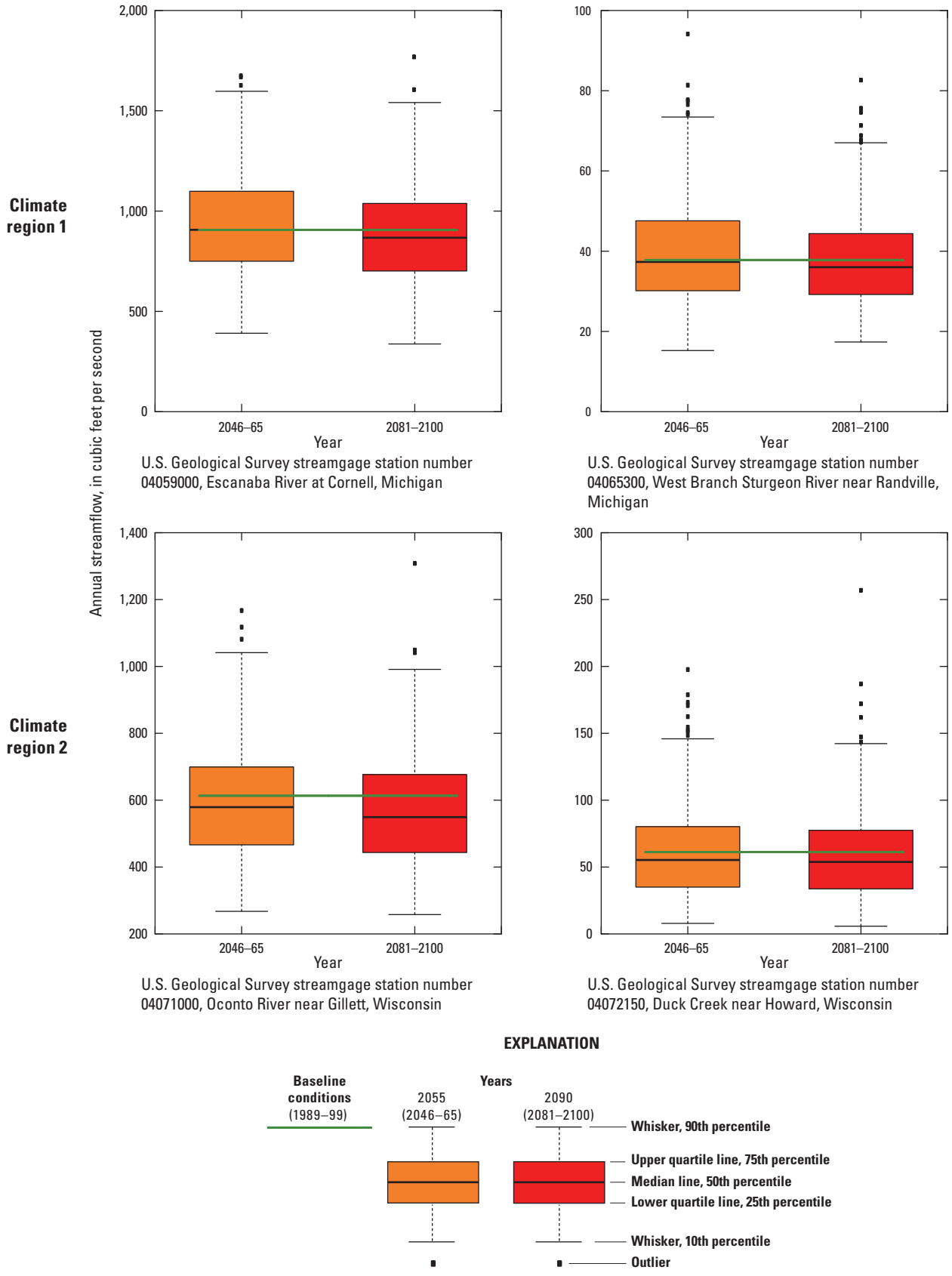

Figure 12. Annual streamflows for selected streamgages of the Lake Michigan Basin for current and future carbon emissions scenario conditions.

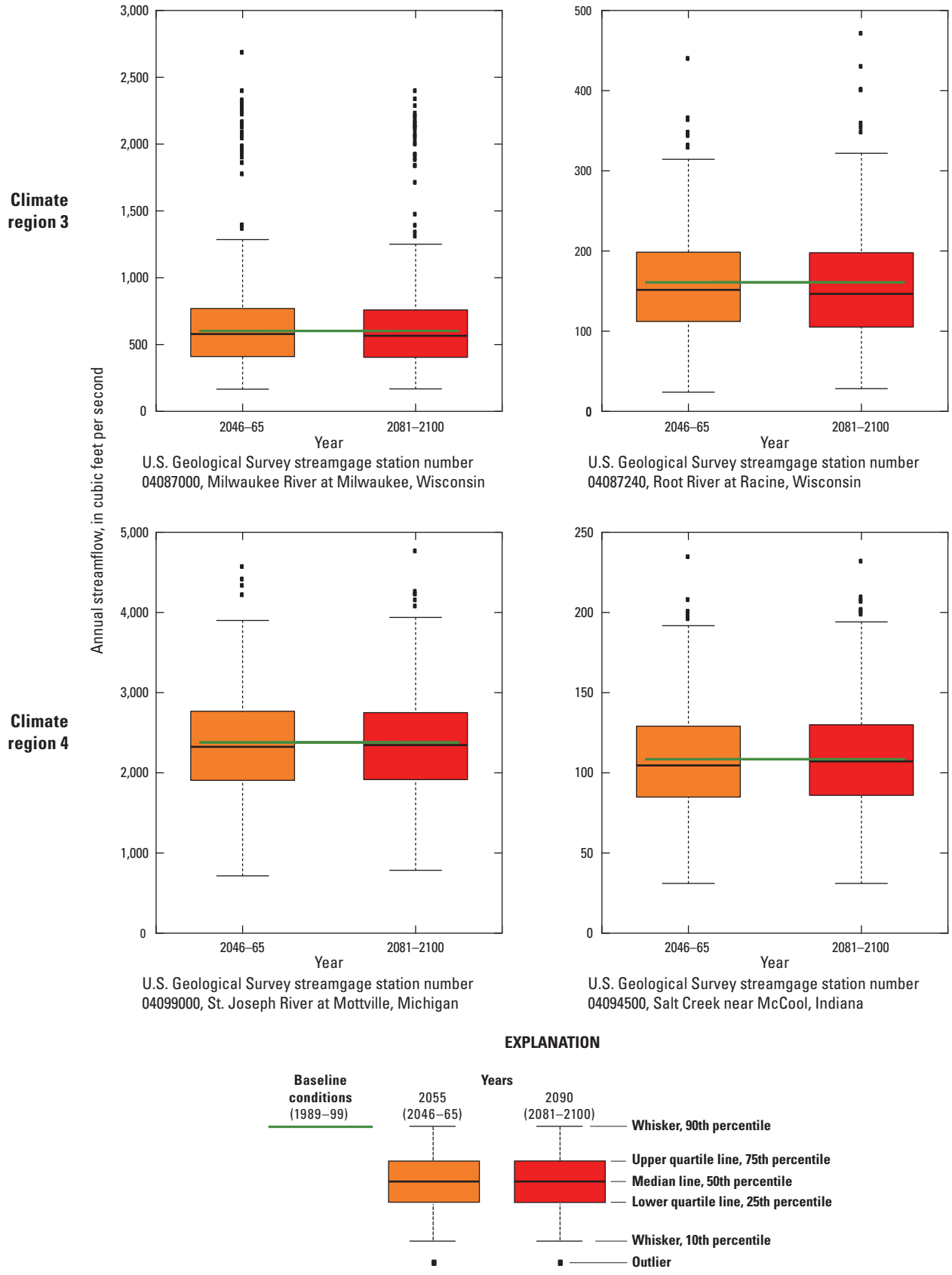

Figure 12. Annual streamflows for selected streamgages of the Lake Michigan Basin for current and future carbon emissions scenario conditions.—Continued

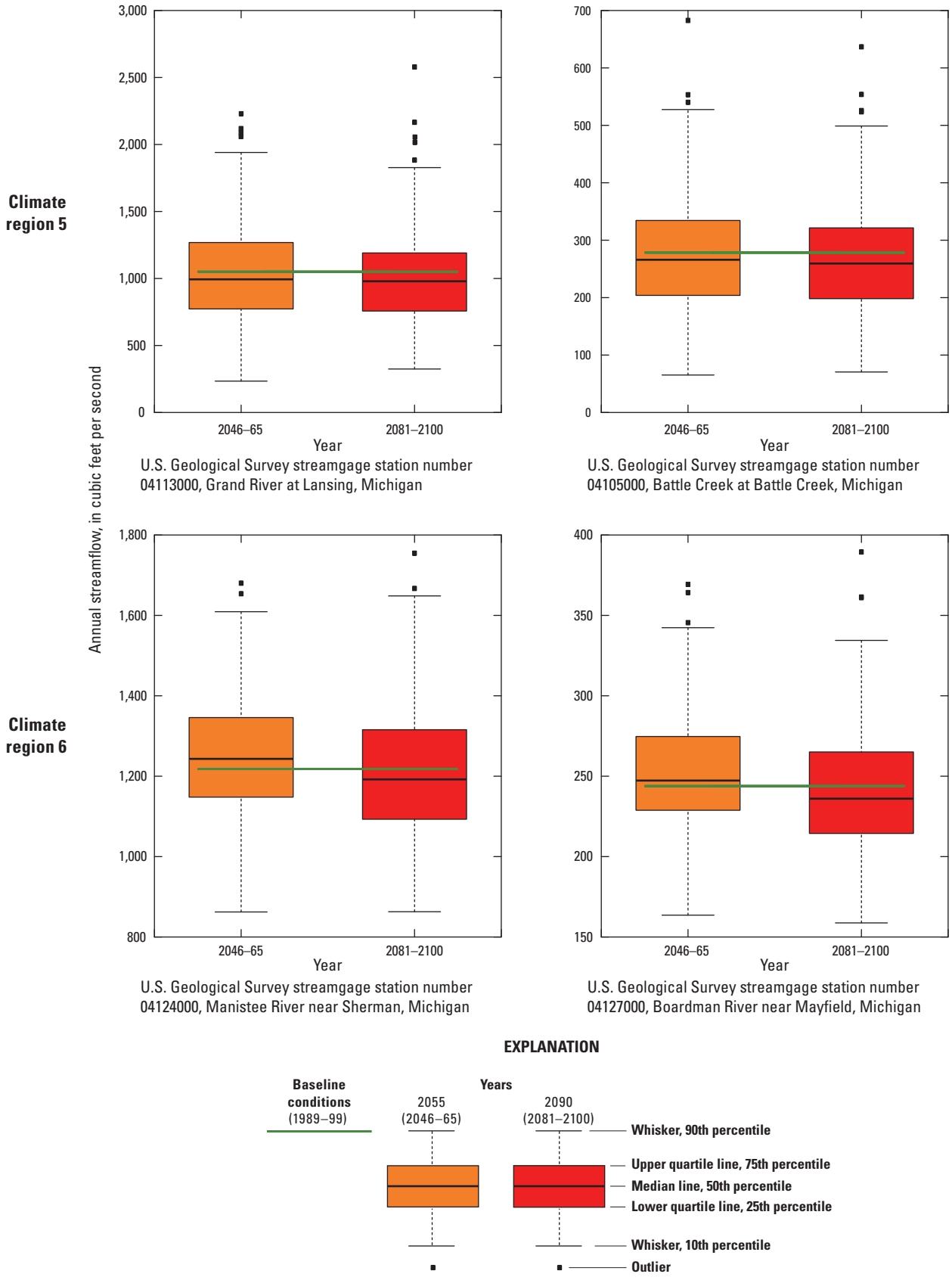

Figure 12. Annual streamflows for selected streamgages of the Lake Michigan Basin for current and future carbon emissions scenario conditions.—Continued

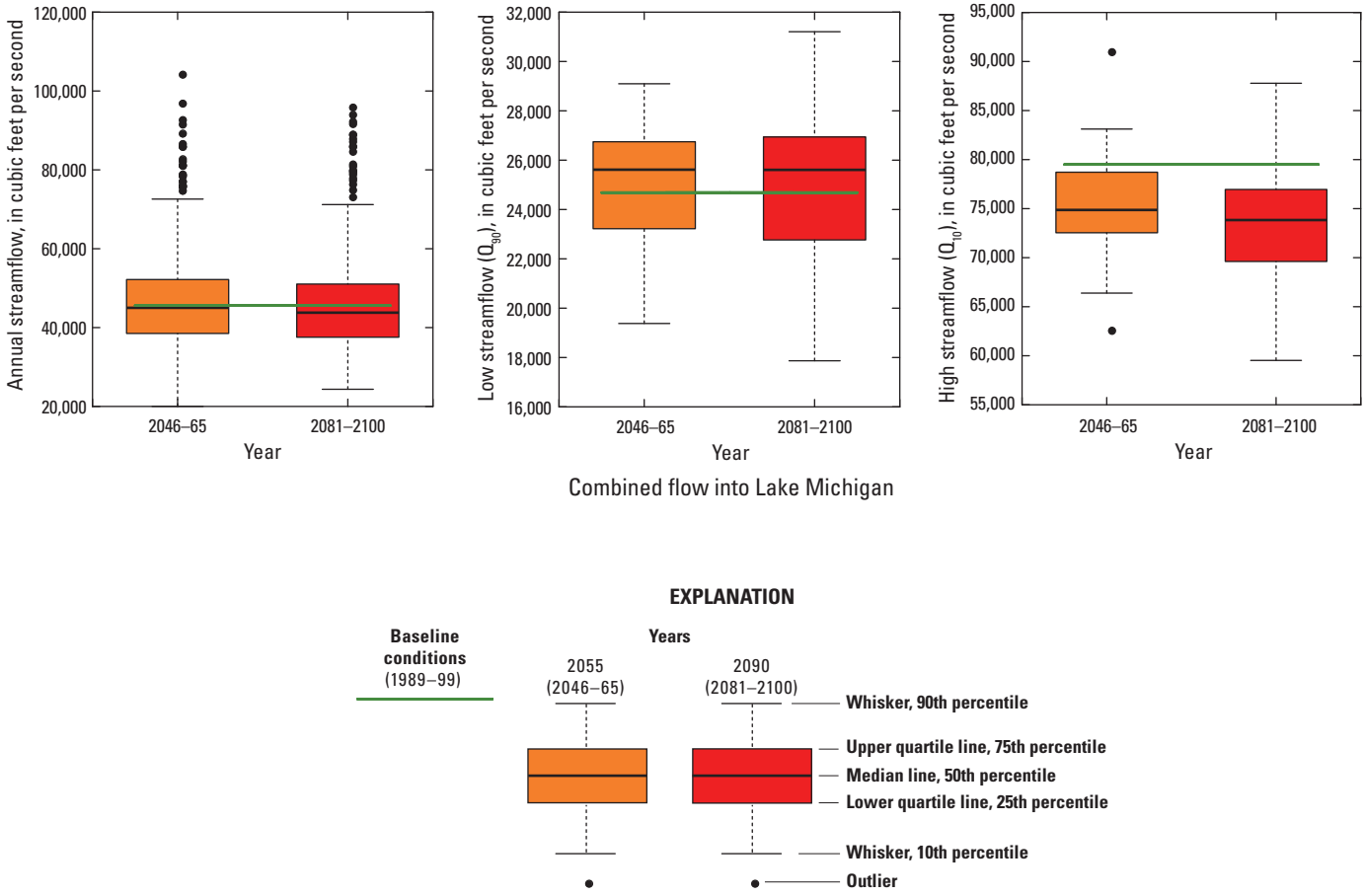

Figure 13. Combined basin flow into Lake Michigan for current and future carbon emissions scenario conditions for annual, high-flow (Q_{10}), and low-flow (Q_{90}) streamflows.

Changes in Subbasin Monthly Streamflows in Six Subregions of the Lake Michigan Basin 2012–2100

Median changes between current and forecasted Q_{10} (high) streamflows show reductions throughout the Lake Michigan Basin (fig. 14), which reflect the dampening of snowmelt dynamics with forecast reductions in water stored in the winter indicated by increased streamflows during January and February (fig. 15). The Q_{90} (low) streamflows show an approximate northwest-southeast gradient (fig. 16) with significant increases in low flow in northwest and no change to decreases in the southeast. It should be noted that the Lake Michigan Basin PRMS model uses a simple linear reservoir to represent the groundwater system in these areas. Thus, PRMS-derived low-flow simulations may be less accurate than simulations that include more sophisticated handling of the groundwater system; forecasts dependent on accurate simulations of groundwater-stream interaction are expected to be less accurate than those forecasts focusing on surface water system response. Moreover, given the regional discretization of the model, error in the simulation of groundwater-stream is expected to be mostly expressed in forecasts of low flow from small subbasins that generate less than 50 cubic feet per second values for Q_{90}.

Generally, monthly simulations show a north-south gradient in climate change effects where forecasts in the northern areas (Regions 1 and 6) of the Lake Michigan Basin are more affected by climate change than the southern areas (Regions 3 and 4) (fig. 15). This result reflects a larger change along the current conditions north-south gradient whereby the north is characterized by larger accumulation of snowpack storage and the associated snow-melt pulse in April (for example, fig. 16A and B versus fig. 16E and F and fig. 17). Changes in the partitioning of winter precipitation reflect increases in air temperature (fig. 10) that are projected to take place by 2100, a result consistent across all GCMs and emission scenarios. Warmer winters are important because they are simulated to have a higher part of winter precipitation falling as rain rather than snow, and more episodic melt-derived streamflow and groundwater recharge spread over the winter months. This winter precipitation that is converted to winter streamflow rather than stored as snow is then unavailable during the spring which is a period of large snowmelt dynamics during current conditions. This effect also is present in the southern areas of the Lake Michigan Basin (fig. 15, Regions 3 and 4), but to a lesser extent because current climate conditions already limit large-scale storage of winter precipitation; therefore, one way to visualize this forecast of possible future

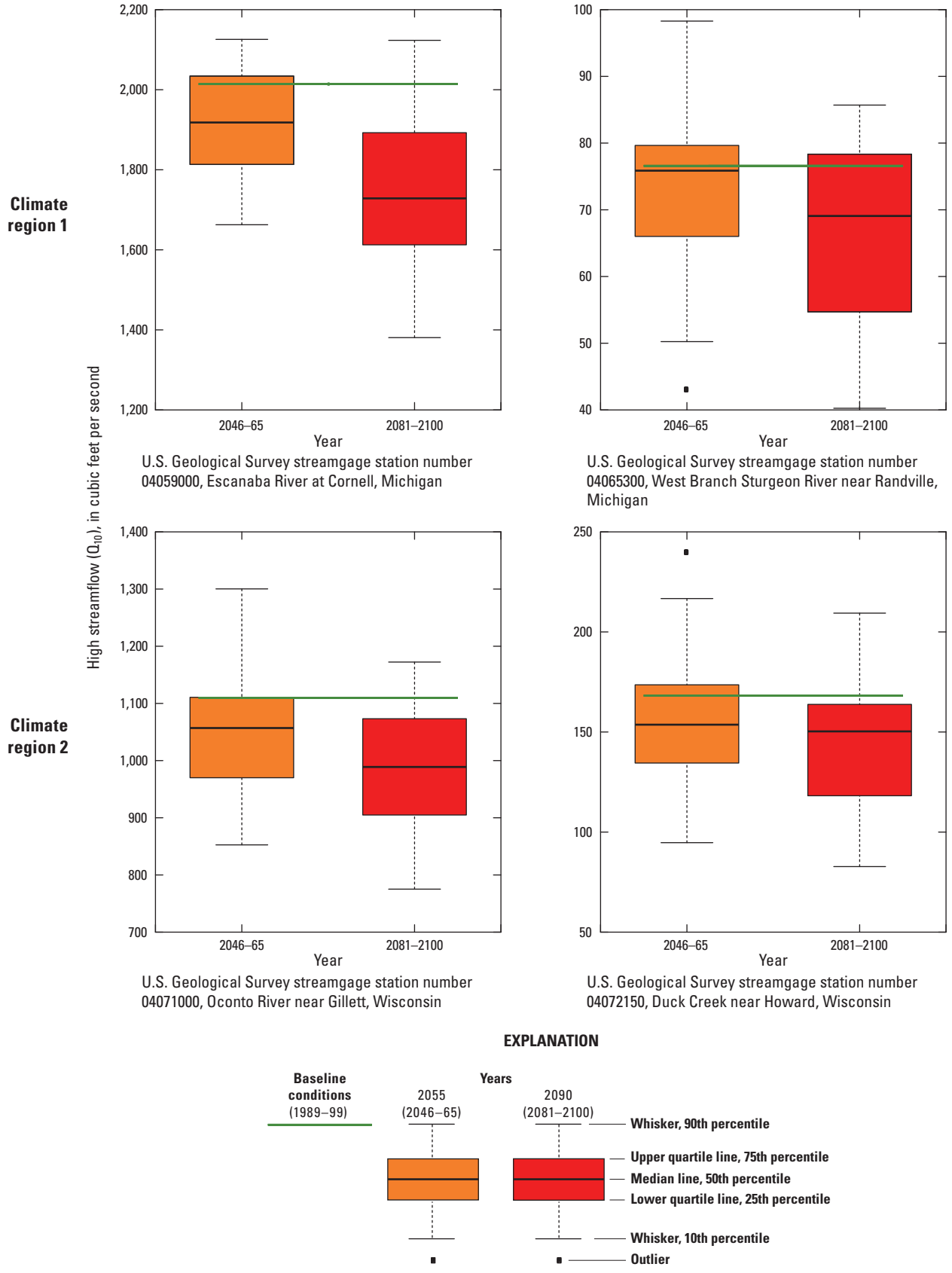

Figure 14. Selected streamgages and current conditions compared to future emission scenarios for high-flow (Q_{10}) streamflows.

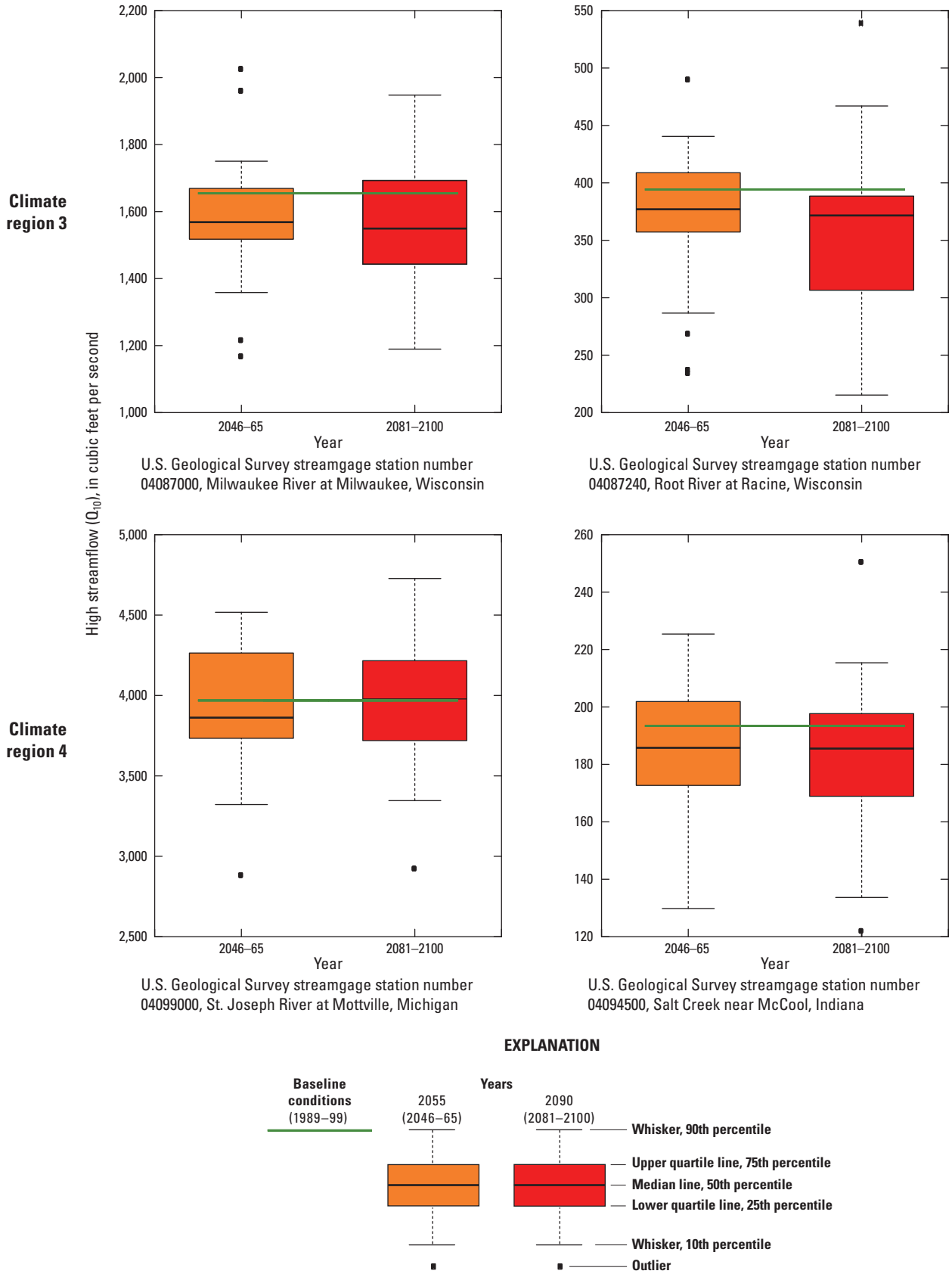

Figure 14. Selected streamgages and current conditions compared to future emission scenarios for high-flow (Q_{10}) streamflows.—Continued

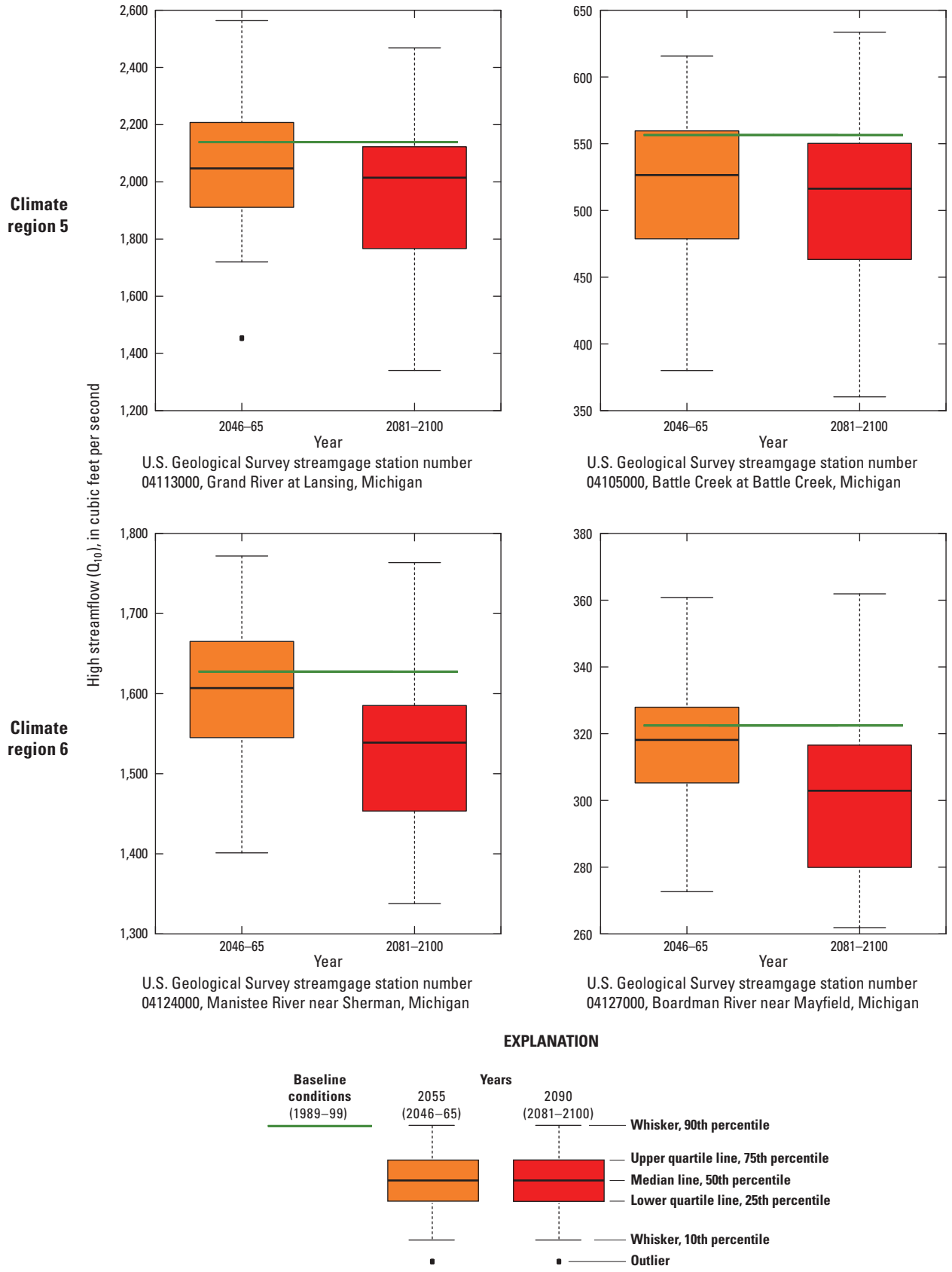

Figure 14. Selected streamgages and current conditions compared to future emission scenarios for high-flow (Q_{10}) streamflows.—Continued

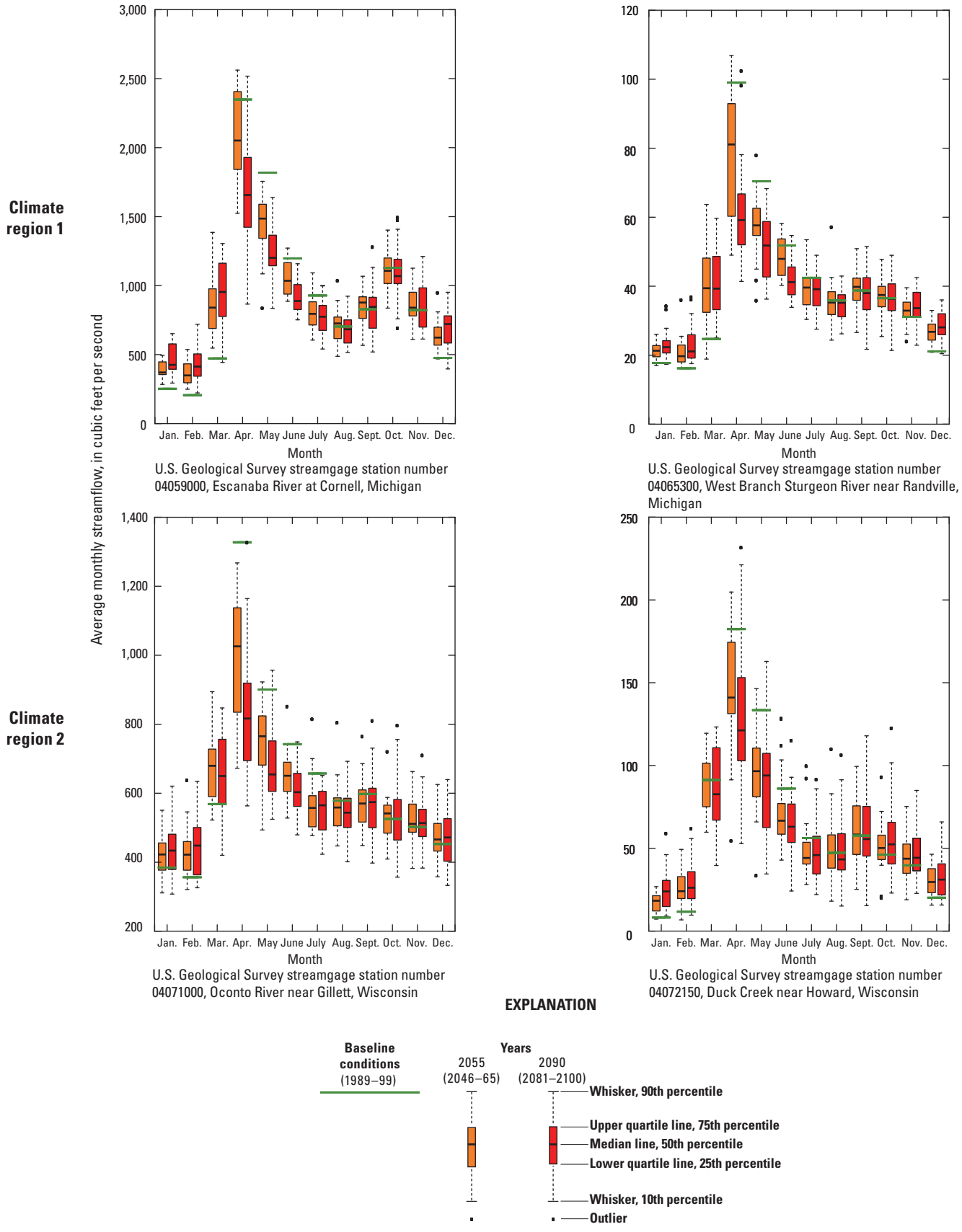

Figure 15. Selected streamgages and current conditions compared to future emission scenarios average mean monthly streamflow.

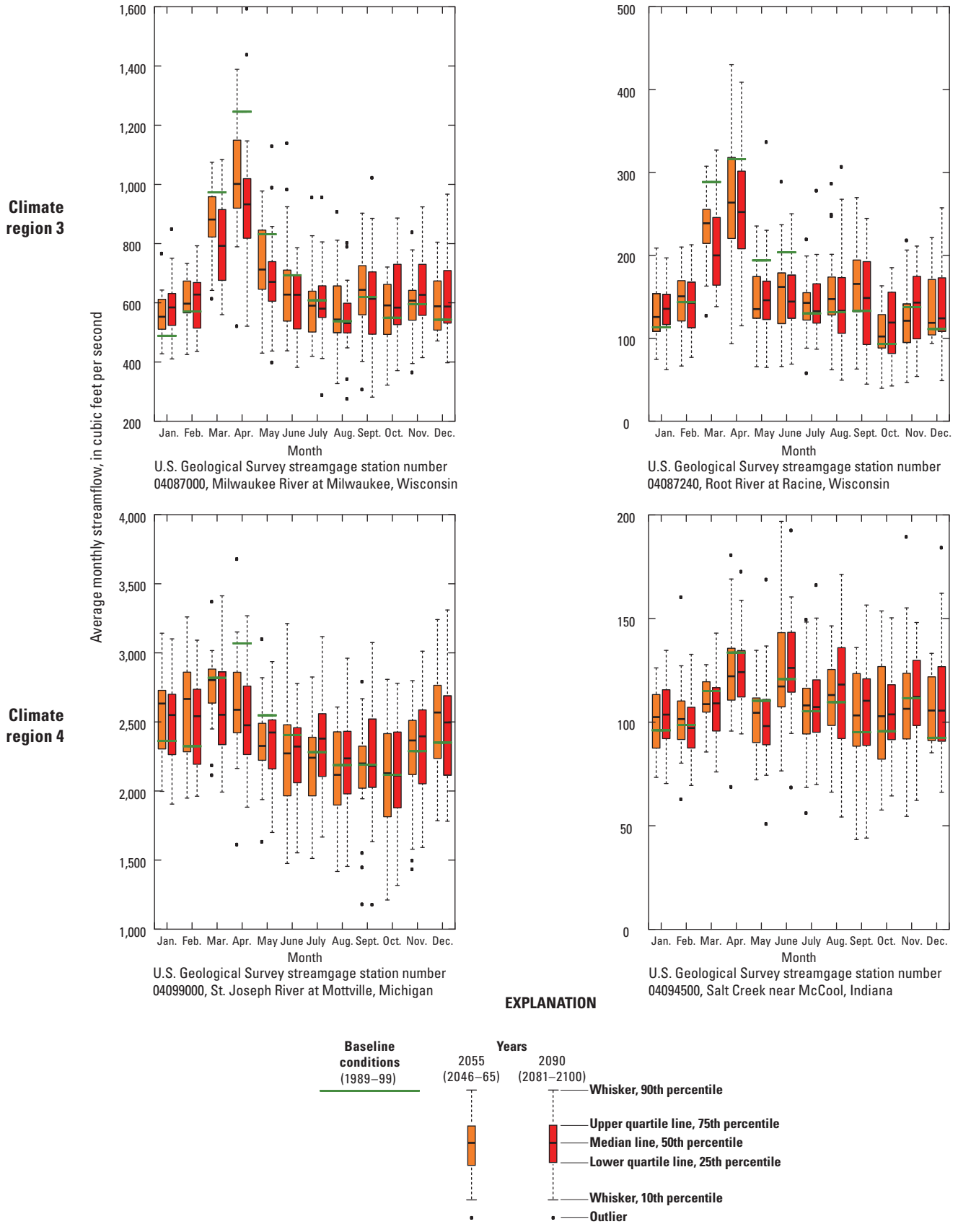

Figure 15. Selected streamgages and current conditions compared to future emission scenarios average mean monthly streamflow.—Continued

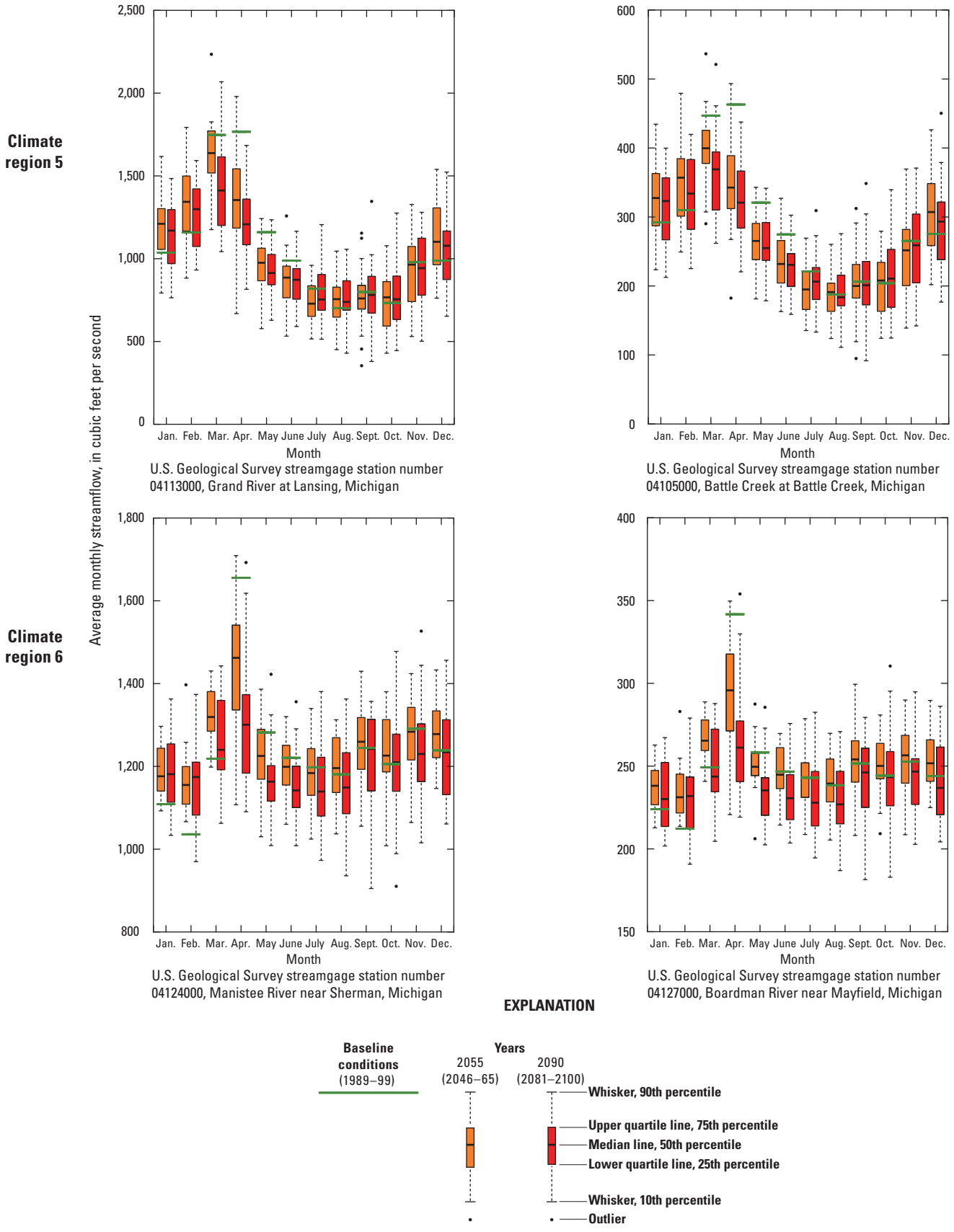

Figure 15. Selected streamgages and current conditions compared to future emission scenarios average mean monthly streamflow.—Continued

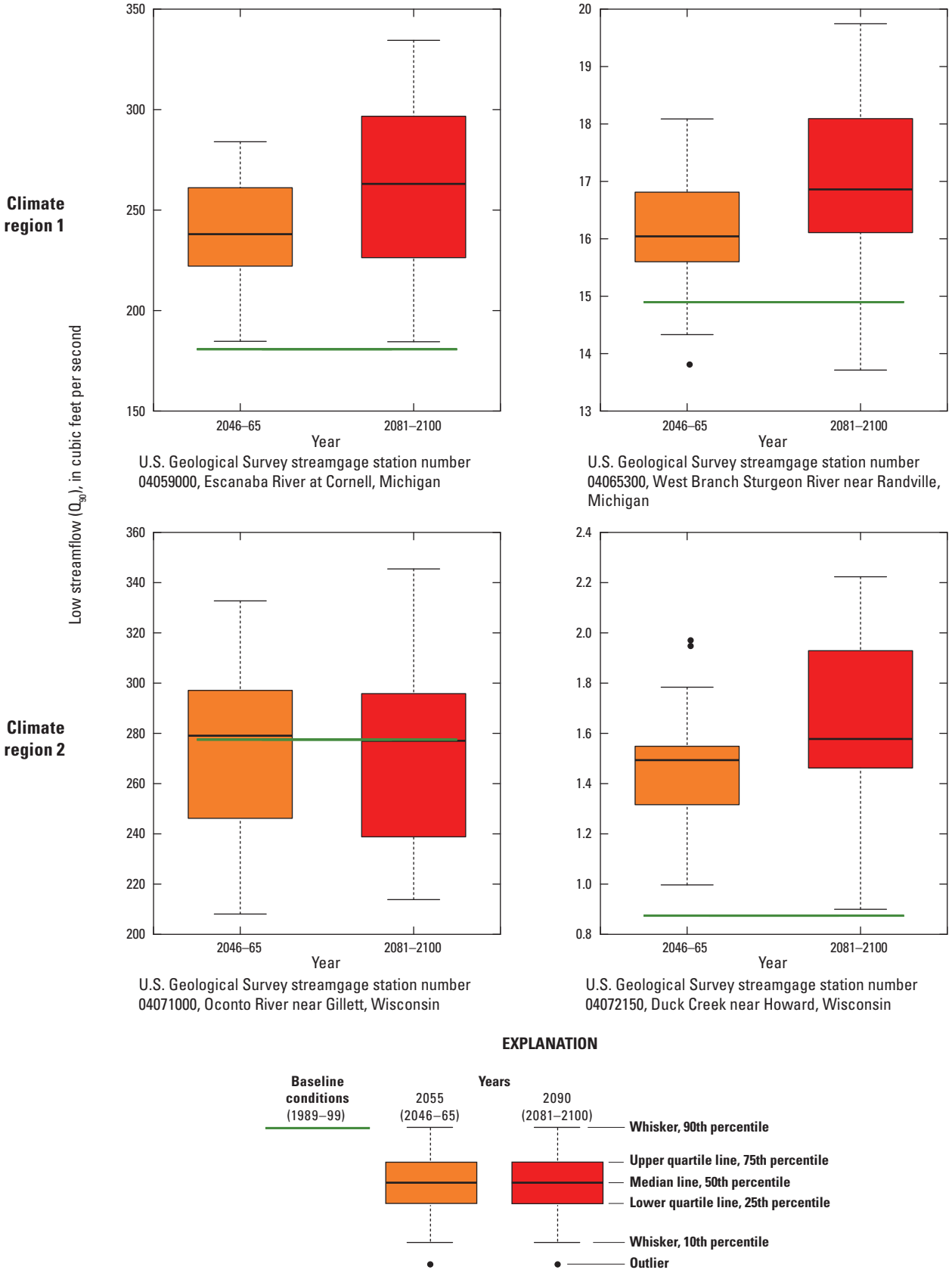

Figure 16. Selected streamgages and current conditions compared to future emission scenarios for low-flow (Q_{90}) streamflows.

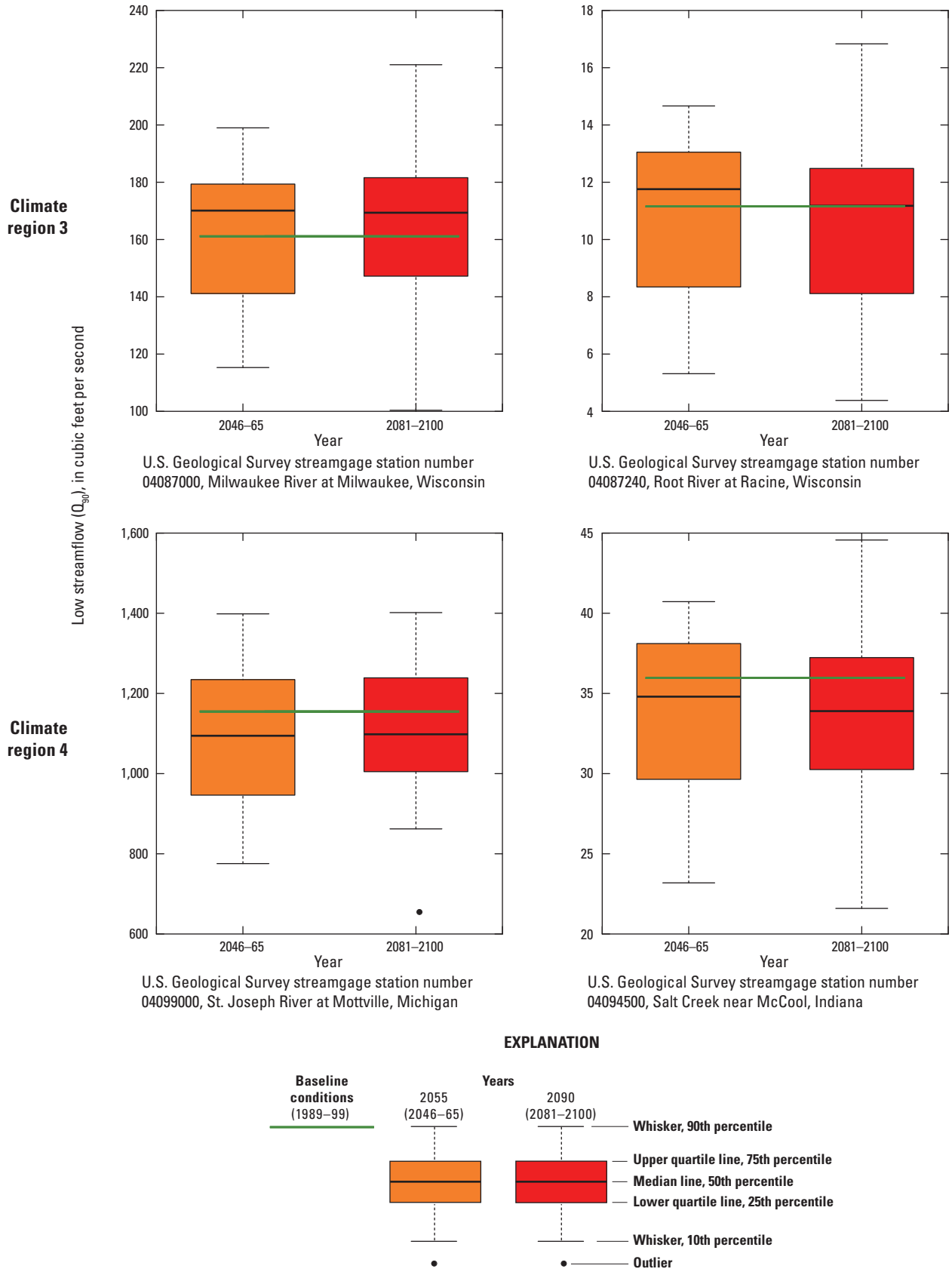

Figure 16. Selected streamgages and current conditions compared to future emission scenarios for low-flow (Q_{90}) streamflows.—Continued

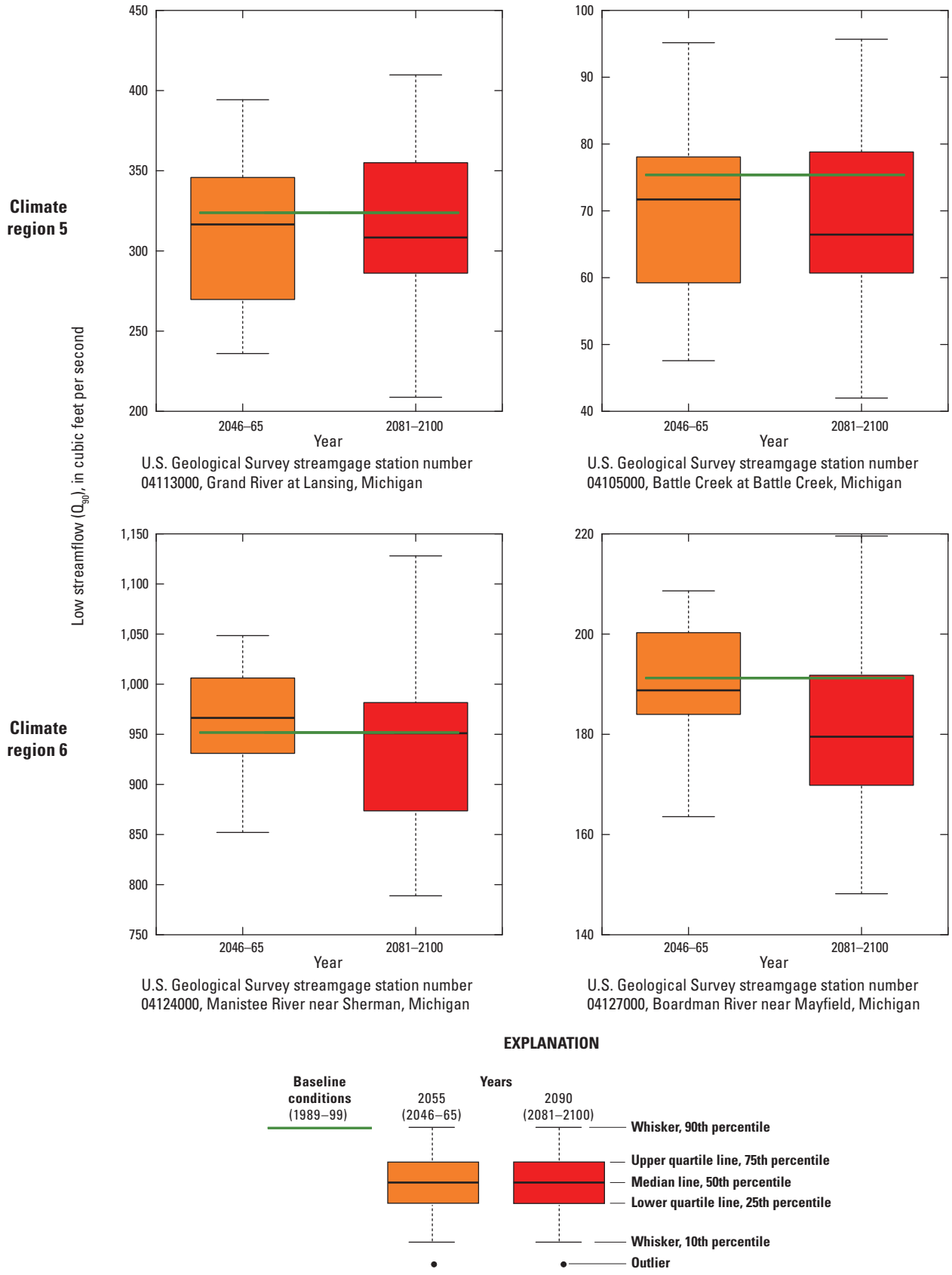

Figure 16. Selected streamgages and current conditions compared to future emission scenarios for low-flow (Q_{90}) streamflows.—Continued

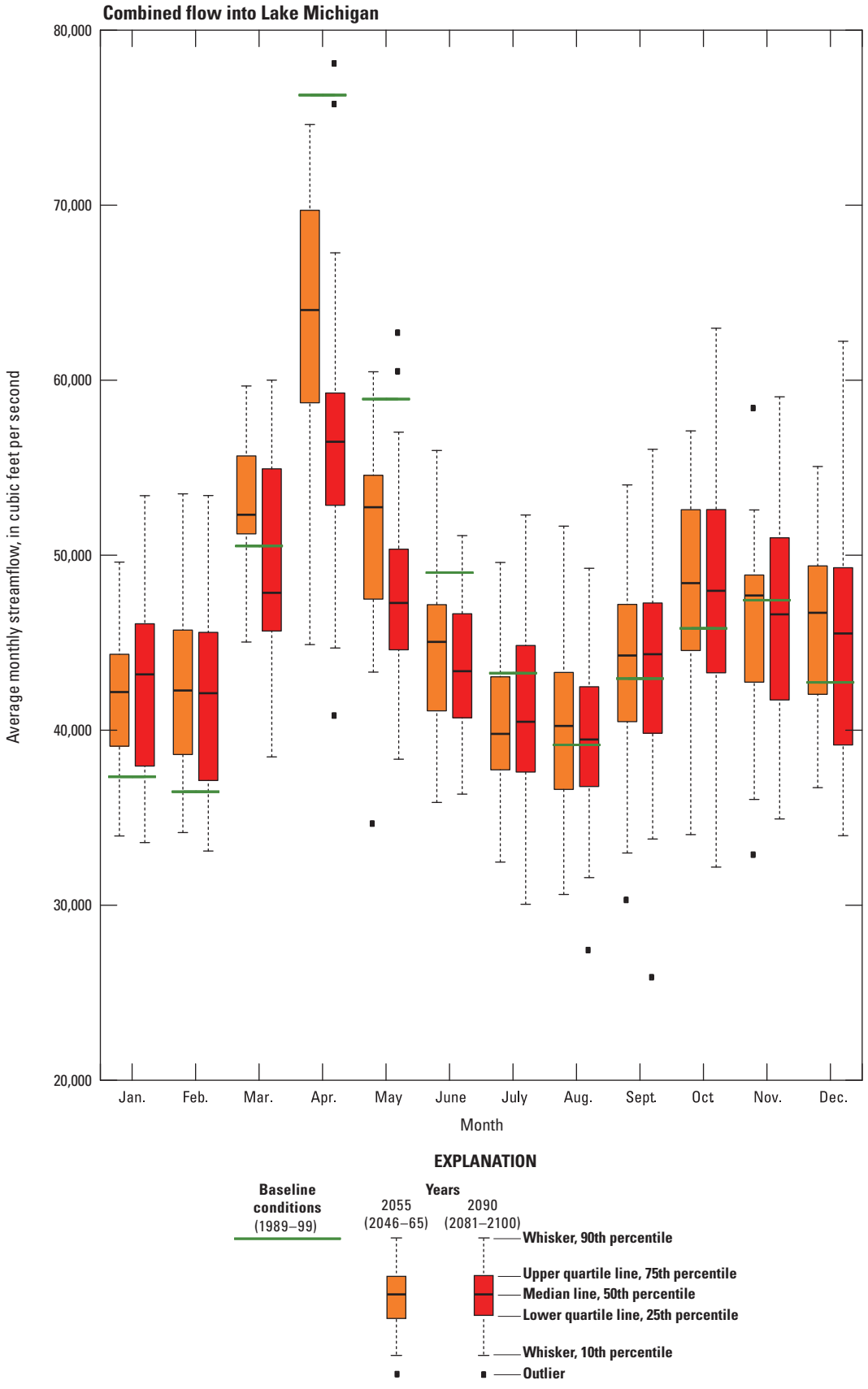

Figure 17. Lake Michigan Basin current conditions compared to future emission scenarios average mean monthly streamflow.

climate in the northern parts of the Lake Michigan Basin is to look at the southern parts of the basin (that is, using differences in space to give insight into differences in time). With this view, hydrograph monthly time series from northern parts of the Lake Michigan Basin become flatter and more similar to that taking place in the southern parts of the basin under current conditions. Hydrographs in the southern parts of the Lake Michigan Basin are forecasted to flatten as well, further reducing the intermonthly dynamics, and are expected to be similar to areas located south of the Lake Michigan Basin under current conditions.

Spatial Changes in Growing Season and Soil Moisture in the Lake Michigan Basin

One result of the potential increased air temperature with changing climate is an appreciable increase in the length of the growing season in the Lake Michigan Basin (fig. 18). This increase is comparable to Christiansen and others (2011), who used a different downscaling approach to the GCM results. Such an increase in growing season length will increase the period of evapotranspiration in the basin, which in turn is expected to affect soil moisture. For example, average conditions during 2081–2100 for August soil moisture have decreased across the Lake Michigan Basin (fig. 19). August was selected because it often is the month of lowest flow in the Lake Michigan Basin. The spatial distribution of decreased August soil moisture coincides with decreases annually for soil moisture across the Lake Michigan Basin (fig. 20). Areas with large wetland expanses (Region 1, fig. 7) show large effects; however, the PRMS hydrologic model constructed here only includes consideration of wetlands within an HRU through the average property specified for that HRU. Therefore, the coarse discretizations of the model, and lack of inclusion of specific wetland water budget processes, preclude more refined estimates of effects in wetland rich areas of the Lake Michigan Basin.

Climate Change Discussion

When total streamflows to Lake Michigan are integrated over time, the long-term input of water is forecast to stay similar to that of current conditions. This lack of change reflects (1) the offsetting effects of forecasted increases in temperature and precipitation in the 21st century by the GCMs (fig. 10), and (2) averaging over large temporal (annual) and spatial (entire Lake Michigan Basin) scales. The range of uncertainty expressed by the eight GCMs (Intergovernmental Panel on Climate Change, 2007) and four carbon emission scenarios is also appreciable, which would in turn affect the uncertainty in the basin flow forecasts. As discussed in the Hydrologic Response to Climate Change Scenarios section, such basin flow forecasts do not equate directly into forecasts of Lake Michigan stage, because changes in other water budget components are not considered in tandem; for example, forecasts of evaporation off Lake Michigan itself are not considered in this work, and this flux is a dominant sink from Lake Michigan (Grannemann and others, 2000).

Changes in the seasonal hydrological dynamics, consistent with warming air temperatures in a northern temperate climate, are forecast across the Lake Michigan Basin, with the largest increase in dampening of the seasonal dynamic taking place in the northern Lake Michigan Basin. Comparison of forecasts of combined annual streamflow into Lake Michigan (fig. 13) and forecasts of monthly streamflows in figures 15 and 17 show a summary point of this work: when streamflows are integrated across the spatial extent of the lake over large timeframes, the effects of climate change are less visible, but when streamflows are analyzed by subbasin and subannual scale, climate change effects are more pronounced. Therefore, these simulated forecasts indicate that effects of climate change may not be substantial, but could appreciably alter ecosystem functions within the Lake Michigan Basin that depend on seasonal dynamics at subannual time periods, such as fish spawning.

Climate effects on decreased storage of winter precipitation are forecasted to result in smaller high (Q_{10}) streamflows throughout the Lake Michigan Basin (fig. 14); however, this result should be viewed with caution because this forecast is calculated using a statistical representation of high stream discharge flow rather than peak height itself, and this effect is mostly a result of simulated changes during the snowmelt period. Many peak flooding events result from extreme precipitation events that take place outside of the spring snowmelt time period, and occurrence of this type of extreme events is forecast to increase with future warming (for example, *http://www.wicci.wisc.edu/publications.php*). Low-flow (Q_{90}) forecasts range from substantial increases in the Upper Peninsula of Michigan to slightly decreasing in the middle and southern parts of the Lake Michigan Basin (fig. 16). This spatial gradient in system response again reflects difference in utility of model outputs: large-scale models are appropriate for outputs such as annual streamflows, which are important for integrating predictions such as Lake Michigan stage forecasts. More localized subbasin water budgets forecasts are not well simulated by the coarse large-scale model because they cannot simulate important smaller scale processes such as mitigating local storage in the basin; therefore, subbasin forecasts reflect effects of increased groundwater recharge (northwest part of the basin) or increased evapotranspiration during the growing season (southern parts of the basin; fig. 18) even if annual streamflow also does not capture the potential important change to the timing of streamflows. Flow timing is important for many societal and restoration activities taking place within the basin. For example, decreases in soil moisture in August and annually (figs. 19 and 20) could be offset by increased irrigation, but removal of water from the subbasins as a result of increased irrigation would decrease the average August streamflows (for example, figs. 15 and 17); such tradeoffs result from changes in seasonal timing of streamflows within the Lake Michigan Basin. Restoration activities that enhance water retention within a subbasin could help mitigate seasonal

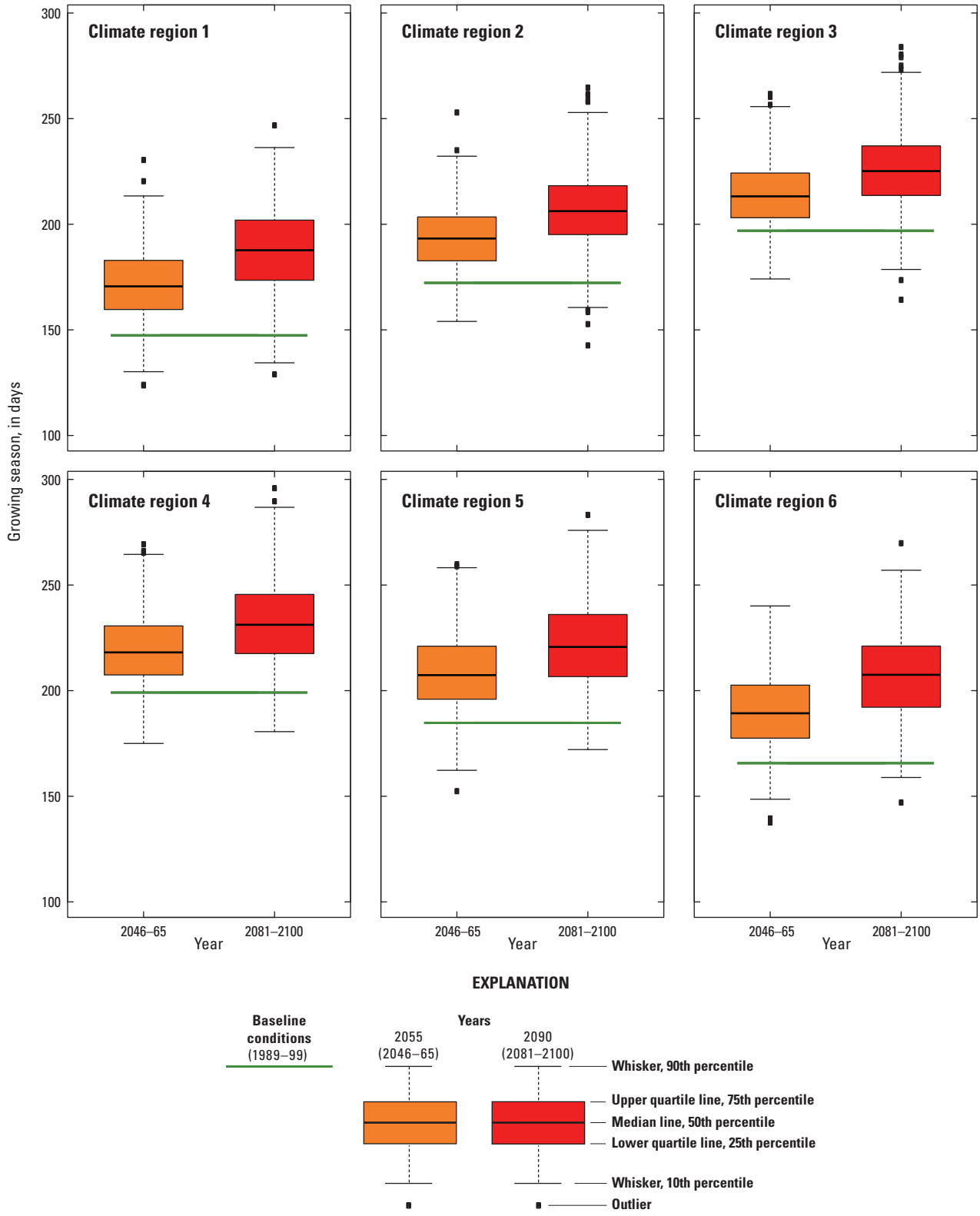

Figure 18. Growing season change by climate region in the Lake Michigan Basin.

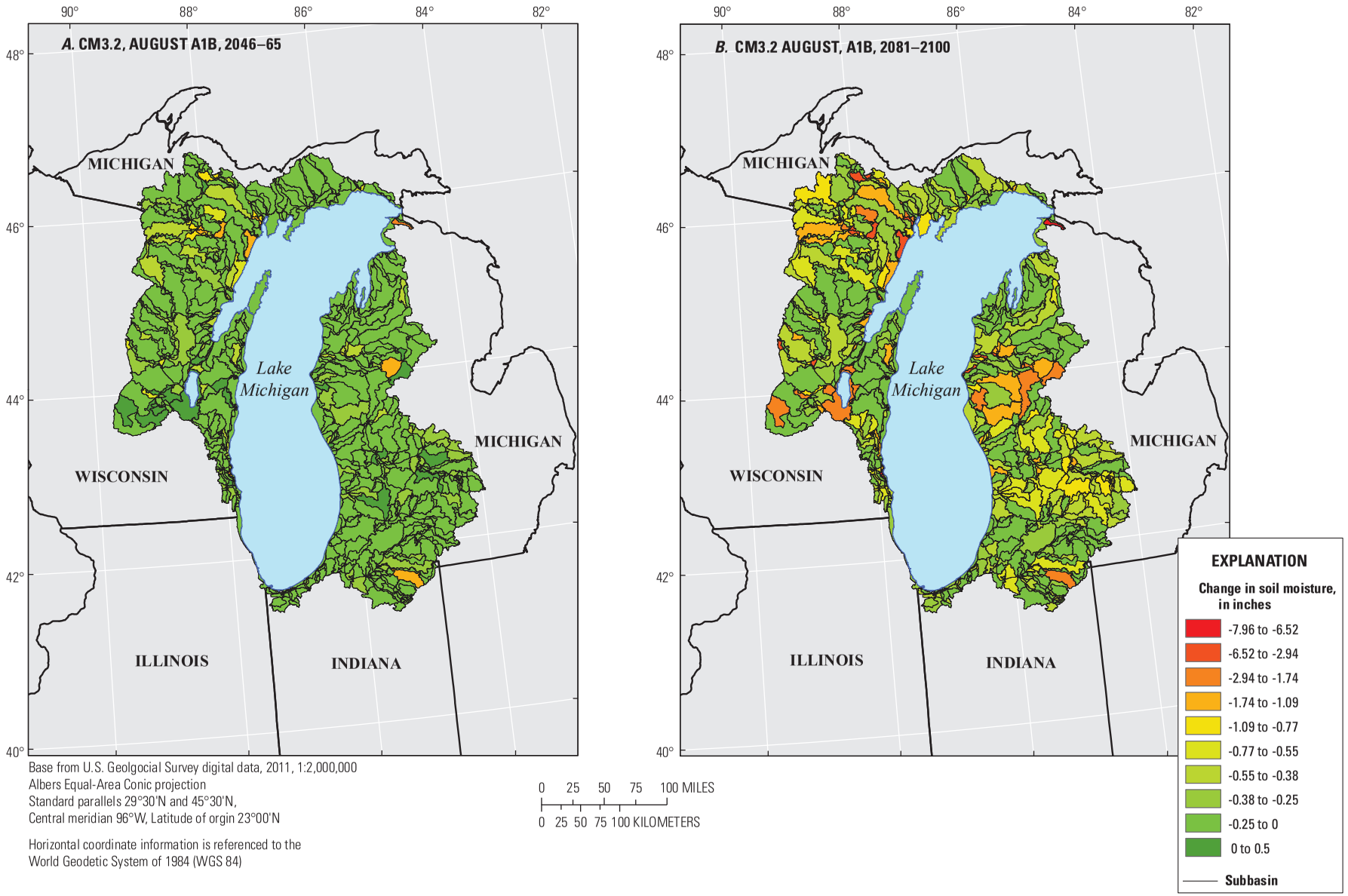

Figure 19. Change in August soil moisture from baseline 1981–2000 to *A*, 2046–2065 and to *B*, 2081–2100.

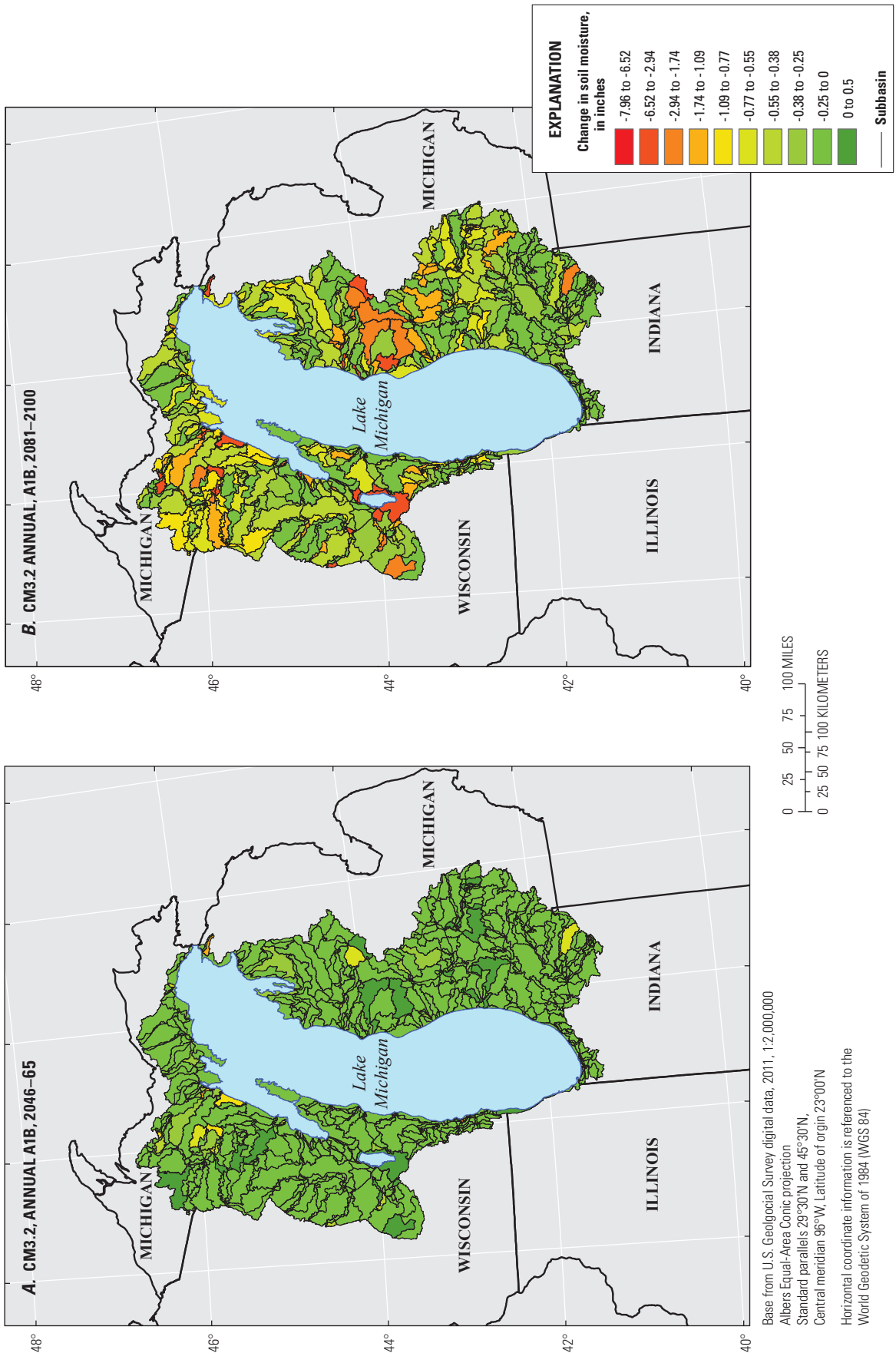

Figure 20. Change in annual soil moisture from baseline 1981–2000 to *A*, 2046–2065 and to *B*, 2081–2100.

short-term shortages of water. Moreover, such mitigating storage would facilitate storage of water during wet years for use during drier years, which in turn provides additional resiliency to the associated aquatic ecosystems.

Finally, it should be noted that this basin-scale view is intended to provide a process-based mechanism to translate possible climate scenarios (for example, Hayhoe and others, 2010) to basin response, and improve future forecasts for Great Lake systems such as lake levels calculated with approximate representations of the basin contributions such as net basin supplies (for example, MacKay and Seglenieks, 2013) and lake-centric approaches (for example, Angel and Kunkel, 2010). It is acknowledged that forecasts of change resulting from future climates are inherently uncertain; therefore, the approach documented here is best considered a tool for informing, and integrating with, the family of existing approaches that have been brought to bear on this important topic.

Limitations and Assumptions

The Lake Michigan Basin PRMS model uses a relatively large piecewise-constant discretization of flow planes within the basin, a discretization suitable for a regional basin model; therefore, it is considered a somewhat coarse simulator of processes happening within subbasins. It is likely that predictions of interest not well served by the regional discretization will need refinement of the regional HRUs. This model limitation will apply most prominently to forecasts that require daily streamflows, such as short term low streamflows Q_7, 10-year (drought low streamflows) or 2-year reoccurrence interval for forecasting sediment transport. The PRMS model code itself uses a number of process simplifications that may have varying degrees of appropriateness across the model domain; for example, the linear reservoir assumption for the groundwater system may not represent a groundwater-dominated stream system well (for example, WEST BRANCH STURGEON RIVER NEAR RANDVILLE, MI, station number 04065300, fig. 11), even if the uncertainty resulting from the global climate scenarios (that is, the envelope of possible results) seems small based on small forecasted changes in annual flows (same station, appendix 2. Furthermore, to the extent that the projected metrics align with the observations used for calibration, the degree of fit shown for a given streamgage in appendix 1 is an indication of the uncertainty associated with forecasts simulated by the Lake Michigan Basin PRMS model. The temperature-based proxy approach for calculating PET can be problematic (Lofgren and others, 2013); the version of PRMS used here calculated PET using such a temperature proxy method. Finally, the climate_hru module (LaFontaine and others, 2013) is an improvement over previous methods of distributing climate across large model domains, but simulations using the downscaled/extrapolated climate data can introduce error and lead to inaccuracies in the simulated streamflow. Further developments to improve PET calculation and down-scaling/extrapolating of climate data and PRMS climatic simulation modules are topics of on-going work.

Summary

The Great Lakes Restoration Initiative (GLRI) is the largest public investment in the Great Lakes in two decades. A task force of 11 Federal agencies developed an action plan to implement the initiative. The U.S. Department of the Interior was one of the 11 agencies that entered into an interagency agreement with the U.S. Environmental Protection Agency as part of the GLRI to complete scientific projects throughout the Great Lakes basin. The U.S. Geological Survey (USGS), a bureau within the Department of the Interior, is involved in the GLRI to provide scientific support to management decisions as well as measure progress of the Great Lakes restoration efforts. This report presents basin-scale simulated current and forecast climatic and hydrologic conditions in the Lake Michigan Basin. The forecasts were obtained by constructing and calibrating a Precipitation-Runoff Modeling System (PRMS) model of the Lake Michigan Basin; the PRMS model was calibrated using a model-independent parameter estimation approach. The Lake Michigan Basin PRMS model was used to simulate potential future hydrology by using four simulated carbon emission scenarios from the World Climate Research Programme's Coupled Model Intercomparison Project phase 3 for eight global climate models (GCMs) that were statistically downscaled and available for use through the USGS GeoData Portal.

The model was calibrated using the computer code PEST (Doherty 2010a, 2010b), which is a universal code for parameter estimation and uncertainty analysis. The PEST optimization algorithm automatically adjusted PRMS input parameters to determine better fits to observed data in a series of model runs. After each model run, simulated model outputs were automatically compared to USGS streamflow measurements. Paramter estimation continued until a best fit between simulated and observed targets was attained.

The calibrated Lake Michigan Basin PRMS model was used to examine four potential climate-change emission scenarios, thus providing potential future hydrologic changes within the Lake Michigan Basin because of changes in climate, which could be used by environmental managers. The GCM projections contain a wide range of future climatic conditions, each of which is used in the Lake Michigan Basin PRMS model to simulate hydrologic responses to the climate scenarios. The four scenarios represent different levels of carbon emissions [one current (2014) and three potential futures] leading to the different greenhouse gas emissions and concentrations during the 21st century, from relatively low (B1), to medium (A1B, to high (A2) concentrations.

The GCMs predicted that the maximum and minimum temperatures in the Lake Michigan Basin will increase in the

future with the minimum temperature increasing more than the maximum temperature. Although the minimum and maximum temperatures were increasing, precipitation results were not as clear, with a general increase in the central tendency for the two periods; however, the variability across the GCMs and emission scenarios was relatively large. Examining the Lake Michigan Basin over such a large area results in some combinations exhibiting temperature and precipitation that are lower than current conditions and some combinations higher than current conditions, and only indicates the coarse overall changes in temperature and precipitation. Generally, monthly simulations indicated a north-south gradient in climate change effects where forecasts in the northern (Regions 1 and 6) areas of the Lake Michigan Basin are more affected by climate change than the southern (Regions 3 and 4) areas. This result reflects the north-south gradient whereby the north is characterized by larger accumulation of snowpack storage and the associated snow-melt pulse. Changes in the partitioning of winter precipitation reflect increases in air temperature that are projected to take place by 2100, a result consistent across all GCMs and emission scenarios.

The median between current and forecasted Q_{10} (high) streamflows indicates reductions throughout the Lake Michigan Basin, which is an indication that there is a dampening of snowmelt dynamics with forecast reductions in water stored in the snowpack. Although the Q_{10} (high) streamflows are indicating reductions, the Q_{90} (low) streamflows indicate an increase in low streamflows with an approximate northwest-southeast gradient, with significant increases in low flow in northwest and no change to decreases in the southeast.

The potential increased air temperature because of changing climate causes an appreciable increase in the length of the growing season in the basin. The increase in growing season length will increase the period of evapotranspiration in the basin, which in turn is expected to affect soil moisture. For example, average conditions during 2081–2100 for August soil moisture have decreased across the Lake Michigan Basin. August was selected because it often is the month of lowest flow in the Lake Michigan Basin. The spatial distribution of decreased August soil moisture coincides with decreases annually for soil moisture across the Lake Michigan Basin. Areas with large wetland expanses such as Region 1 indicate large effects.

The Lake Michigan Basin PRMS model can be used as a tool for the Great Lakes restoration effort to answer many potential questions about long-term restoration investments related to potential changes in land use and climate change. For example, coupling the hydrological output (streamflows) from the Lake Michigan Basin PRMS model with the Spatially Referenced Regression on Watershed (SPARROW) model framework can be used to estimate nutrient concentrations in streams and loadings to Lake Michigan in response to changes in land use and climate. The Lake Michigan Basin PRMS model also can be applied to wildlife diseases; indices of hydrologic alteration can be related to historical spatial and temporal changes in wildlife diseases, and the relations can be used to forecast potential impacts of land use and climate on wildlife diseases. The model outputs will have applicability to a variety of biological, ecological, and hydrological efforts in the Lake Michigan Basin.

References

Angel, J.R., and Kunkel, K.E, 2010, The response of Great Lakes water levels to future climate scenarios with an emphasis on Lake Michigan-Huron: Journal of the Great Lakes Research, v. 36, p. 51–58.

Beven, K.J., 1993, Prophecy, reality and uncertainty in distributed hydrological modeling: Advances in Water Resources, v. 16, p. 41–51.

Beven, K.J., and Binley, A.M., 1992, The future of distributed models—Model calibration and uncertainty prediction: Hydrological Processes, v. 6, p. 279–298.

Beven, K.J., and Freer, J., 2001, Equifinality, data assimilation, and uncertainty estimation in mechanistic modelling of complex environmental systems: Journal of Hydrology, v. 249, p. 11–29.

Blodgett, D.L., 2013, The U.S. Geological Survey Climate Geo Data Portal—An integrated broker for climate and geospatial data: U.S. Geological Survey Fact Sheet 2013–3019, 2 p., [Also available at *http://pubs.usgs.gov/fs/2013/3019*.]

Cherkauer, K.A., and Sinha, T., 2010, Hydrologic impacts of projected future climate change in the Lake Michigan region: Journal of the Great Lakes Research, v. 36, p. 33–50.

Christiansen, D.E., Markstrom, S.L., and Hay, L.E., 2011, Impacts of climate change on growing season in the United States: Earth Interactions, v. 15, p.1–17.

Coon, W.F., Murphy, E.A., Soong, D.T., and Sharpe, J.B., 2011, Compilation of watershed models for tributaries to the Great Lakes, United States, as of 2010, and identification of watersheds for future modeling for the Great Lakes Restoration Initiative: U.S. Geological Survey Open-File Report 2011–1202, 23 p. [Also available at *http://pubs.usgs.gov/of/2011/1202*.]

Doherty, J., 2003, Ground water model calibration using pilot points and regularization: Ground Water, v. 41, no. 2, p. 170–177.

Doherty, J., and Hunt, R.J., 2010, Response to comment on "Two statistics for evaluating parameter identifiability and error reduction": Journal of Hydrology, v. 380, p. 489–496.

Doherty, J., 2010a, PEST, Model-independent parameter estimation—User manual (5th ed.): Brisbane, Australia, Watermark Numerical Computing, 336 p.

Doherty, J., 2010b, Addendum to the PEST manual: Brisbane, Australia, Watermark Numerical Computing, 293 p.

Environmental Systems Research Institute, Inc., 2004, Getting to know ArcGIS Desktop: Redlands, California, [variously paged].

Farnsworth, R.K., Thompson, E.K., and Peck, E.L., 1982, Evaporation atlas for the contiguous 48 United States: National Oceanic and Atmospheric Administration Technical Report NWS 33, 41 p.

Feinstein, D.T., Hunt, R.J., and Reeves, H.W., 2010, Regional groundwater-flow model of the Lake Michigan Basin in support of Great Lakes Basin water availability and use studies: U.S. Geological Survey Scientific Investigations Report 2010–5109, 379 p., [Also available at *http://pubs.usgs.gov/sir/2010/5109/.]*

Fenneman, N.M., and Johnson, D.W., 1946, Physical divisions of the United States: U.S. Geological Survey, scale 1:7,000,000.

Government of Canada and U.S. Environmental Protection Agency, 1995, The Great Lakes—An environmental atlas and resource book: EPA 905–B–95–001, 46 p.

Grannemann, N.G., Hunt, R.J., Nicholas, J.R., Reilly, T.E., and Winter, T.C., 2000, The importance of ground water to the Great Lakes Region: U.S. Geological Survey Water-Resources Investigations Report 00–4008, 12 p., [Also available at *http://pubs.er.usgs.gov/publication/wri004008.]*

Hay, L.E., Leavesley, G.H., Clark, M.P., Markstrom, S.L., Viger, R.J., and Umemoto, M., 2006, Step wise, multiple objective calibration of a hydrologic model for a snowmelt dominated basin: Journal of the American Water Resources Association, v. 42, no. 4, p. 877–890.

Hayhoe, K., VanDorn, J., Croley, T., Schlegal, N., and Wuebbles, D.J., 2010, Regional climate change projections for Chicago and the US Great Lakes: Journal of the Great Lakes Research, v. 36, p. 7–21.

Homer, C., Huang, C., Yang, L., Wylie, B., and Coan, M., 2004, Development of a 2001 National Landcover Database for the United States: Photogrammetric Engineering and Remote Sensing, v. 70, no. 7, p. 829–840.

Horizon Systems Corporation, 2006, National Hydrography Dataset Plus (NHDPlus): Horizon Systems Corporation, accessed March 16, 2012, at *http://www.horizon-systems.com/nhdplus/*.

Hunt, R.J., and Doherty, J., 2006, A strategy of constructing models to minimize prediction uncertainty, *in* International Conference of the International Ground Water Modeling Center, 7th, Golden, Colo., 2006, Proceedings: Golden, Colo., Colorado School of Mines, p. 56–60.

Hunt, R.J., Doherty, J., and Tonkin, M.J., 2007, Are models too simple? Arguments for increased parameterization: Ground Water, v. 45, no. 3, p. 254–262, *http://dx.doi.org/10.1111/j.1745-6584.2007.00316.x*.

Hunt, R.J., Walker, J.F., Selbig, W.R., Westenbroek, S.M., and Regan, R.S., 2013, Simulation of climate-change effects on streamflow, lake water budgets, and stream temperature using GSFLOW and SNTEMP, Trout Lake Watershed, Wisconsin: U.S. Geological Survey Scientific Investigations Report 2013–5159, 118 p., [Also available at *http://pubs.usgs.gov/sir/2013/5159/.*]

Intergovernmental Panel on Climate Change, 2007, Summary for policymakers, in Solomon, S., Qin, D., Manning, M., Chen, Z., Marquis, M., Averyt, K.B., Tignor, M., and Miller, H.L., eds., Climate change 2007—The physical science basis, contributions of working group 1 to the fourth assessment report of the Intergovernmental Panel on Climate Change: Cambridge and New York, Cambridge University Press, 18 p.

Jakeman, A.J., and Horneberger, G.M., 1993, How much complexity is warranted in a rainfall-runoff model?: Water Resources Research, v. 29, no. 8, p. 2637-2649, *http://dx.doi.org/10.1029/93WR00877*

LaFontaine, J.H., Hay, L.E., Viger, R.J., Markstrom, S.L., Regan, R.S., Elliott, C.M., and Jones, J.W., 2013, Application of the Precipitation-Runoff Modeling System (PRMS) in the Apalachicola–Chattahoochee–Flint River Basin in the southeastern United States: U.S. Geological Survey Scientific Investigations Report 2013–5162, 118 p., [Also available at *http://pubs.usgs.gov/sir/2013/5162/.*]

Lofgren, B.M., and Gronewold, A.D., 2013, Reconciling alternative approaches to projecting hydrologic impacts of climate change: Bulletin of the American Meteorological Society, v. 94, no. 10, p. ES133–ES135, *http://dx.doi.org/10.1175/BAMS-D-13-00037.1*

Lofgren, B.M, Gronewold, A.D, Acciaioli, A., Cherry, J., Steiner, A., and Watkins, D., 2013,

Methodological approaches to projecting the hydrologic impacts of climate change: Earth Interactions, v. 17, p. 1–19.

MacKay, M., and Seglenieks, F., 2013, On the simulation of Laurentian Great Lakes water levels under projections of global climate change: Climatic Change, v. 117, p. 55-67, *http://dx.doi.org/10.1007/s10584-012-0560-z*

Markstrom, S.L., Hay, L.E., Ward-Garrison, C.D., Risley, J.C., Battaglin, W.A., Bjerklie, D.M., Chase, K.J., Christiansen, D.E., Dudley, R.W., Hunt, R.J., Koczot, K.M., Mastin, M.C., Regan, R.S., Viger, R.J., Vining, K.C., and Walker, J.F., 2011, Integrated watershed—Scale response to climate change for selected basins across the United States: U.S. Geological Survey Scientific Investigations Report 2011–5077, [Also available at *http://pubs.usgs.gov/sir/2011/5077/*.]

Markstrom, S.L., Niswonger, R.G., Regan, R.S., Prudic, D.E., and Barlow, P.M., 2008, GSFLOW—Coupled ground-water and surface-water flow model based on the integration of the Precipitation-Runoff Modeling System (PRMS) and the Modular Ground-Water Flow Model (MODFLOW-2005): U.S. Geological Survey Techniques and Methods, chap. 6, book D1, 240 p.

Miller, I., and Freund, J.E., 1977, Probability and statistics for engineers (2d ed.): Englewood Cliffs, N.J., Prentice-Hall, Inc, 529 p.

Moore, C., and Doherty, J., 2005. The role of the calibration process in reducing model predictive error: Water Resources Research, v. 41, no. 5, 14 p,

Moriasi, D.N., Arnold, J.G., Van Liew, M.W., Binger, R.L., Harmel, R.D., and Veith, T.L., 2007, Model evaluation guidelines for systematic quantification of accuracy in watershed simulations:

Transactions of the American Society of Agricultural and Biological Engineers, v. 50, no. 3, p. 885–900.

Nash, J.E., and Sutcliffe, J.V., 1970, River flow forecasting through conceptual models part I—A discussion of principles: Journal of Hydrology, v. 10, no. 3, p. 282–290.

National Geophysical Data Center, 1998, GEOphysical DAta System - Next Generation (GEODAS) gridded data format: accessed April 2008, at *http://www.ngdc.noaa.gov/mgg/gdas/gd_designagrid.html?dbase=grdglb*.

National Oceanic and Atmospheric Administration, 2010, Lake Michigan Basin land cover change report 1985–2010: accessed March 2014, at *http://www.csc.noaa.gov/digitalcoast/publications/lake-michigan-basin-land-cover-change*.

National Oceanic and Atmospheric Administration Cooperative Observer Program, 2014, National Weather Service database: accessed June 2010, at *http://www.nws.noaa.gov/om/coop/*.

Notaro, M., Lorenz, D., Vimont, D., Vavrus, S., Kucharik, C., and Franz, K., 2011, 21st century Wisconsin snow projections based on an operational snow model driven by statistically downscaled climate data: International Journal of Climatology, v. 31, p. 1615–1633.

Open Geospatial Consortium, Inc., 2006, OpenGIS Web Map Service Implementation Specification: accessed June 2010, at *http://www.opengeospatial.org/standards/wms*.

Robertson, D.M., and Saad, D.A., 2011, Nutrient inputs to the Laurentian Great Lakes by source and watershed estimated using SPARROW watershed models: Journal of the American Water Resources Association, v. 47, no. 5, p. 1011–1033, *http://dx.doi.org/10.1111/j.1752-1688.2011.00574.x.*

Rutherford, E.S., 2008, Lake Michigan's tributary and nearshore fish habitats, *in* Clapp, D.F., and Horns, W., eds.,The State of Lake Michigan in 2005: Ann Arbor, Mich., Great Lakes Fishery Commission, Special Publication 08-02, p. 7–17, [Also available at *http://www.glerl.noaa.gov/pubs/fulltext/2008/20080068.pdf*.]

Sheets, R.A., and Simonson, L.A., 2006, Compilation of regional ground-water divides for principal aquifers corresponding to the Great Lakes Basin: U.S. Geological Survey Scientific Investigations Report 2006–5102, 23 p.

Simley, J., 2008, Applying the National Hydrography Dataset: Water Resources Impact, v. 10, no. 1, p. 5–8.

Tikhonov, A.N., 1963a, Solution of incorrectly formulated problems and the regularization method: Soviet Mathematics Doklady, v. 4, p. 1035–1038.

Tikhonov, A.N., 1963b, Regularization of incorrectly posed problems: Soviet Mathematics Doklady, v. 4, p. 1624–1637.

Tonkin, M., and Doherty, J., 2005, A hybrid regularized inversion methodology for highly parameterized models: Water Resources Research, vol. 41, 16 p., *http://dx.doi.org/10.1029/2005WR003995*.

U.S. Department of Agriculture, 1994, State Soil Geographic (STATSGO) Database: Fort Worth, Tex., Data use information, Soils Conservation Service, National Cartography and Geographic Information System Center.

U.S. Geological Survey, 2007, National Elevation Dataset Database: accessed October 2007, at *http://ned.usgs.gov*.

Viger, R.J., and Leavesley, G.H., 2007, The GIS Weasel user's manual: U.S. Geological Survey Techniques and Methods, book 6, chap. B4, 201 p., [Also available at *http://pubs.usgs.gov/tm/2007/06B04/*.]

Viger, R.J., Hay, L.E., Jones, J.W., and Buell, G.R., 2010, Effects of including surface depressions in the application of the Precipitation-Runoff Modeling System in the Upper Flint River Basin, Georgia: U.S. Geological Survey Scientific Investigation Report 2010–5062, 36 p.

Walker, J.F., Hunt, R.J., Doherty, J., and Hay, L., 2009, Processing time-series data to calibrate a surface-water model in small headwater watersheds, *in* PEST Conference, 1st, Potomac, Md., 2009, Proceedings: Potomac, Md, 304 p.

Ward-Garrison, C., Markstrom, S.L., and Hay, L.E., 2009, Downsizer—A graphical user interface-based application for browsing, acquiring, and formatting time-series data for hydrologic modeling: U.S. Geological Survey Open-File Report 2009–1166, 27 p.

Westenbroek, S.M., Doherty, J., Walker, J.F., Kelson, V.A., Hunt, R.J., and Cera, T.B., 2012, Approaches in highly parameterized inversion—TSPROC, a general time-series processor to assist in model calibration and result summarization: U.S. Geological Survey Techniques and Methods, book 7, chap. C7, 79 p., 3 apps.

Wolock, D.M., 2003, Flow characteristics at U.S. Geological Survey streamgages in the conterminous United States: U.S. Geological Survey Open-File Report 03–146, accessed June 2008, at *http://pubs.er.usgs.gov/publication/ofr03146*.

Wuebbles, D.J., Hayhoe, K., and Parzen, J., 2010, Introduction—Assessing the effects of climate change on Chicago and the Great Lakes: Journal of the Great Lakes Research, v. 36, p. 1–6.

Appendixes 1–5

Appendix 1. Precipitation-Runoff Modeling System (PRMS) Statistical Graphs

The graphs compare the observed and simulated values for annual mean, monthly mean, monthly mean base flow, and mean monthly streamflows in the Lake Michigan Basin Precipitation-Runoff Modeling System model. Appendix 1 is available for download at *http://pubs.usgs.gov/sir/2014/5175/downloads/appendix_1.pdf*.

Appendix 2. Annual Climate Change Boxplots

The boxplots show the annual streamflow climate change ensembles for the annual periods of 2046–2065 and 2081–2100 for streamgages in the Lake Michigan Basin Precipitation-Runoff Modeling System model. Appendix 2 is available for download at *http://pubs.usgs.gov/sir/2014/5175/downloads/appendix_2.pdf*.

Appendix 3. Mean Monthly Climate Change Boxplots

The boxplots show the mean monthly streamflow climate change ensembles for the annual periods of 2046–2065 and 2081–2100 for streamgages in the Lake Michigan Basin Precipitation-Runoff Modeling System model. Appendix 3 is available for download at *http://pubs.usgs.gov/sir/2014/5175/downloads/appendix_3.pdf*.

Appendix 4. High Streamflow Climate Change Boxplots

The boxplots show the annual Q_{10} (high) streamflow climate change ensembles for the annual periods of 2046–2065 and 2081–2100 for streamgages in the Lake Michigan Basin Precipitation-Runoff Modeling System model. Q_{10} is defined as streamflow that is equaled or exceeded by only 10 percent of the streamflow on record. Appendix 4 is available for download at *http://pubs.usgs.gov/sir/2014/5175/downloads/appendix_4.pdf*.

Appendix 5. Low Streamflow Climate Change Boxplots

The boxplots show the annual Q_{90} (low) streamflow climate change ensembles for the annual periods of 2046–2065 and 2081–2100 for streamgages in the Lake Michigan Basin Precipitation-Runoff Modeling System model. Q_{90} is defined as streamflow that is equaled or exceeded by 90 percent of the streamflow on record. Appendix 5 is available for download at *http://pubs.usgs.gov/sir/2014/5175/downloads/appendix_5.pdf*.

Publishing support provided by:
Rolla Publishing Service Center

For more information concerning this publication, contact:
Director, USGS Iowa Water Science Center
P.O. Box 1230
Iowa City, IA 52244
(319) 337–4191

Or visit the Iowa Water Science Center Web site at:
http://ia.water.usgs.gov/

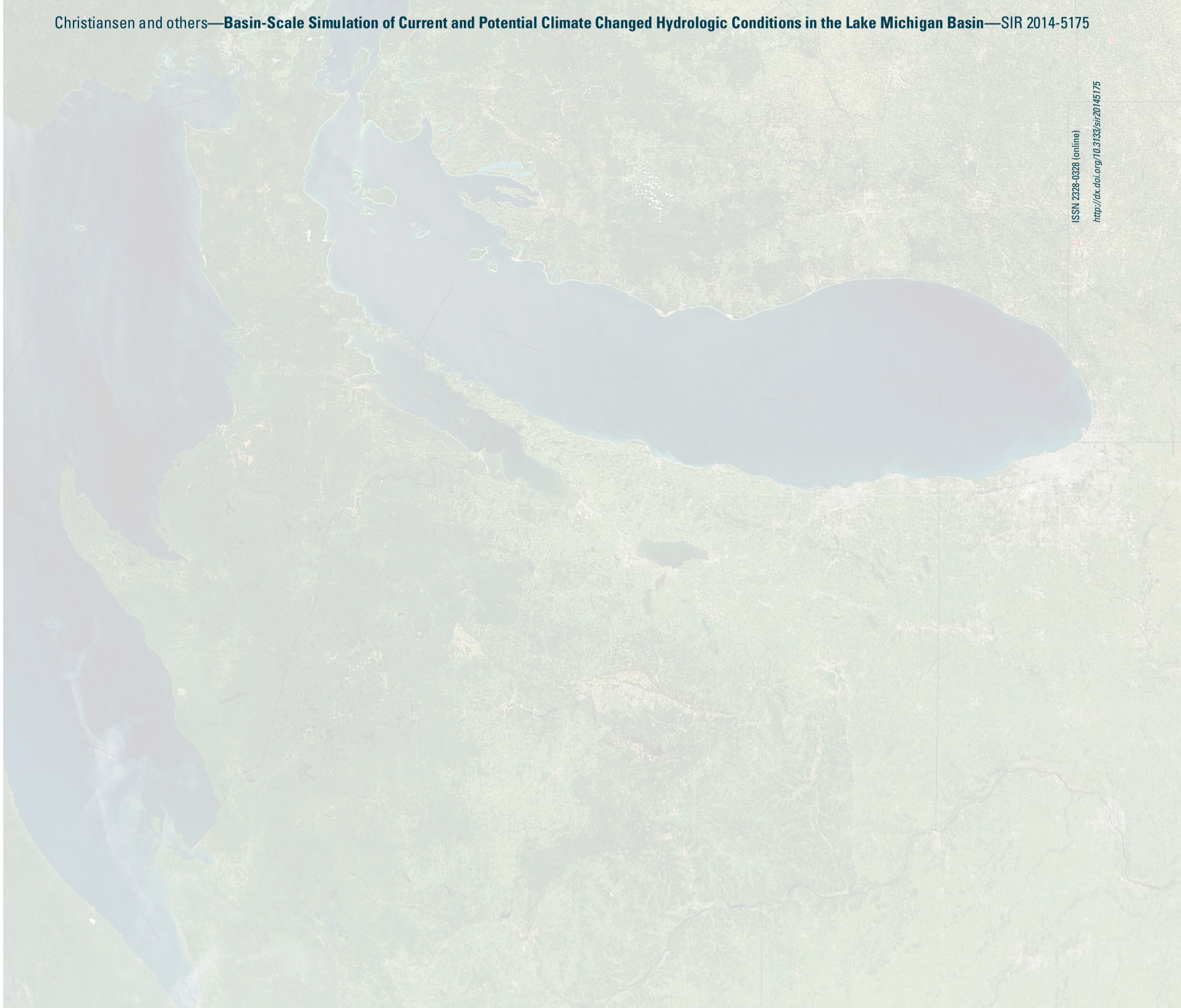

ISSN 2328-0328 (online)
http://dx.doi.org/10.3133/sir20145175